Electronic Supporting Information

Accurate Prediction of $T_{1/2}$ Variation with Pressure in Solid State Spin Crossover by *Ab Initio* Methods: the $[Co^{II}(dpzca)_2]$ case

Luca Bondì,[a,b] Sally Brooker*,[a] and Federico Totti*,[b]

[a]Department of Chemistry and MacDiarmid institute for Advanced 60 Materials and Nanotechnology, University of Otago, PO Box 56, Dunedin, 9054 New Zealand.
[b]Department of Chemistry 'Ugo Schiff' and INSTM Research Unit, University of Florence, 50019 Sesto Fiorentino, Italy.

Corresponding author email: sbrooker@chemistry.otago.ac.nz
Corresponding author email: federico.totti@unifi.it

Table of Contents

1. Computational Protocol

All periodic calculations were performed with the CP2K 6.1 quantum chemistry software,[1] which employs the Gaussian-plane waves formalism (GPW). Norm-conserving Goedecker-Tetter-Hutter (GTH) pseudopotentials[2-4] along with double zeta basis set with polarisation functions (DZVP-MOLOPT-SR) were employed for C, N, O, H atoms and DZVP-MOLOPT-SR-GTH basis set was applied to Co atoms. A cut-off of 450 Ry was applied for the plane wave expansion.[5]

The Anisimov simplified version[6] of the *DFT*+U approach[7] was used (U_{eff}). The U_{eff} parameters were chosen to match the experimental X-ray data observables (cell parameters and atomic positions) of both $\mathbf{1}_{cryst,LS}$ and $\mathbf{1}_{cryst,HS}$ at 1 bar of pressure along with the corresponding $T_{1/2}$ value (*abrupt* $T_{1/2}\uparrow$ from ref[8]). Tests on U_{eff} values for Co, N, C, O, and H atoms were performed with revPBE functional[9] with rVV10[10-11] as non-local VdW correlation functional. The exact reproduction of the average $T_{1/2}$ value (171 K) for the *abrupt* component of the *SCO* at 1 bar proved be very sensitive to the U_{eff} values chosen for the *d* orbitals of the cobalt ion (Co(*d*)) whilst the reproduction of the crystallographic parameters was needed to tune the U_{eff} on the *p*-orbitals on the nitrogen atoms (N(*p*); Table S2-S3). In such a framework, the best computational set up was achieved with U_{eff}(Co(*d*)) = 1.15 *eV* and U_{eff}(N(*p*)) = 3.0 *eV*. Cell optimisations were performed to very tight levels of convergence for the wavefunction (1.0×10^{-9} Hartree) and for the atomic forces (1.0×10^{-8} Hartree $bohr^{-1}$).

Hessian matrices were calculated and checked to ensure that no imaginary eigenvalues values were present. Being performed at the Γ point, 3*N*-3 frequencies (optical modes) were computed and used to calculate the thermodynamic quantities (see below, Tables S14-S19).

This procedure was repeated for six out the seven pressures (1800, 2100, 2500, 2900, 3900 bar) reported in ref[8] at which the experimental *SCO* activity of $\mathbf{1}_{cryst}$ was measured. For p = 4300 bar, $\mathbf{1}_{cryst,HS}$ did not reach satisfying convergence criteria. Finally, IR/Raman spectra were calculated for $\mathbf{1}_{cryst,LS}$ and $\mathbf{1}_{cryst,HS}$ in vacuum and in the charge field built over the optimised structures obtained at the end of the calculations performed with CP2K6.1 package and re-run with ORCA4.1 code,[12] using PBE functional[13] and def2-TZVPP basis sets.[14-16] Two different kind of calculations were performed: (i) re-optimising the isolated $[Co^{II}(\boldsymbol{dpzca})_2]$ ($\mathbf{1}_{iso,LS}$ and $\mathbf{1}_{iso,HS}$) molecules in vacuum and (ii) re-

optimising the structures of one [Co(***dpzca***)$_2$] molecule in a charge field (**1**$_{cf,LS}$ and **1**$_{cf,HS}$) produced by the 3x3x1 supercell obtained at the end of the cell optimisation with CP2K6.1 code for each pressure. The charge field was set by replacing each atom kind with the respective Mulliken charge at the Potential Energy (*PES)* minima; the 3x3x1 supercell was obtained by replicating the original crystalline unit cells nine times. For both **1**$_{cf,LS}$ and **1**$_{cf,HS}$*:* three times along the shorter *a-* and *c-axes* and once along the longer *b-axes*.

The effects of the cell shrinking were monitored by looking at the angular distortions within the complex, using a variety of parameters (Equations S1-S6 and Table S10); ***RMSD*** measures the average divergence between atomic position when the studied system is compared to a reference (in this study, the molecules in **1**$_{cryst,LS}$ and **1**$_{cryst,HS}$ at p = 1 bar) (Equation S1); **<D>** describes the average Co-N bond distance). **ζ** is the sum of the differences between individual Co-N bond distance *vs*. the mean Co-N bond (Equation S2);[17] **Δ** is the average of the differences between individual Co-N bond distance vs. the mean Co-N bond (Equation S3);[18] **Σ** describes the local angular deviation from the *cis* octahedral angles of 90° (Equation S4);[19] **Θ** measures the trigonal torsion, which is defined as the degree of twist from a perfect octahedron towards trigonal prismatic: it is obtained by the sum of the differences of the absolute value of all 24 unique angles (Equation S5).[20] Finally, **Ω** measures the three angles, ω, of each of the eight triangles (24 angles in total) found in a perfect octahedron (Equation S6).[21] For a perfect octahedral geometry, all the distortion parameters (**Σ**, **Θ**, **Ω**) are equal to zero. **<D>**, **ζ**, **Δ**, **Σ**, **Θ**, were calculated using OctaDist 2.6.1 software;[22] ***RMSD*** was calculated using VMD software.[23]

2. Computational Protocol Validation

1.1. U_{eff} Tuning in Geometry Optimisation Procedure

Calculated curves for geometry optimisation performed on crystalline **1**$_{cry}$ at different values of U_{eff}(Co(*d*)) are reported in Figure S2. U_{eff}(Co(*d*)) range spreads from 3.0 *eV* (not reported in Figure S2 as $\Delta H_{el,HS-LS} < 0$ *eV*; detail in Table S1) to 1.5 *eV*. For ΔU_{eff}(Co(*d*) = 1.5 *eV*, $\Delta H_{el,HS-LS}$ change is about 3.0 *eV*; this is more than enough to change the magnetic response of **1**$_{cry}$ from physically wrong (from U_{eff} = 3.0 *eV*, $\Delta H_{el,HS-LS} < 0$ *eV*), fully *HS* (U_{eff} = 2.5 *eV*), *SCO*-active (U_{eff} = 2.375 *eV* to U_{eff} = 2.25 *eV*), almost fully *LS* before 400K (U_{eff} = 2.0 *eV*) and, finally, fully *LS* (U_{eff} = 1.5 *eV*).

Specifically, by decreasing U_{eff} magnitude of 0.125 *eV* (from U_{eff} = 2.375 *eV* to U_{eff} = 2.25 *eV*), the calculated $T_{1/2}$ rises of 200K (Table S1). The fragility of the *SCO* phenomenon should be extremely clear: even if the U_{eff} term can be used to fine-tune the $\Delta H_{el,HS-LS}$ gap, it is extremely complicated to get the exact value of experimental $T_{1/2}$; indeed, for small variation in U_{eff} magnitude, the *SCO* phenomenon shifts largely. Finally, the best value of U_{eff} to reproduce the experimental *SCO* transition of **1**$_{cry}$ was set at 2.35 *eV* ($T_{1/2}$ = 175 K, Table S1).

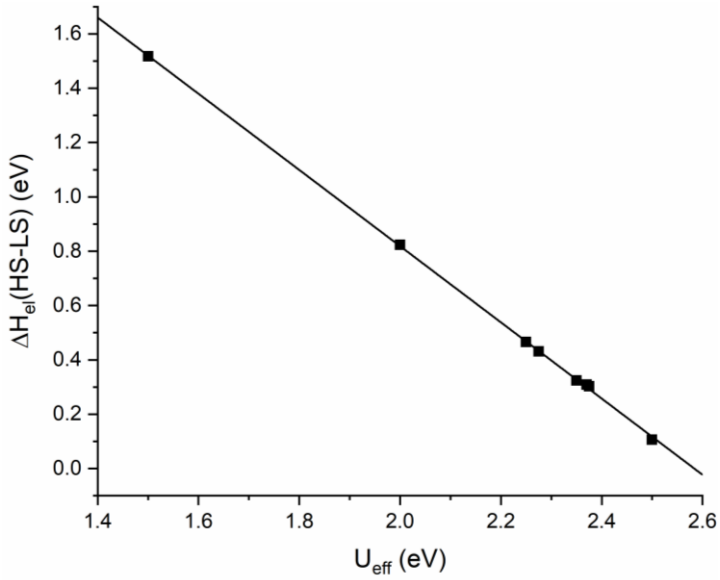

Figure S1. *Correlation line established between the applied localising potential Hubbard U (U_{eff}) to the Co^{II} d-orbitals. Reported line describes an extremely good correlation between the magnitude of the $\Delta H_{el,HS-LS}$ gap (eV) vs. the applied U_{eff} (eV).*

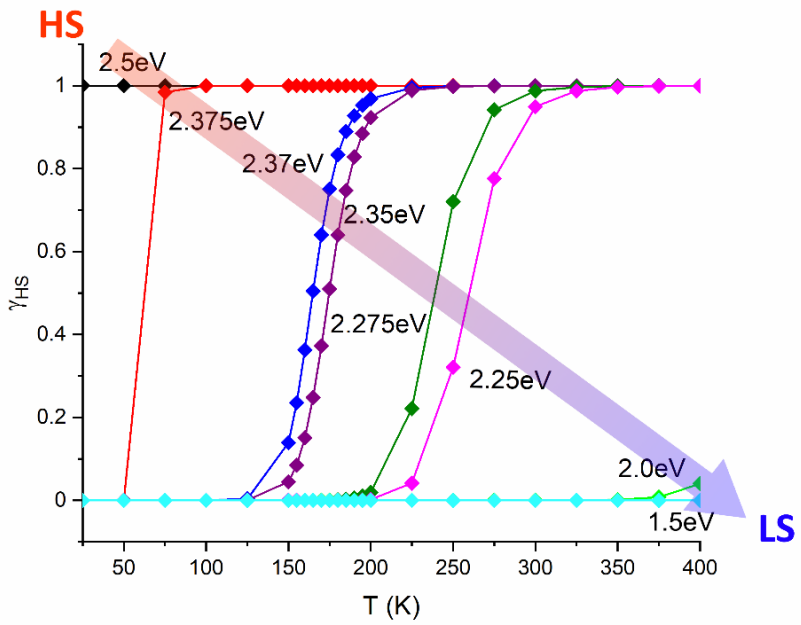

Figure S2. *Reported results of the regular SCO transition of [Co^{II}(**dpzca**)$_2$] for different values of U_{eff} (from 2.5 eV to 1.5 eV). Normal modes were calculated from a first calculation on **1**$_{cry,LS}$ and **1**$_{cry,HS}$ without applying any U_{eff}. Next, $\Delta H_{el,HS-LS}$ gap (eV) was obtained by proceed with a further step of cell optimisation by applying various U_{eff} terms at Co(d) orbitals. Colour code: U_{eff} = 2.5 eV (black), U_{eff} = 2.375 eV (red), U_{eff} = 2.37 eV (blue), U_{eff} = 2.35 eV (purple), U_{eff} = 2.275 eV (olive), U_{eff} = 2.25 eV (magenta), U_{eff} = 2.0 eV (light green), U_{eff} = 1.5 eV (light blue).*

Table S1. *Results of calculated electronic Enthalpy (H) for on* $\mathbf{1}_{cry,LS}$ *and* $\mathbf{1}_{cry,HS}$ *at different values of* U_{eff} *obtained in the protocol of geometry optimisation to the* $\Delta H_{el,HS-LS}$ *gap at the experimental* $T_{1/2}$*. In the last column on the right are reported theoretical values of* $T_{1/2}$ *at the different applied Hubbard potentials.*

U_{eff} (eV)	$H_{el,HS}$ (H)	$H_{el,LS}$ (H)	$H_{el,HS-LS}$ (H)	$\Delta H_{el,HS-LS}$ (Ev)	$T_{1/2}$ (K)
3.0	-1718.070	-1718.010	-0.059	-1.625	*HS*
2.5	-1716.936	-1716.940	0.003	0.105	*HS*
2.375	-1716.938	-1716.949	0.011	0.302	$50 < T_{1/2} < 75$
2.37	-1716.938	-1716.949	0.011	0.308	165
2.35	-1716.938	-1716.950	0.012	0.324	175
2.275	-1716.939	-1716.955	0.015	0.430	$225 < T_{1/2} < 250$
2.25	-1716.939	-1716.957	0.017	0.465	$250 < T_{1/2} < 275$
2	-1716.944	-1716.974	0.030	0.823	$T_{1/2} > 400$
1.5	-1716.957	-1717.013	0.056	1.517	*LS*

1.2. U_{eff} Tuning for Cell Parameters in Cell Optimisation Procedure

Table S2. *Final cell parameters obtained in the protocol validation step of applying further* U_{eff} *for improving the emulation of on* $\mathbf{1}_{cry,HS}$ *at pressure 1 bar.*

LS	***Cell Parameters***						***U_{eff}***				
	a /Å	***b /Å***	***c /Å***	***α /°***	***β /°***	***γ /°***	***Co(d)***	***N(p)***	***O(p)***	***C(p)***	***H(s)***
EXP	**8.668**	**27.656**	**8.514**	**90.00**	**91.52**	**90.00**	**-**	**-**	**-**	**-**	**-**
	8.578	27.275	8.167	90.03	91.33	90.12	1.6	0	0	0	0
	8.577	27.276	8.168	90.03	91.38	90.10	1.75	0	0	0	0
	8.576	27.279	8.168	90.03	91.39	90.10	1.8	0	0	0	0
	8.575	27.286	8.169	90.05	91.42	90.12	1.875	0	0	0	0
	8.566	27.289	8.175	90.09	91.47	90.07	1.9	0	0	0	0
	8.575	27.237	8.186	90.00	91.48	90.23	1.65	1	0	0	0
	8.573	27.25	8.186	89.95	91.27	90.22	1.65	1.5	0	0	0
	8.569	27.238	8.197	89.96	91.19	90.23	1.65	2	0	0	0
	8.375	27.532	8.367	89.93	90.78	90.04	1.65	3	0	0	0
	8.566	27.243	8.200	89.97	91.15	90.25	1.65	2	0	0	0
	8.556	**8.555**	**27.342**	**89.98**	**90.07**	**89.97**	**1.15**	**3**	**0**	**0**	**0**
	8.375	27.532	8.367	89.94	90.77	90.04	1.65	3	0	0	0
	8.574	27.155	8.184	90.02	91.60	90.19	1.65	2	0	2	0
	8.38	27.561	8.386	89.96	90.76	89.92	2	3	0	2	0
	8.382	27.581	8.393	89.99	90.77	89.89	2	3	0	3	0

Table S3. *Final cell parameters obtained in the protocol validation step of applying further* U_{eff} *for improving the emulation of* $\mathbf{1}_{cry,LS}$ *at pressure 1 bar.*

HS	***Cell Parameters***						***U_{eff}***				
	a /Å	***b /Å***	***c /Å***	***α /°***	***β /°***	***γ /°***	***Co(d)***	***N(p)***	***O(p)***	***C(p)***	***H(s)***
EXP	**8.795**	**8.795**	**27.918**	**90.00**	**90.00**	**90.00**	**-**	**-**	**-**	**-**	**-**
	8.590	8.556	26.982	90.20	90.08	90.16	1.6	0	0	0	0
	8.586	8.553	29.963	90.19	90.07	90.15	1.75	0	0	0	0
	8.618	8.629	27.406	90.04	90.00	89.95	1.8	0	0	0	0
	8.656	8.665	27.536	90.03	90.00	89.97	1.875	0	0	0	0
	8.665	8.676	27.566	90.03	90.00	89.97	1.9	0	0	0	0
	8.590	8.569	26.991	90.24	90.19	90.10	1.65	1	0	0	0
	8.589	8.563	27.001	90.23	90.19	90.13	1.65	1.5	0	0	0
	8.567	8.567	27.046	90.18	90.38	89.99	1.65	2	0	0	0
	8.572	8.571	27.399	89.96	90.10	90.01	1.65	3	0	0	0
	8.584	8.561	26.967	90.24	90.19	90.11	1.65	2	0	2	0
	8.300	**27.355**	**8.282**	**89.86**	**90.84**	**89.73**	**1.15**	**3**	**0**	**0**	**0**
	8.586	8.585	27.369	89.98	90.05	90.01	2	3	0	2	0
	8.592	8.591	27.382	89.98	90.05	90.01	2	3	0	3	0
	8.615	8.610	27.086	89.99	90.01	90.02	2	3	3	3	1
	8.607	8.613	27.191	89.91	90.18	89.92	2	3	0	3	1

1.3. U_{eff}(Co(*d*)) Tuning in Cell Optimisation Procedure

Table S4. *Results of calculated electronic Enthalpy (H) for on* $\mathbf{1}_{cry,LS}$ *and* $\mathbf{1}_{cry,HS}$ *at different values of* U_{eff} *obtained in the protocol of cell optimisation to the* $\Delta H_{el,HS-LS}$ *gap at the experimental* $T_{1/2}$*. In the last column on the right are reported theoretical values of* $T_{1/2}$ *at the different applied Hubbard potentials.*

U_{eff} / eV	$H_{el,HS}$ / H	$H_{el,LS}$ / H	$H_{el,HS-LS}$ / H	$\Delta H_{el,HS-LS}$ / eV	$T_{1/2}$ (K)
2.35	-1716.96	-1716.95	-0.013	-0.361	*HS*
1.75	-1713.68	-1713.66	-0.013	-0.348	*HS*
1.25	-1713.70	-1713.71	0.014	+0.373	75 < $\mathbf{T_{1/2}}$ < 100
1.15	-1713.70	-1713.71	0.012	+0.322	175
1.00	-1713.71	-1713.72	0.019	+0.526	275 < $\mathbf{T_{1/2}}$ < 300
0.75	-1713.72	-1713.75	0.030	+0.813	$\mathbf{T_{1/2}}$ > 400
0.50	-1713.72	-1713.77	0.044	+1.199	*LS*
0.25	-1713.73	-1713.79	0.058	+1.571	*LS*
0.00	-1713.75	-1713.81	0.069	+1.881	*LS*

Table S5. *Error analysis of divergence between the calculated and the experimental unit cell parameters at the available pressures of 1 bar (*$\mathbf{1}_{cry,HS,1bar}$ *and* $\mathbf{1}_{cry,LS,1bar}$*) and 4300 bar (*$\mathbf{1}_{cry,LS,4300bar}$*). Note that each calculation is performed at the absolute temperature of 0 K. 1 bar = 10*$^{-4}$ *Pa.*

Cell Param.	$\mathbf{1}_{cry,HS}$			$\mathbf{1}_{cry,LS}$		
	1 bar			1 bar		4300 bar
	Exp.	Calc.	%	Exp.	Calc.	%
a /Å	8.795	8.556	-2.7%	8.668	8.366	-3.5%
b /Å	8.795	8.555	-2.7%	27.656	27.536	-0.4%
c /Å	27.918	27.342	-2.1%	8.514	8.357	-1.8%
α /°	90.00	89.979	-0.1%	90.00	89.971	-0.1%
β /°	90.00	90.065	+0.1%	91.52	90.925	-0.7%
γ /°	90.00	89.969	-0.1%	90.00	89.901	-0.1%
Av. Error	-	-	1.3%			1.1%

2. Additional Structural Data

$$RMSD = \sqrt{\frac{1}{n}\sum_{i=1}^{n}((v_{ix} - w_{ix})^2 + \left(v_{iy} - w_{iy}\right)^2 + (v_{iz} - w_{iz})^2)} \qquad \text{(Eq. S1)}$$

$$\zeta = \sum_{i=1}^{6} |d_i - d_{mean}| \qquad \text{(Eq. S2)}$$

$$\Delta = \frac{1}{6}\sum_{i=1}^{6}\left(\frac{|d_i - d_{mean}|}{d_{mean}}\right)^2 \qquad \text{(Eq. S3)}$$

$$\Sigma = \sum_{i=1}^{12} |90 - \phi_i| \qquad \text{(Eq. S4)}$$

$$\Theta = \sum_{i=1}^{24} |90 - \theta_i| \qquad \text{(Eq. S5)}$$

$$\Omega = \sum_{i=1}^{24} |60 - \omega_i| \qquad \text{(Eq. S6)}$$

Table S6. *Reported variation in the cell volume for on* ***1****cry,LS* *and* ***1****cry,HS* *at different pressures. Reference system is considered at the external pressure of 1 bar. Results are reported in Å³.*

p / bar	*HS* / Å³	*LS* / Å³	% *HS*	% *LS*
1	2001.27	1925.80	-	-
1800	1978.99	1906.64	-22.28 (-1.11%)	-46.16 (-2.36%)
2100	1974.65	1903.71	-26.62 (-1.33%)	-49.09 (-2.51%)
2500	1970.41	1899.97	-30.86 (-1.54%)	-52.83 (-1.54%)
2900	1960.62	1893.81	-40.65 (-2.03%)	-58.99 (-3.02%)
3900	1970.20	1862.75	-31.07 (-1.55%)	-90.05 (-4.61%)
4300	1965.55	1897.99	-35.72 (-1.78%)	-54.81 (-2.81%)

Table S7. *Reported correlation factor in the analysis of the variation of the structural parameters of the unit cell for on* ***1****cry,LS* *and* ***1****cry,HS* *versus the seven different pressures (and related experimental* $T_{1/2}$*).*

		R^2 (pressure)	R^2 ($T_{1/2}$(exp.))
1cry,*LS*	**a** / **Å**	0.47 (Fig. S3)	0.41 (Fig. S4)
	b / **Å**	0.54 (Fig. S5)	0.64 (Fig. S6)
	c / **Å**	0.63 (Fig. S7)	0.13 (Fig. S8)
	α / **°**	0.74 (Fig. S9)	0.77 (Fig. S10)
	β / **°**	0.64 (Fig. S11)	0.70 (Fig. S12)
	γ / **°**	0.39 (Fig. S13)	0.36 (Fig. S14)
1cry,*HS*	**a** / **Å**	0.71 (Fig. S15)	0.49 (Fig. S16)
	b / **Å**	0.59 (Fig. S17)	0.58 (Fig. S18)
	c / **Å**	0.93 (Fig. S19)	0.86 (Fig. S20)
	α / **°**	0.20 (Fig. S21)	0.23 (Fig. S22)
	β / **°**	0.23 (Fig. S23)	0.25 (Fig. S24)
	γ / **°**	0.20 (Fig. S25)	0.21 (Fig. S26)

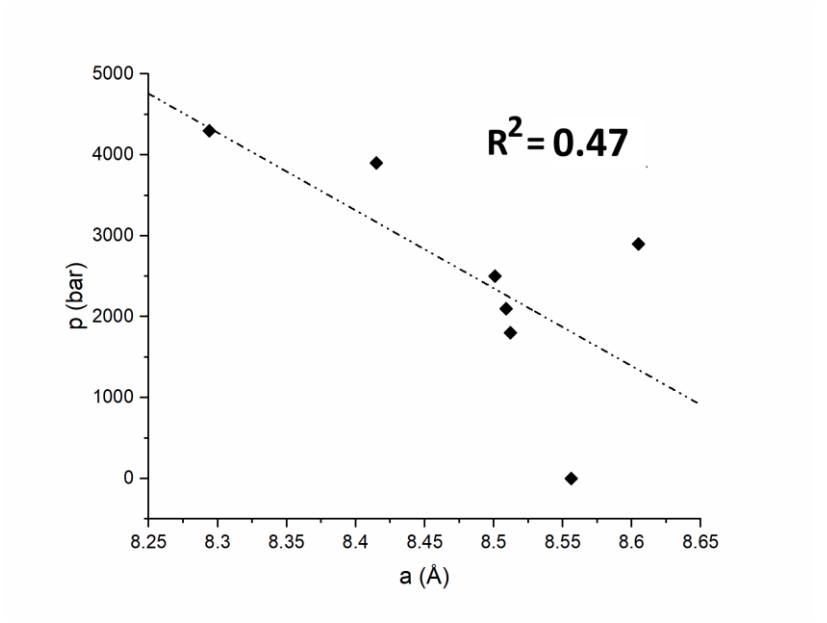

Figure S3. *Reported correlation factor R^2 for the variation of the length of the a-axis of* ***1****$_{cry,LS}$ at the pressure increase (R^2 = 0.47).*

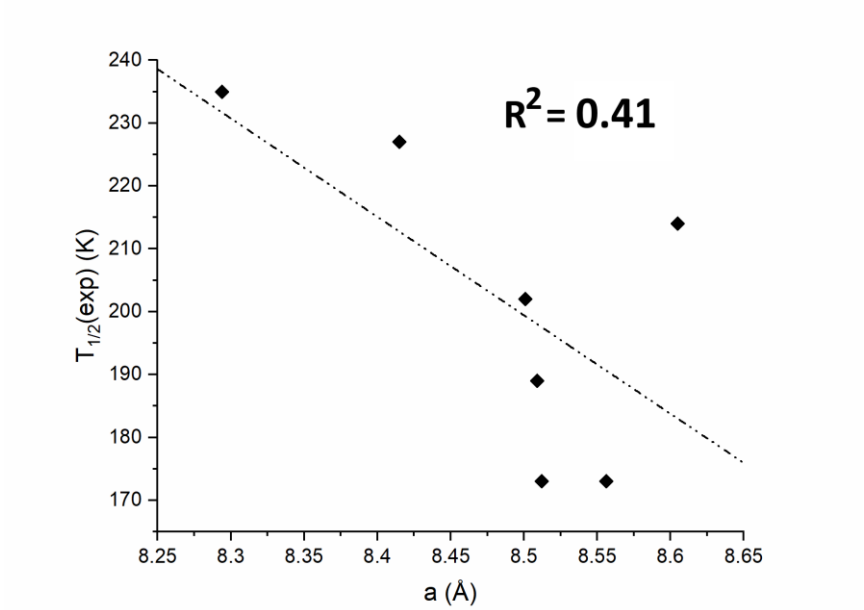

Figure S4. *Reported correlation factor R^2 for the variation of the length of the a-axis of* ***1****$_{cry,LS}$ at the increase of the measured $T_{1/2}$ (R^2 = 0.41).*

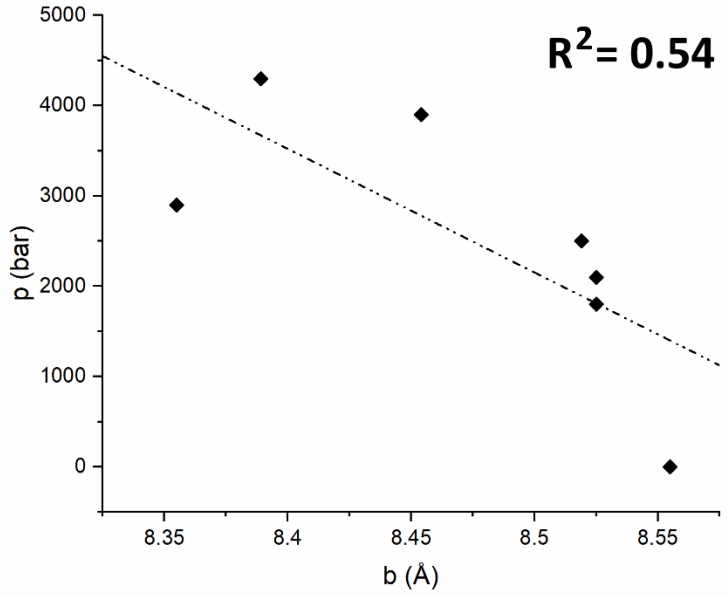

Figure S5. *Reported correlation factor R^2 for the variation of the length of the b-axis of* ***1****$_{cry,LS}$ at the pressure increase (R^2 = 0.54).*

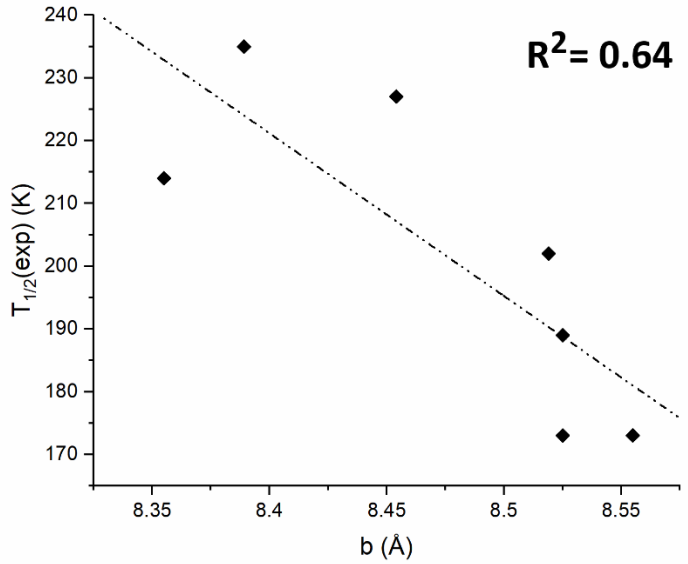

Figure S6. *Reported correlation factor R^2 for the variation of the length of the b-axis of* ***1****$_{cry,LS}$ at the increase of the measured $T_{1/2}$ (R^2 = 0.64).*

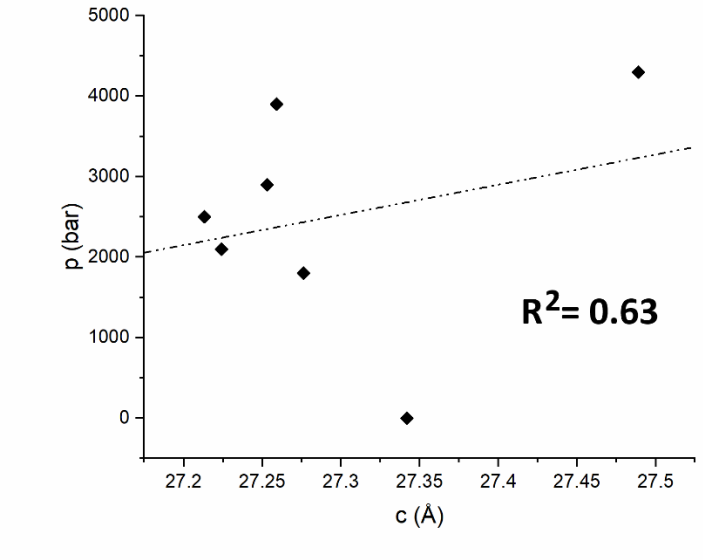

Figure S7. *Reported correlation factor R^2 for the variation of the length of the c-axis of* ***1****$_{cry,LS}$ at the pressure increase (R^2 = 0.63).*

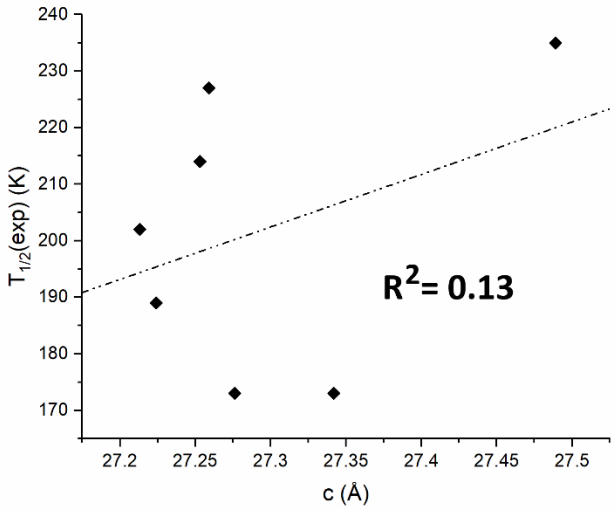

Figure S8. *Reported correlation factor R^2 for the variation of the length of the c-axis of* ***1****$_{cry,LS}$ at the increase of the measured $T_{1/2}$ (R^2 = 0.13).*

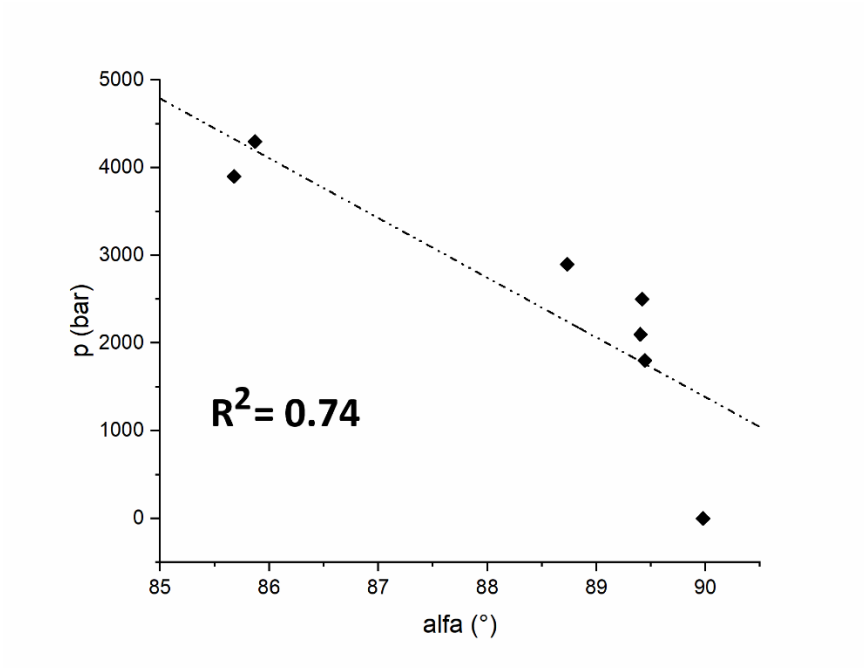

Figure S9. *Reported correlation factor R^2 for the variation of the magnitude of the α angle of* ***1****$_{cry,LS}$ at the pressure increase (R^2 = 0.74).*

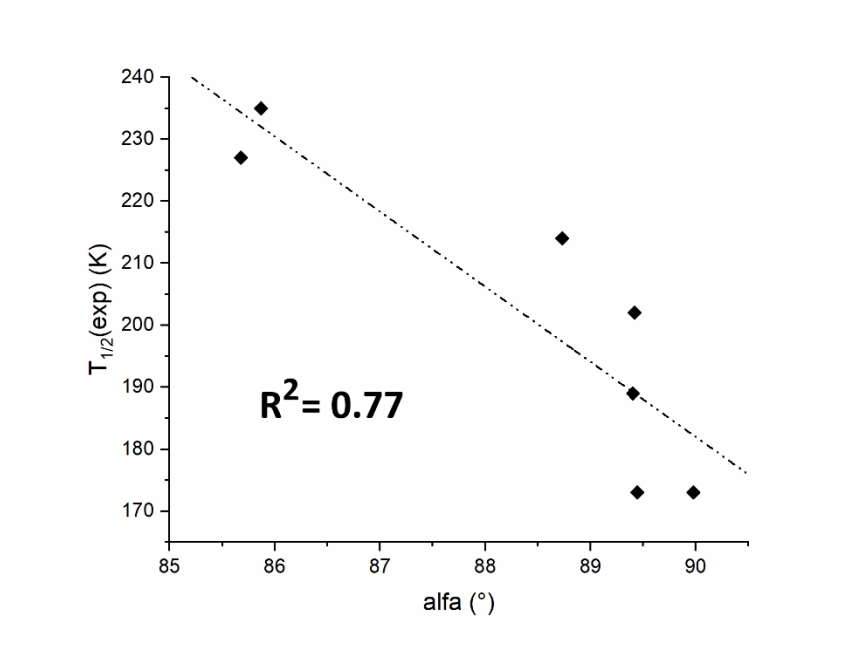

Figure S10. *Reported correlation factor R^2 for the variation of the magnitude of the α angle of* ***1****$_{cry,LS}$ at the increase of the measured $T_{1/2}$ (R^2 = 0.70).*

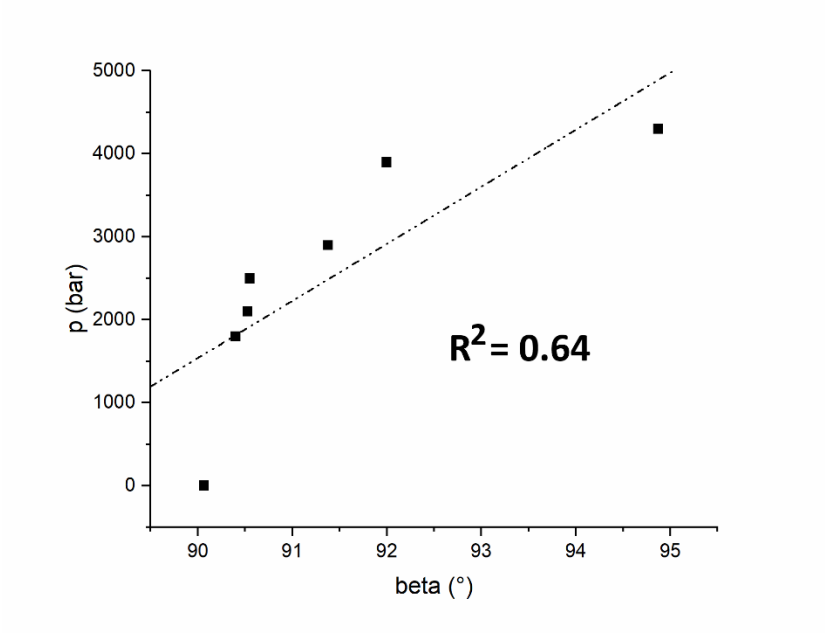

Figure S11. *Reported correlation factor R^2 for the variation of the magnitude of the β angle of* ***1****$_{cry,LS}$ at the pressure increase (R^2 = 0.64).*

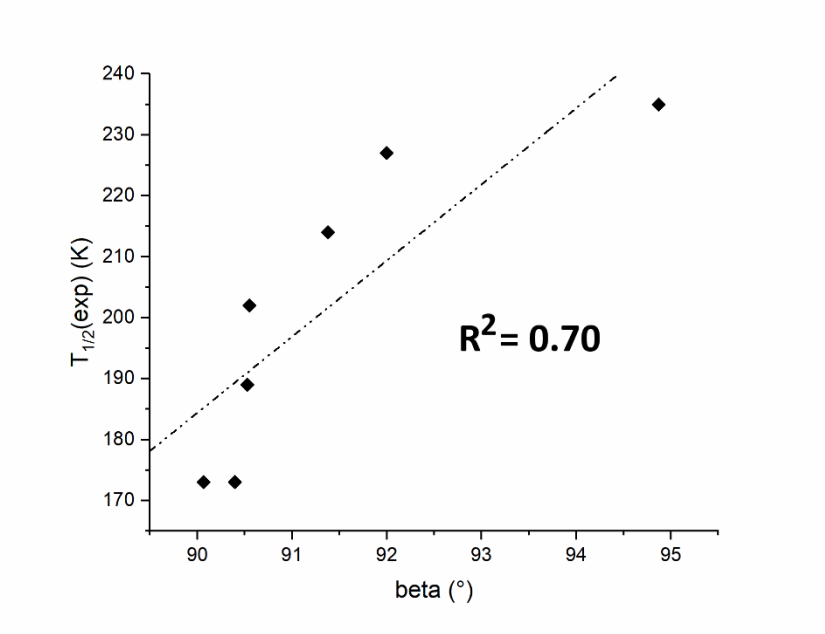

Figure S12. *Reported correlation factor R^2 for the variation of the magnitude of the β angle of* ***1****$_{cry,LS}$ at the increase of the measured $T_{1/2}$ (R^2 = 0.70).*

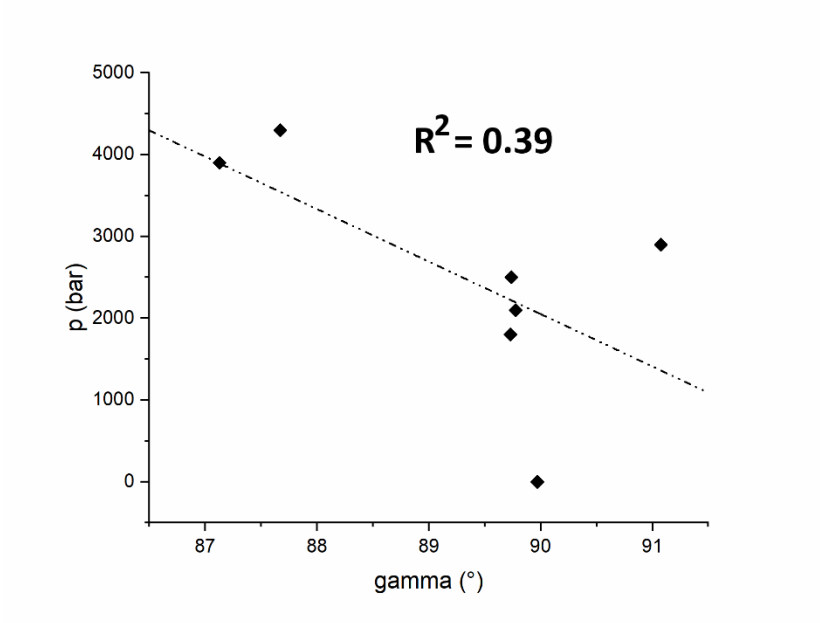

Figure S13. *Reported correlation factor R^2 for of the variation of the magnitude of the γ angle of* ***1****$_{cry,LS}$ at the pressure increase (R^2 = 0.39).*

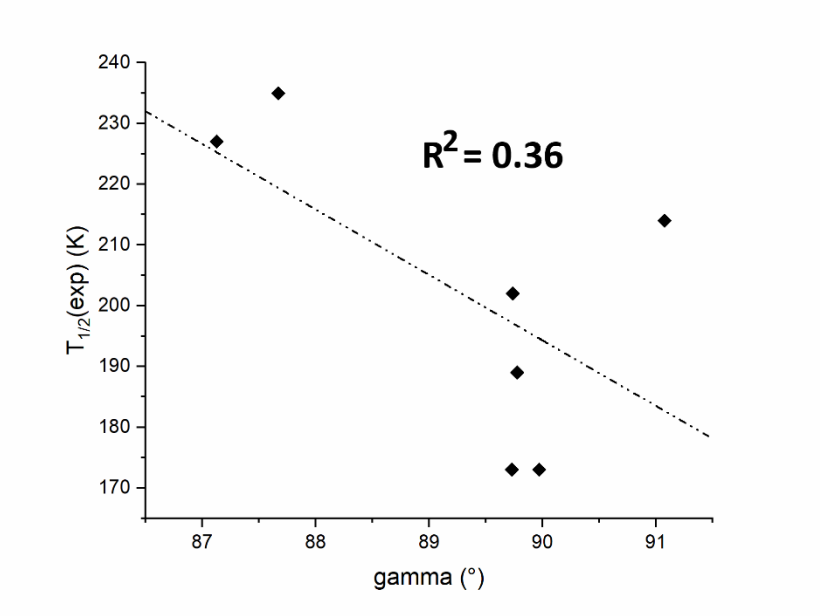

Figure S14. *Reported correlation factor R^2 for the variation of the magnitude of the γ angle of* ***1****$_{cry,LS}$ at the increase of the measured $T_{1/2}$ (R^2 = 0.36).*

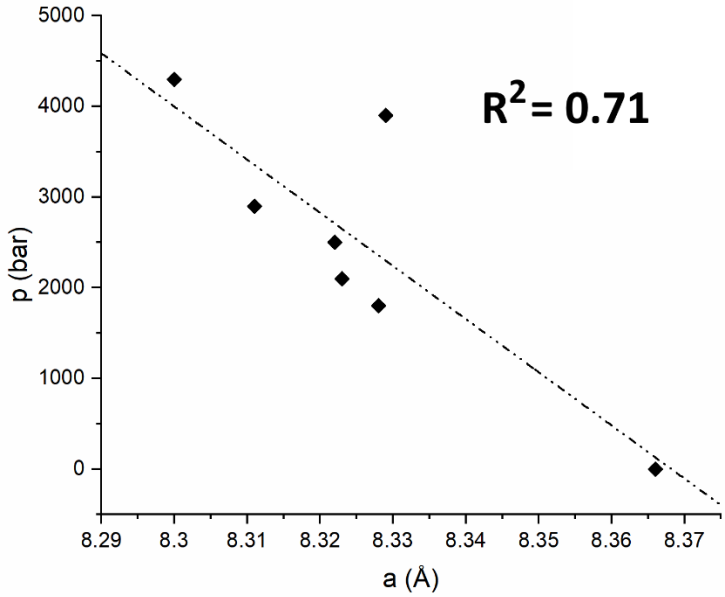

Figure S15. *Reported correlation factor R^2 for the variation of the length of the a-axis of* ***1****$_{cry,HS}$ at the pressure increase (R^2 = 0.71).*

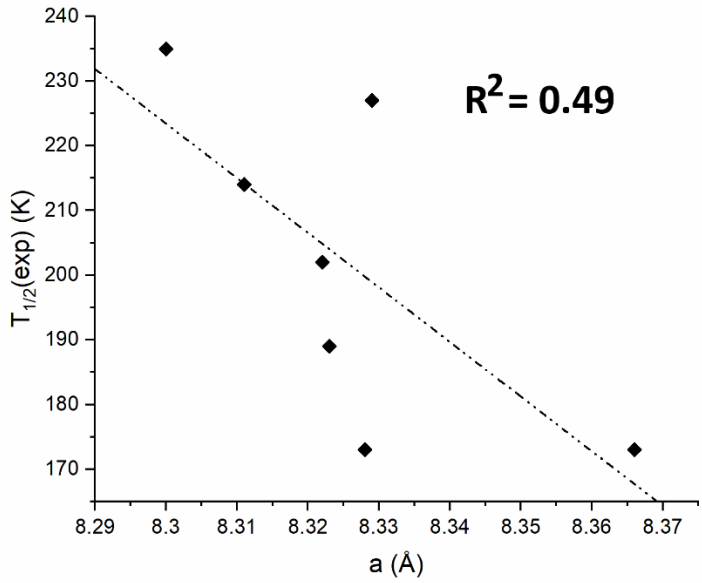

Figure S16. *Reported correlation factor R^2 for the variation of the length of the a-axis of* ***1****$_{cry,HS}$ at the increase of the measured $T_{1/2}$ (R^2 = 0.49).*

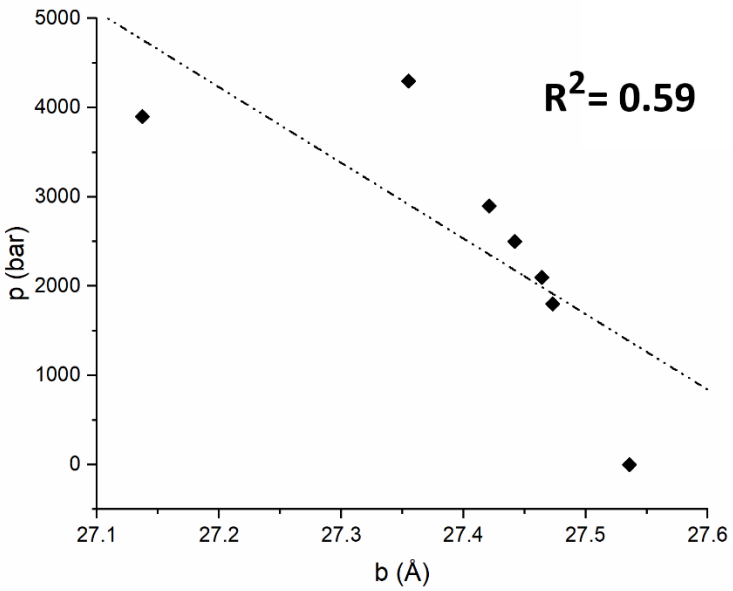

Figure S17. *Reported correlation factor R^2 for the variation of the length of the b-axis of* ***1****$_{cry,HS}$ at the pressure increase (R^2 = 0.59).*

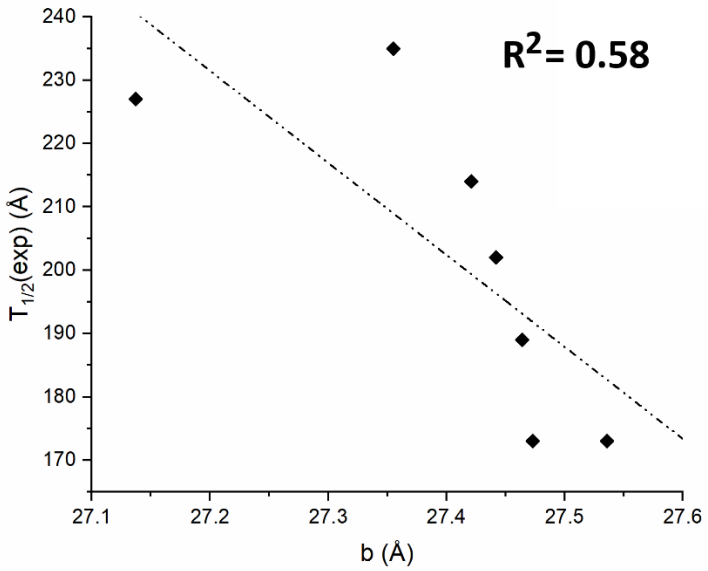

Figure S18. *Reported correlation factor R^2 for the variation of the length of the b-axis of* ***1****$_{cry,HS}$ at the increase of the measured $T_{1/2}$ (R^2 = 0.58).*

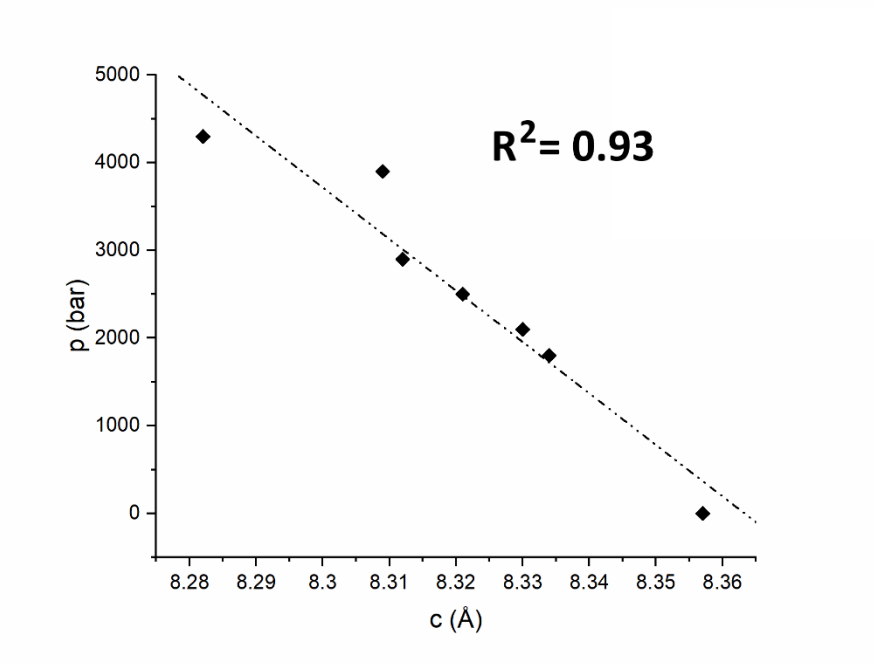

Figure S19. *Reported correlation factor R^2 for of the variation of the length of the c-axis of* ***1****$_{cry,HS}$ at the pressure increase (R^2 = 0.93).*

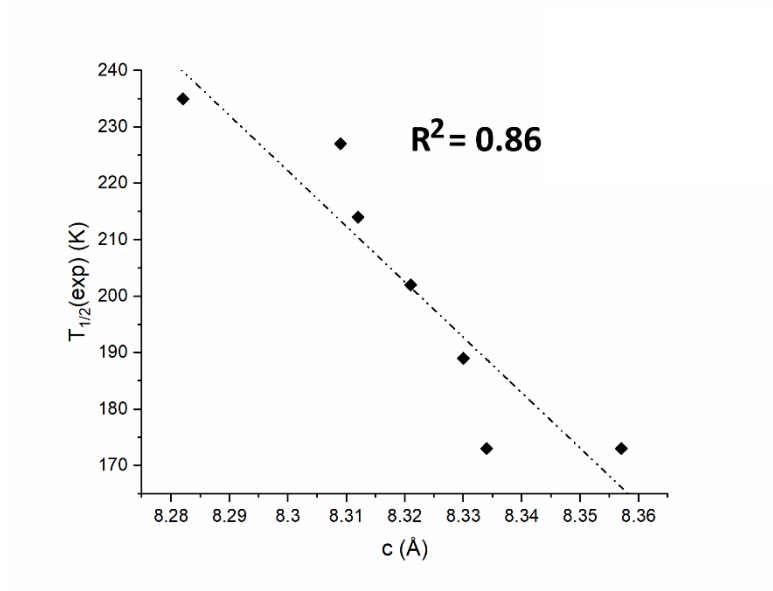

Figure S20. *Reported correlation factor R^2 for the variation of the length of the c-axis of* ***1****$_{cry,HS}$ at the increase of the measured $T_{1/2}$* (R^2 = 0.86).

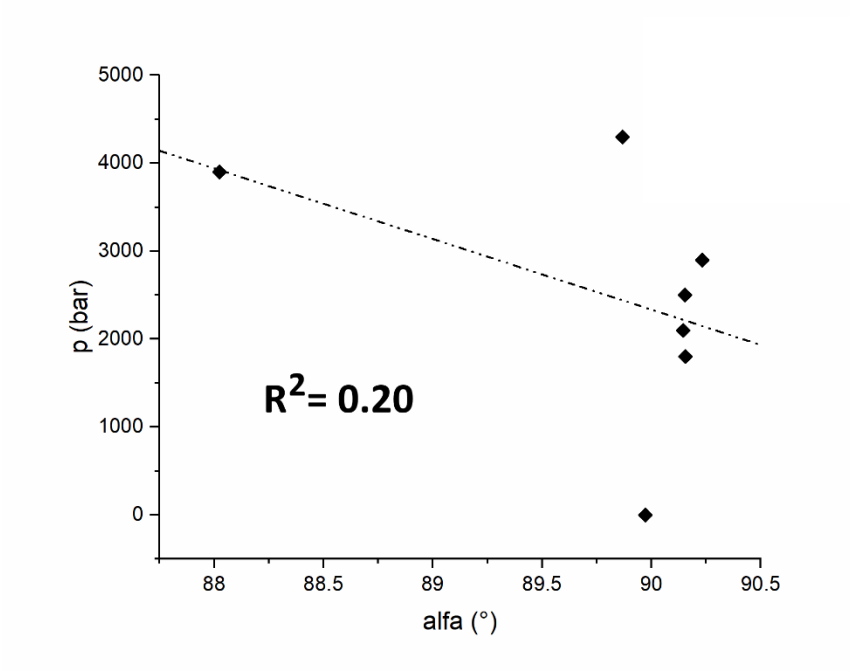

Figure S21. *Reported correlation factor R^2 for the variation of the magnitude of the α angle of* ***1****$_{cry,HS}$ at the pressure increase (R^2 = 0.20).*

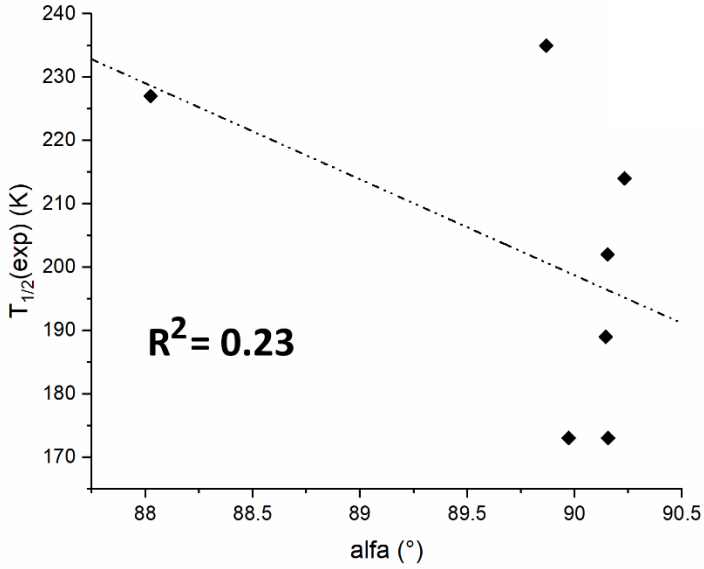

Figure S22. *Reported correlation factor R^2 for the variation of the magnitude of the α angle of* ***1****$_{cry,HS}$ at the increase of the measured $T_{1/2}$ (R^2 = 0.23).*

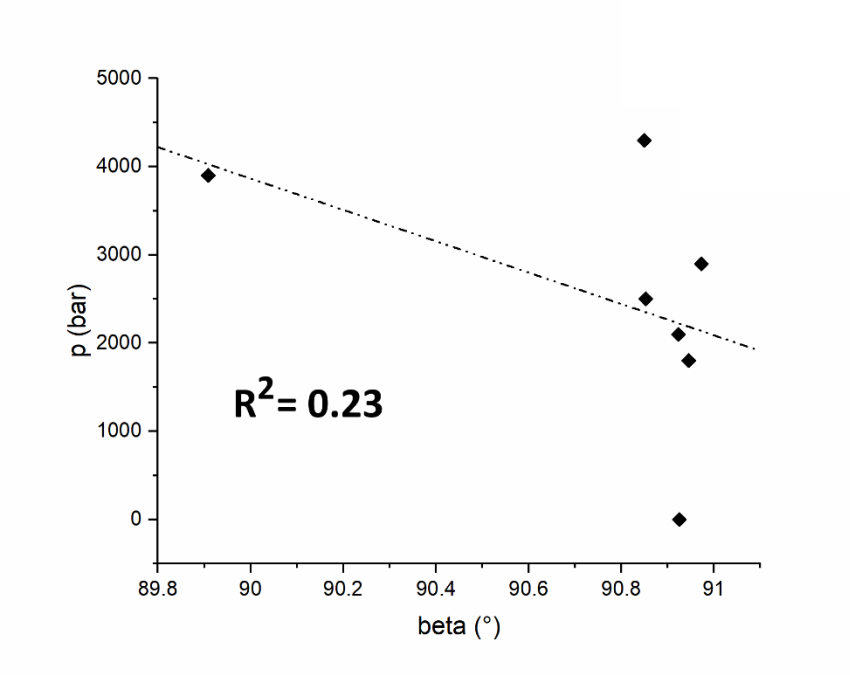

Figure S23. *Reported correlation factor R^2 for the variation of the magnitude of the β angle of* ***1****$_{cry,HS}$ at the pressure increase (R^2 = 0.23).*

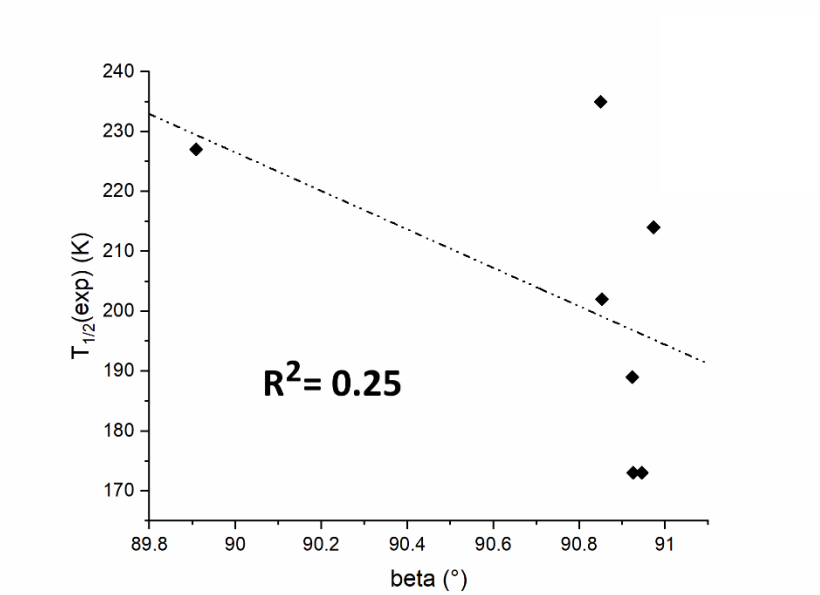

Figure S24. *Reported correlation factor R^2 for the variation of the magnitude of the β angle of* ***1****$_{cry,HS}$ at the increase of the measured $T_{1/2}$ (R^2 = 0.25).*

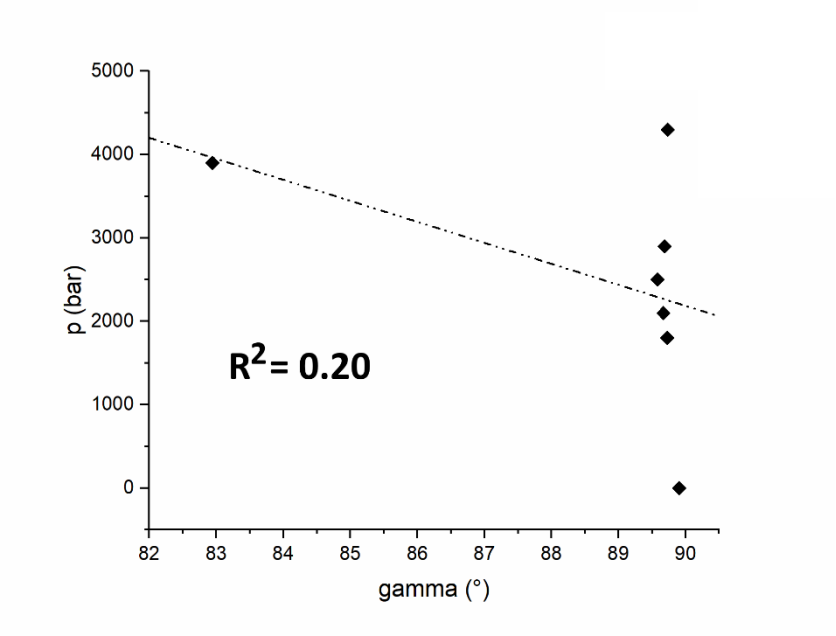

Figure S25. *Reported correlation factor R^2 for the variation of the magnitude of the γ angle of* ***1****$_{cry,HS}$ at the pressure increase (R^2 = 0.20).*

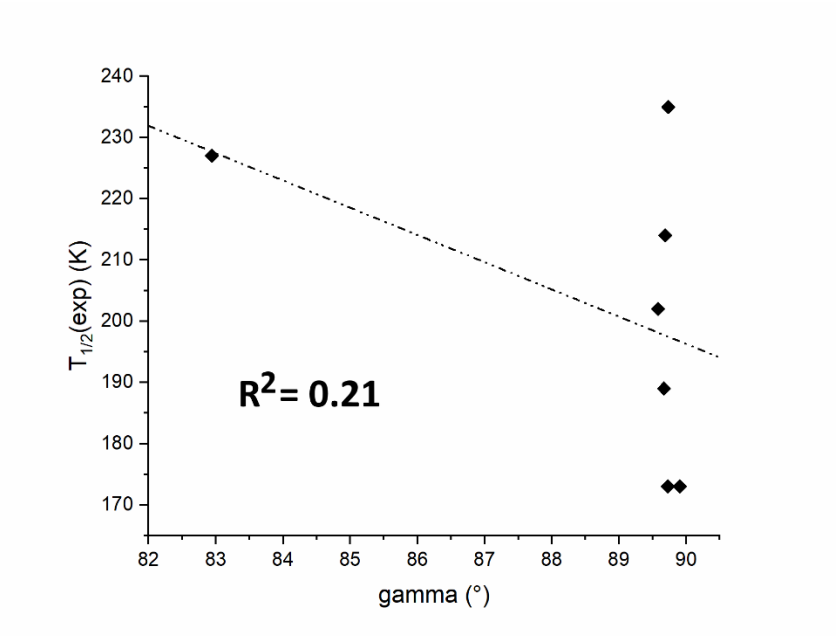

Figure S26. *Reported correlation factor R^2 for the variation of the magnitude of the γ angle of* ***1****$_{cry,HS}$ at the increase of the measured $T_{1/2}$ (R^2 = 0.21).*

2.1. Structural Distortions vs. Pressure

Table S8. *Reported variation of structural parameters (internal to [Co(**dpzca**)$_2$]: Co-N bond length and Σ octahedral distortion and external: Co-Co intermolecular distance) obtained after procedure of cell optimisation for* ***1$_{cry,LS}$*** *at different pressures.*

LS	**Cell Parameters**		
pressure	**Co1-Co2 / Å**	**Co2-Co3 / Å**	**Co3-Co4 / Å**
1	8.177	10.540	8.176
1800	8.171	10.500	8.161
2100	8.167	10.499	8.157
2500	8.161	10.498	8.152
2900	8.127	10.464	8.154
3900	8.123	10.455	8.133
4300	8.114	10.464	8.122

Table S9. *Reported variation of structural parameters (internal to [Co(**dpzca**)$_2$]: Co-N bond length and Σ octahedral distortion and external: Co-Co intermolecular distance) obtained after procedure of cell optimisation for* ***1$_{cry,HS}$*** *at different pressures.*

HS	**Cell Parameters**		
pressure	**Co1-Co2 / Å**	**Co2-Co3 / Å**	**Co3-Co4 / Å**
1	8.057	8.064	8.070
1800	8.013	8.072	8.062
2100	7.987	8.059	8.056
2500	7.991	8.061	8.066
2900	8.029	8.018	8.200
3900	8.028	8.007	8.199
4300	8.028	8.007	8.199

Table S10. *Calculated structural distortion parameters for crystallographic and calculated structures (DFT) for 1cryst at different pressures (1, 1800, 2100, 2500, 2900, 3900, 4300 bar), along with the experimental $T_{1/2}$ from ref[8] and the calculated $T_{1/2}$). 1 bar = 10^{-4} Pa.*

Pressure / bar		***1***	***4300***	***1***	***1800***	***2100***	***2500***	***2900***	***3900***	***4300***	***R^2 [pressure]***	***R^2 [$T_{1/2}$(exp)]***
$T_{1/2}$ (exp) / K		***Exp. x-ray***		***173***	***173***	***189***	***202***	***214***	***218***	***235***		
$T_{1/2}$ (calc) / K				***171***	***164***	***190***	***173***	***LS***	***LS***	***-***		
$1_{cryst,LS}$	***RMSD / Å***	-	-	-	0.03221	0.04415	0.05004	0.06016	0.06482	0.07082	**0.92** (Fig. 6)	**0.98** (Fig. 6)
	<D> / Å	2.03444	2.0505	1.98033	1.97843	1.98299	1.97794	1.97733	1.97365	1.97700	0.43 (Fig. S27)	0.38 (Fig. S33)
	ζ / Å	0.63404	0.4964	0.26140	0.25693	0.26407	0.25610	0.25331	0.23631	0.25671	0.34 (Fig. S28)	0.24 (Fig. S34)
	Δ (geom.)	0.00318	0.0020	0.00057	0.00054	0.00066	0.00054	0.00053	0.00049	0.00057	0.07 (Fig. S29)	0.09 (Fig. S35)
	Σ / °	76.0830	89.8708	69.3796	69.3845	70.5836	69.4735	69.5518	68.0682	69.199	0.17 (Fig. S30)	0.15 (Fig. S36)
	Θ / °	271.161	306.325	230.475	230.731	235.439	231.269	231.510	221.259	231.135	0.13 (Fig. S31)	0.09 (Fig. S37)
	Ω / °	127.36	143.16	126.84	119.64	130.00	126.68	126.80	117.28	127.00	0.06 (Fig. S32)	1.3E-8 (Fig. S38)
$1_{cryst,HS}$	***RMSD / Å***	-	-	-	0.04131	0.05112	0.05195	0.13196	0.25527	0.33967	**0.95** (Fig. 6)	**0.78** (Fig. 6)
	<D> / Å	2.11373	-	2.08150	2.07902	2.07916	2.07866	2.07788	2.07954	2.07784	0.58 (Fig. S27)	0.45 (Fig. S33)
	ζ / Å	0.25709	-	0.13399	0.13028	0.13310	0.13233	0.12746	0.13108	0.13081	0.26 (Fig. S28)	0.21 (Fig. S34)
	Δ (geom.)	0.00046	-	0.00021	0.00020	0.00021	0.00021	0.00021	0.00021	0.00020	0.01 (Fig. S29)	0.01 (Fig. S38)
	Σ / °	110.620	-	104.228	103.785	104.296	104.171	103.966	104.442	104.045	0.01 (Fig. S30)	0.03 (Fig. S36)
	Θ / °	344.334	-	335.121	334.596	336.809	336.455	338.072	336.264	336.287	0.22 (Fig. S31)	0.36 (Fig. S37)
	Ω / °	164.74	-	169.49	169.64	171.44	171.12	173.96	167.16	171.92	0.01 (Fig. S32)	0.07 (Fig. S38)
$1_{cryst,LS-HS}$	***ΔRMSD/Å***	-	-	9.60	9.61	9.63	9.59	9.58	9.56	9.63	0.02 (Fig. S42)	0.02 (Fig. S43)
	ΔΘ / °	-	-	104.6461	103.8654	101.3695	105.1858	106.5625	115.0052	105.1516	0.60 (Fig. S44)	0.22 (Fig. S45)

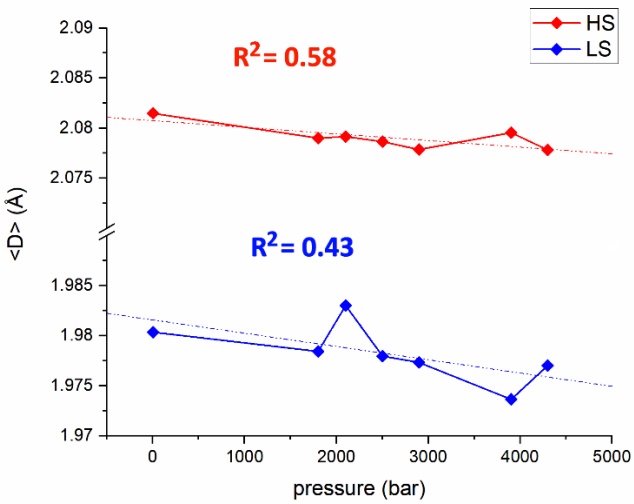

Figure S27. *Reported effects of the pressure increase vs the average* ***<D$_{Co-N}$>*** *distance. Trend line reports the correlation factor for* ***1$_{cry,HS}$*** *(red, R^2 = 0.58) and LS [Co(**dpzca**)$_2$] (blue, R^2 = 0.43).*

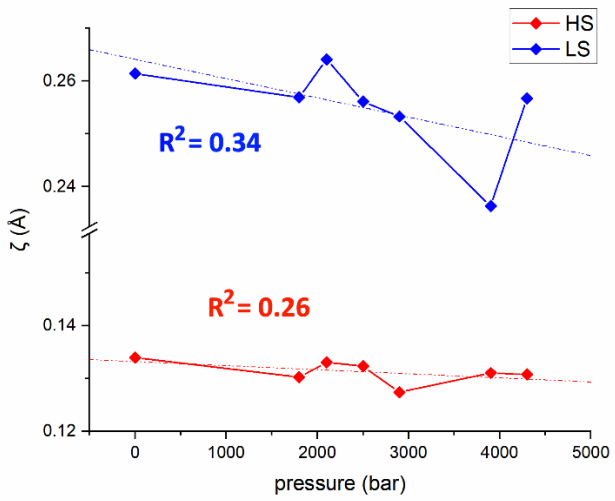

Figure S28. *Reported effects of the pressure increase vs the sum of the Co-N bond differences from <D$_{Co-N}$>,* ***ζ****. Trend line reports the correlation factor for* ***1$_{cry,HS}$*** *(red, R^2 = 0.26) and* ***1$_{cry,LS}$*** *(blue, R^2 = 0.34).*

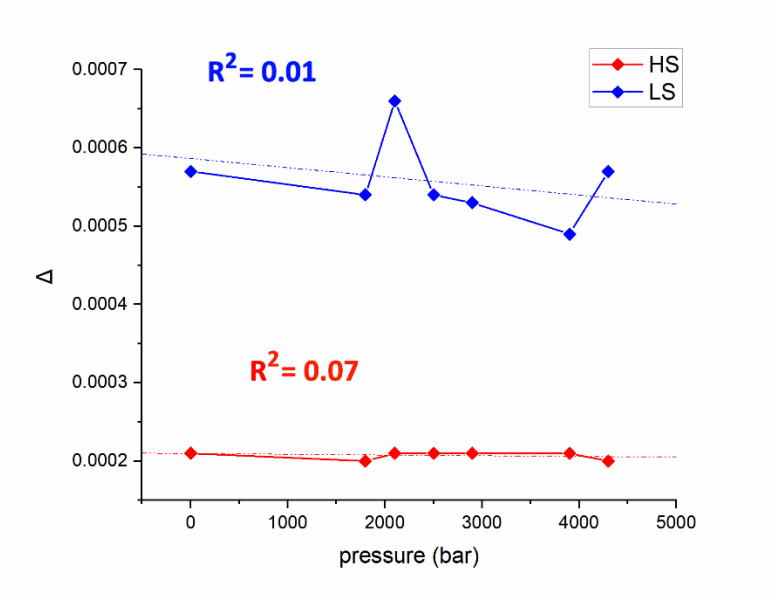

Figure S29. *Reported effects of the pressure increase vs the averaged Co-N bond deviation from <D_{Co-N}>,* ***Δ****. Trend line reports the correlation factor for* ***1****$_{cry,HS}$ (red, R^2 = 0.07) and* ***1****$_{cry,LS}$ (blue, R^2 = 0.01).*

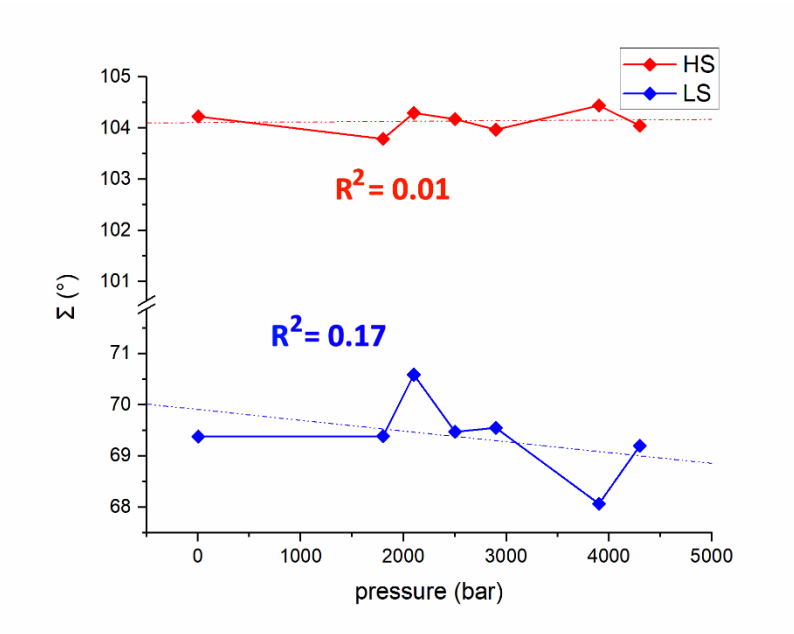

Figure S30. *Reported effects of the pressure increase vs the octahedral distortion parameter* ***Σ****. Trend line reports the correlation factor for* ***1****$_{cry,HS}$ (red, R^2 = 0.01) and* ***1****$_{cry,LS}$ (blue, R^2 = 0.17).*

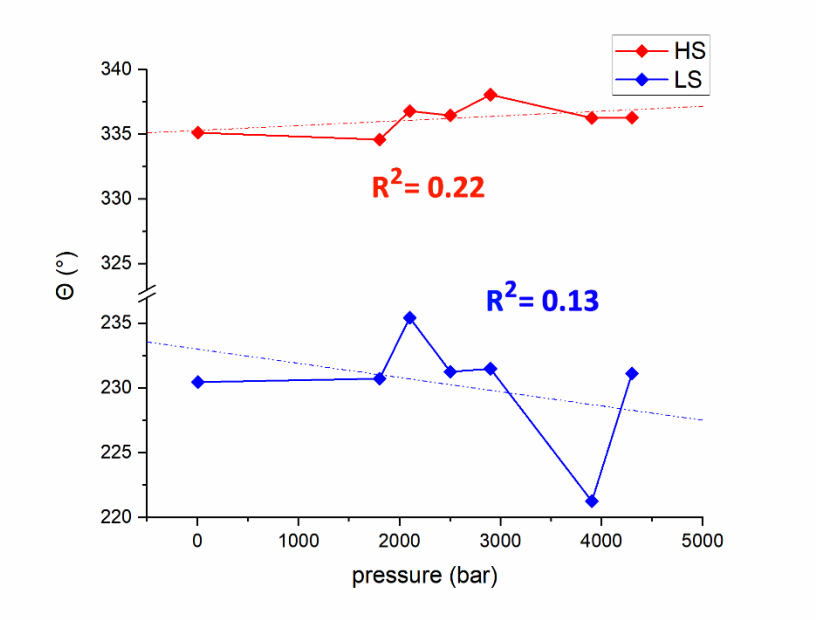

Figure S31. *Reported effects of the pressure increase vs the trigonal torsion parameter* ***Θ****. Trend line reports the correlation factor for* $\mathbf{1}_{cry,HS}$ *(red,* R^2 *= 0.22) and* $\mathbf{1}_{cry,LS}$ *(blue,* R^2 *= 0.13).*

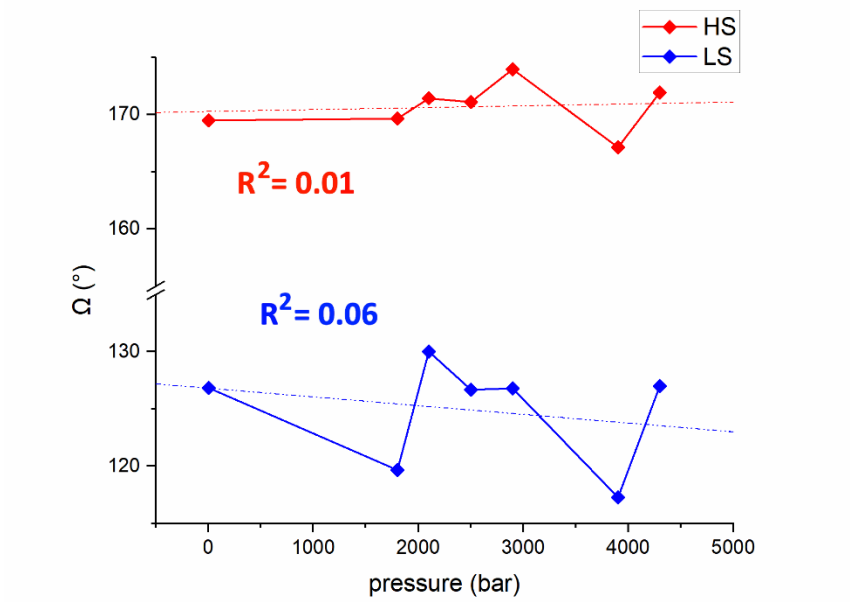

Figure S32. *Reported effects of the pressure increase vs the distortion parameter* ***Ω****. Trend line reports the correlation factor for* $\mathbf{1}_{cry,HS}$ *(red,* R^2 *= 0.01) and* $\mathbf{1}_{cry,LS}$ *(blue,* R^2 *= 0.06).*

2.2. Structural Distortions vs. Measured $T_{1/2}$

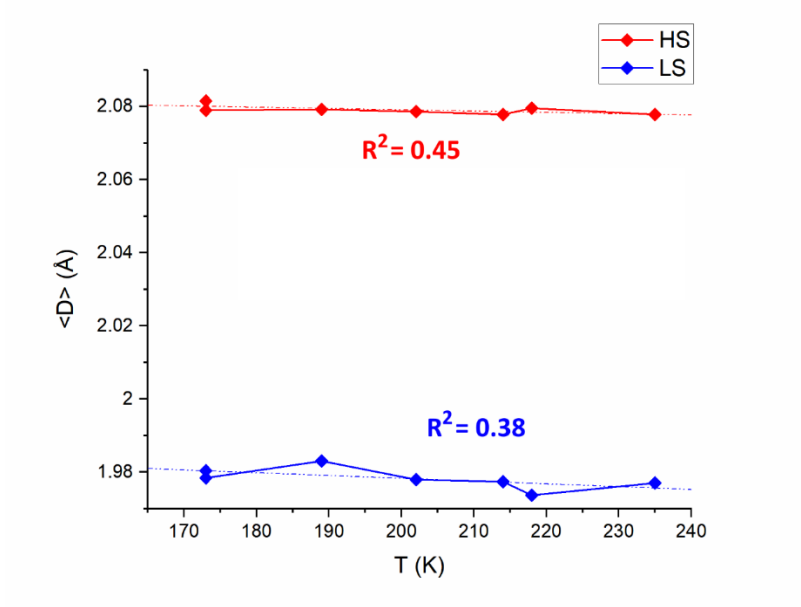

Figure S33. *Reported effects of the measured $T_{1/2}$ values at pressure increase vs the vs the average* **$<D_{Co\text{-}N}>$** *distance. Trend line reports the correlation factor for* **$1_{cry,HS}$** *(red, R^2 = 0.45) and* **$1_{cry,LS}$** *(blue, R^2 = 0.38).*

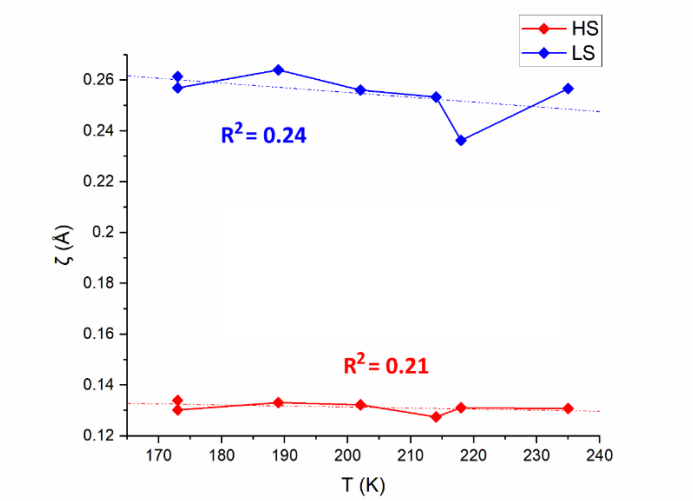

Figure S34. *Reported effects of the measured $T_{1/2}$ values at pressure increase vs the sum of the Co-N bond differences from $<D_{Co\text{-}N}>$,* ***ζ****. Trend line reports the correlation factor for* **$1_{cry,HS}$** *(red, R^2 = 0.21) and* **$1_{cry,LS}$** *(blue, R^2 = 0.24).*

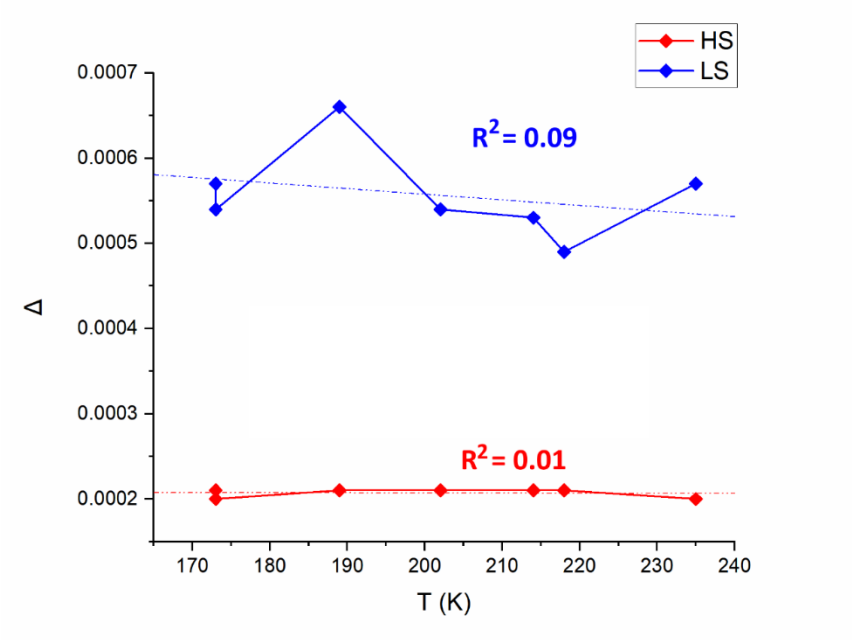

Figure S35. *Reported effects of the measured $T_{1/2}$ values at pressure increase vs the averaged Co-N bond deviation from <D_{Co-N}>, **Δ**. Trend line reports the correlation factor for **1**$_{cry,HS}$ (red, R^2 = 0.01) and **1**$_{cry,LS}$ (blue, R^2 = 0..09).*

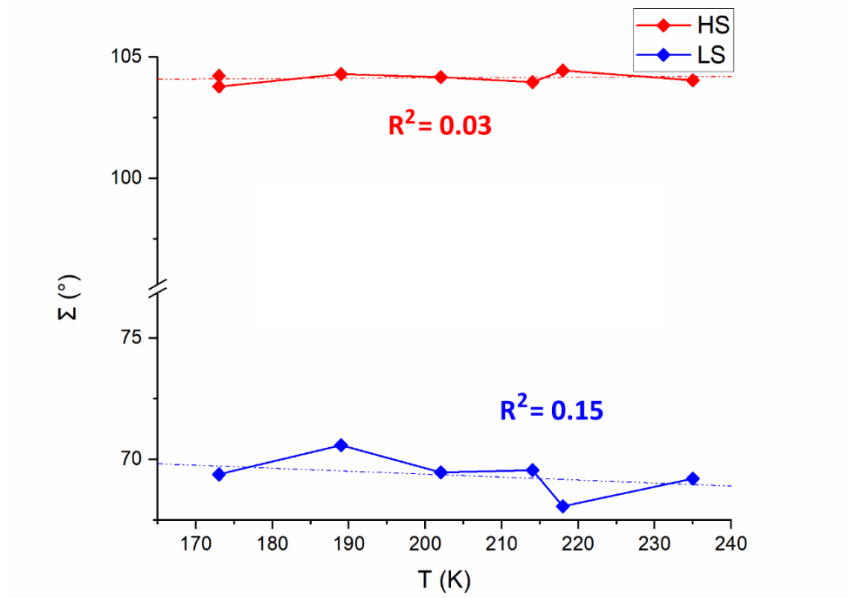

Figure S36. *Reported effects of the measured $T_{1/2}$ values at pressure increase vs the octahedral distortion parameter **Σ**. Trend line reports the correlation factor for **1**$_{cry,HS}$ (red, R^2 = 0.03) and **1**$_{cry,LS}$ (blue, R^2 = 0.15).*

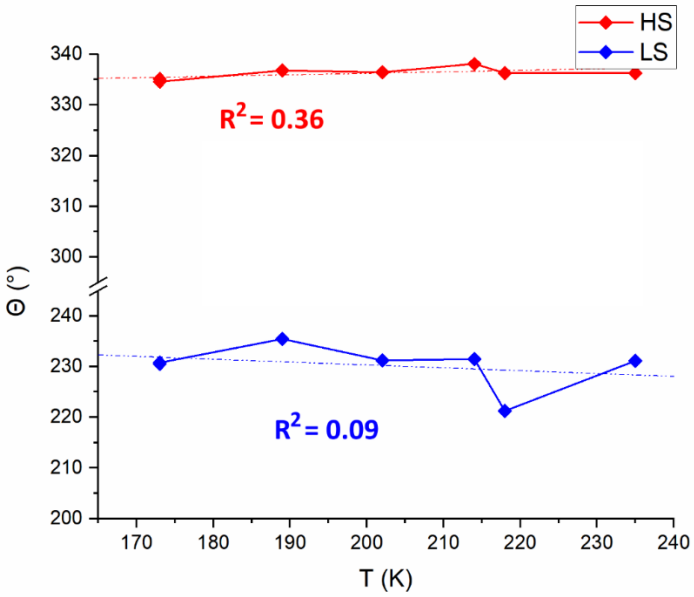

Figure S37. *Reported effects of the measured $T_{1/2}$ values at pressure increase vs the trigonal torsion parameter* ***Θ****. Trend line reports the correlation factor for* ***1****$_{cry,HS}$ (red, R^2 = 0.95) and* ***1****$_{cry,LS}$ (blue, R^2 = 0.92).*

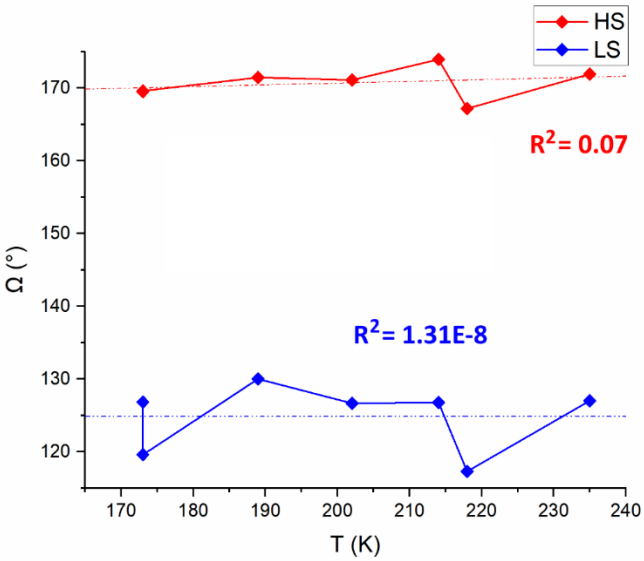

Figure S38. *Reported effects of the $T_{1/2}$ values at pressure increase vs the distortion parameter* ***Ω****. Trend line reports the correlation factor for* ***1****$_{cry,HS}$ (red, R^2 = 0.07) and* ***1****$_{cry,LS}$ (blue, R^2 = 1.13E-8).*

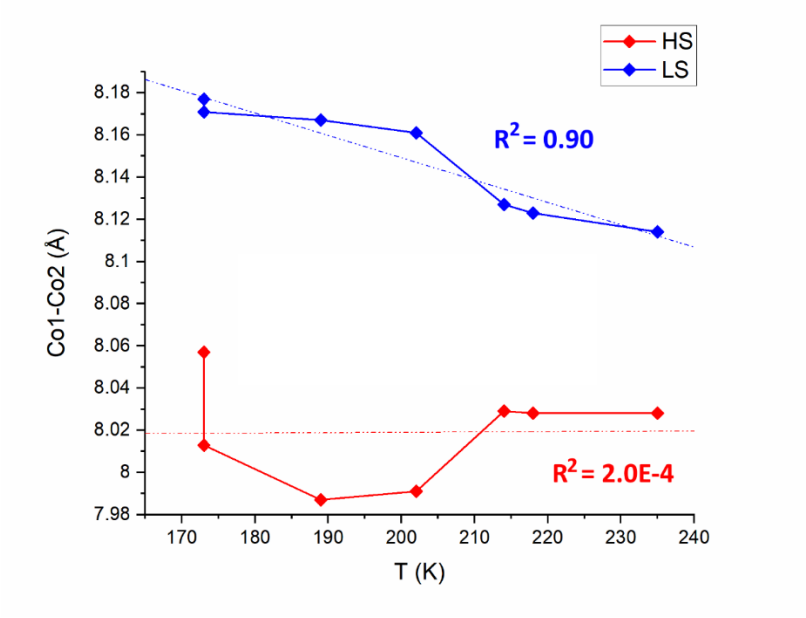

Figure S39. *Reported effects of the measured $T_{1/2}$ values at pressure increase vs the intermolecular Co-Co ions distance (d(Co1-Co2)). Trend line reports the correlation factor for* ***1****$_{cry,HS}$ (red, R^2 = 2.0E-4) and* ***1****$_{cry,LS}$ (blue, R^2 = 0.90).*

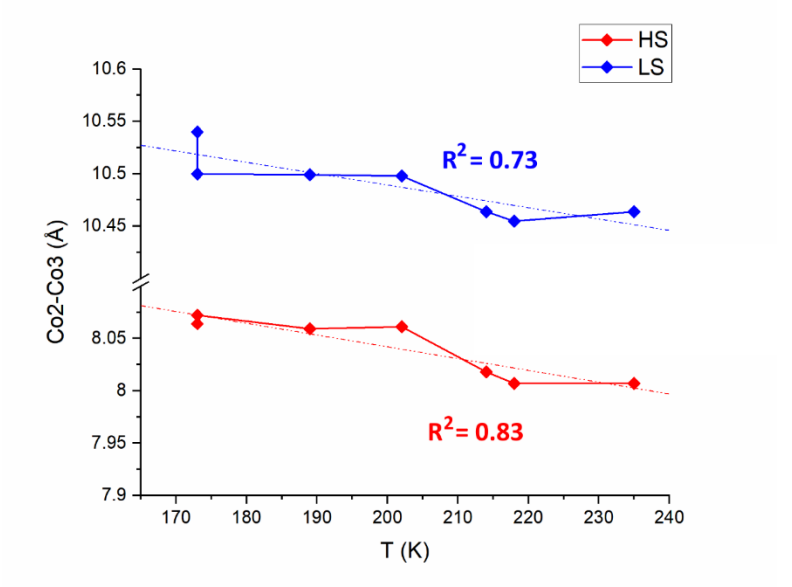

Figure S40. *Reported effects of the measured $T_{1/2}$ values at pressure increase vs the intermolecular Co-Co ions distance (d(Co2-Co3)). Trend line reports the correlation factor for* ***1****$_{cry,HS}$ (red, R^2 = 0.83) and* ***1****$_{cry,LS}$ (blue, R^2 = 0.73).*

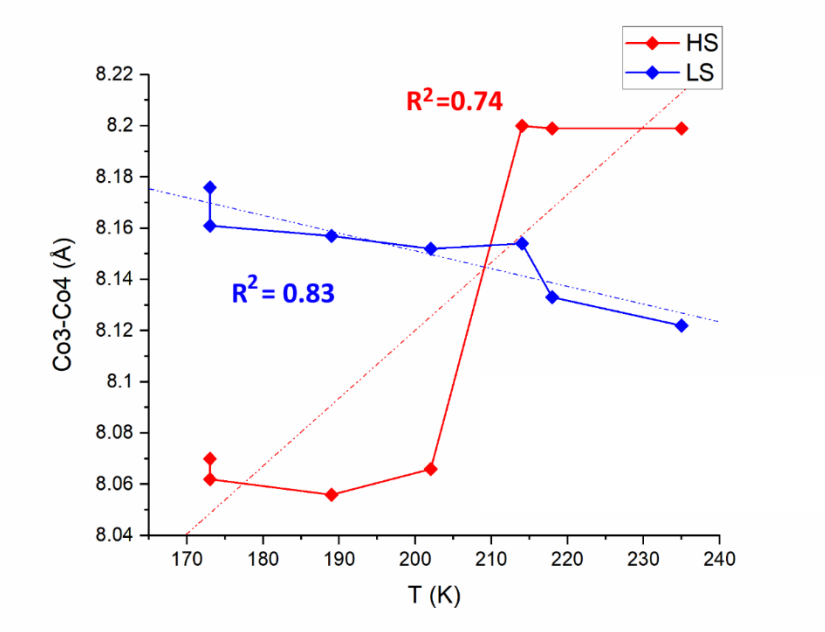

Figure S41. *Reported effects of the measured $T_{1/2}$ values at pressure increase vs the intermolecular Co-Co ions distance (d(Co3-Co4)). Trend line reports the correlation factor for* ***1****$_{cry,HS}$ (red, R^2 = 0.74) and* ***1****$_{cry,LS}$ (blue, R^2 = 0.83).*

2.3. Structural Distortions associated with Spin State Transition

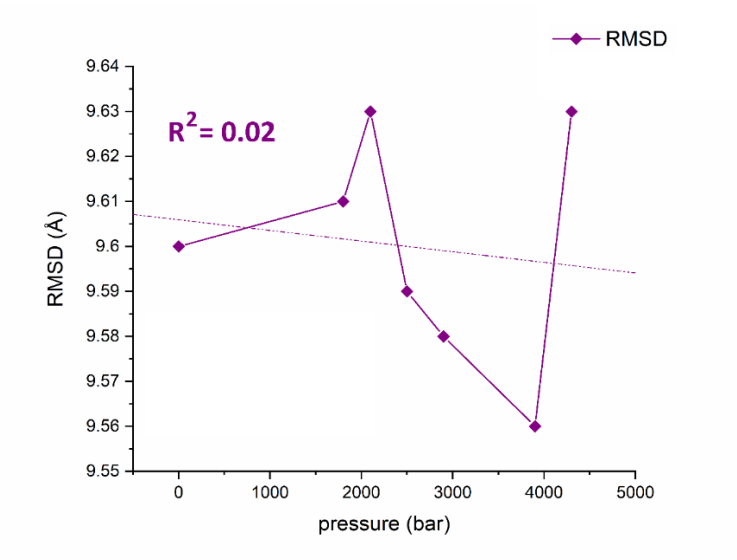

Figure S42. *Reported effects of the pressure increase vs the* ***ΔRMSD*** *variation from* ***1****$_{cry,LS}$* *to* ***1****$_{cry,HS}$*. *Trend line reports the [p vs ΔRMSD] correlation factor (purple, R^2 = 0.02).*

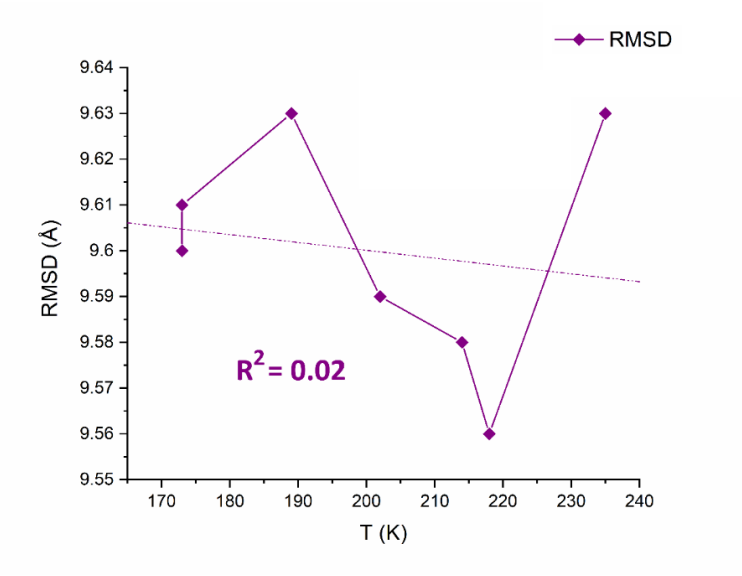

Figure S43. *Reported effects of the measured $T_{1/2}$ at the pressure increase vs the* ***ΔRMSD*** *variation from* ***1****$_{cry,LS}$* *to* ***1****$_{cry,HS}$*. *Trend line reports the [$T_{1/2}$ vs ΔRMSD] correlation factor (purple, R^2 = 0.02).*

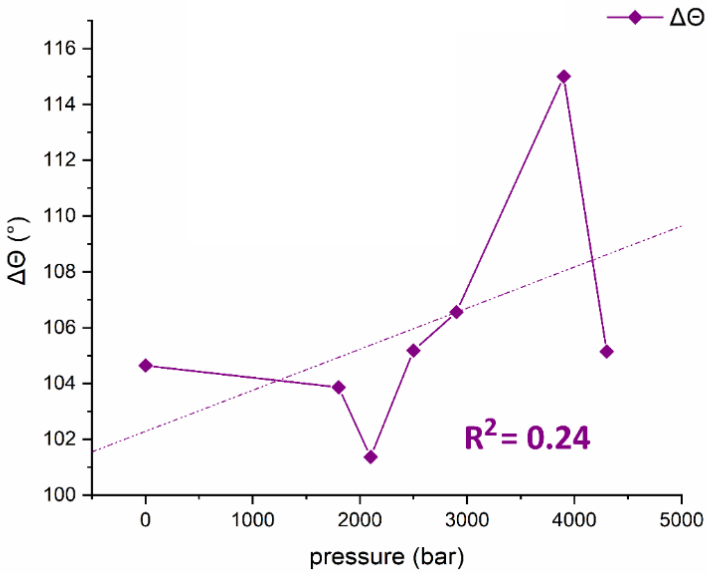

Figure S44. *Reported effects of the pressure increase vs the variation of the trigonal torsion parameter* ***ΔΘ*** *from* ***1****cry,LS* *to* ***1****cry,HS*. *Trend line reports the [p vs. ΔΘ] correlation factor (purple, R^2 = 0.24).*

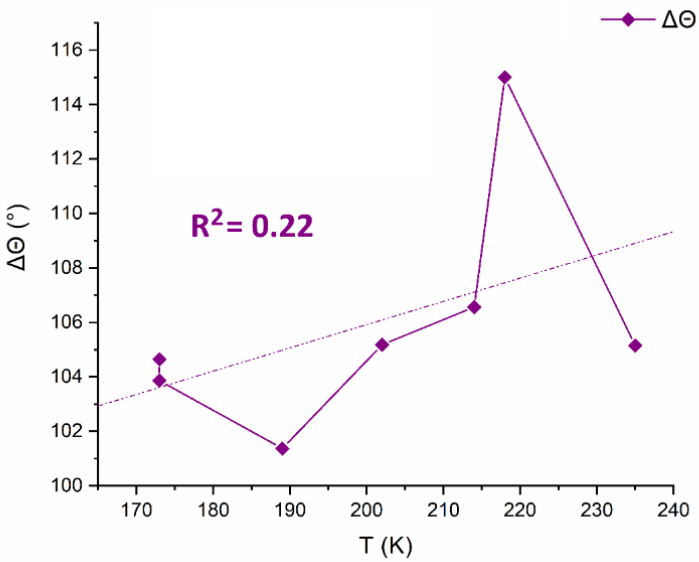

Figure S45. *Reported effects of the measured $T_{1/2}$ at the pressure increase vs the variation of the trigonal torsion parameter* ***ΔΘ*** *from* ***1****cry,LS* *to* ***1****cry,HS*. *Trend line reports the [$T_{1/2}$ vs. ΔΘ] correlation factor (purple, R^2 = 0.22).*

3. Additional Electronic Data

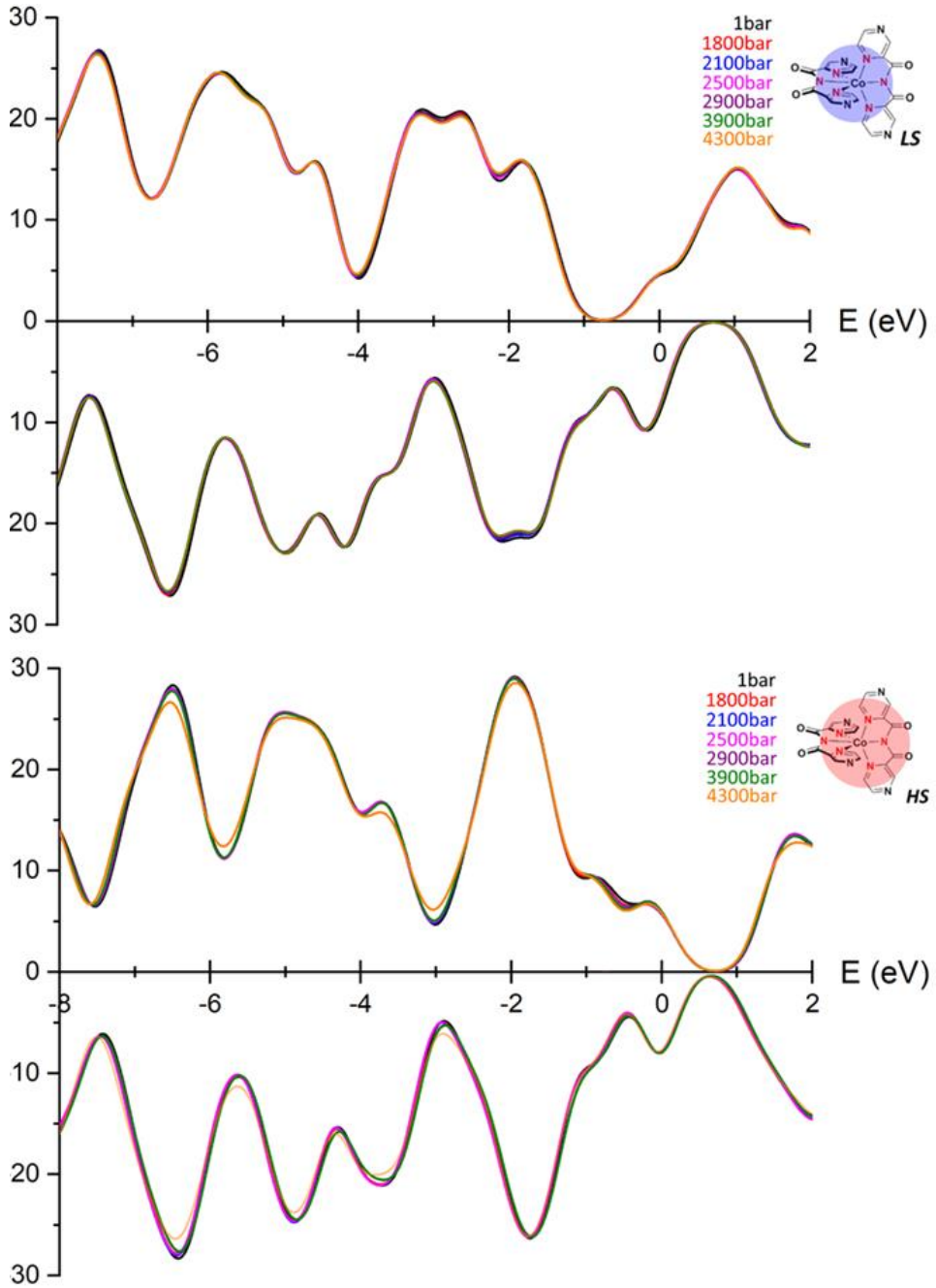

Figure S46. *Calculated PDOS for* $\mathbf{1}_{cryst,LS}$ *(top) and* $\mathbf{1}_{cryst,HS}$ *(bottom) across the whole pressure range (1 bar < p < 4300 bar) in the energy range between -8 eV and +2 eV. For each spin state are reported α- (+y axis) and β-orbitals (-y axis). Colour code: 1 bar (black), 1800 bar (red), 2100 bar (blue), 2500 bar (magenta), 2900 bar (purple), 3900 bar (olive), 4300 bar (orange). 1 bar =* 10^{-4} *Pa.*

Table S11. *Reported correlation factor in the analysis of the variation of twelve characteristic peaks for TDOS and LDOS of* ***1***$_{cry,LS}$ *and to* ***1***$_{cry,HS}$ *versus the seven different pressures (and related experimental* $T_{1/2}$*).*

p / bar			***1***	***1800***	***2100***	***2500***	***2900***	***3900***	***4300***	***R^2(p)***	***R^2 ($T_{1/2}$(exp))***
$T_{1/2}$(exp.) / K			***173***	***173***	***189***	***202***	***214***	***227***	***235***		
DOS	***Figure***	***Energy / eV***	***Intensities***								
1.LS_ TDOS	*7*	*-1.9*	*25.34*	*25.23*	*24.96*	*24.67*	*24.62*	*24.57*	*24.04*	*0.84 (Fig. S47)*	*0.92 (Fig. S59)*
2.LS_ TDOS	*7*	*-2.6*	*42.13*	*41.54*	*41.45*	*41.38*	*41.34*	*41.12*	*40.92*	*0.97 (Fig. S48)*	*0.74 (Fig. S60)*
3.LS_ TDOS	*7*	*-3.1*	*42.44*	*41.91*	*41.81*	*41.74*	*41.76*	*41.51*	*41.46*	*0.97 (Fig. S49)*	*0.74 (Fig. S61)*
4.LS_ PDOS(α)	*S46*	*-2.1*	*13.89*	*14.21*	*14.31*	*14.32*	*14.53*	*14.55*	*14.65*	*0.97 (Fig. S50)*	*0.84 (Fig. S62)*
5.LS_ PDOS(α)	*S46*	*-2.6*	*20.73*	*20.53*	*20.42*	*20.42*	*20.38*	*20.35*	*20.24*	*0.97 (Fig. S51)*	*0.81 (Fig. S63)*
6.LS_ PDOS(α)	*S46*	*-3.2*	*20.93*	*20.67*	*20.67*	*20.61*	*20.63*	*20.46*	*20.41*	*0.97 (Fig. S52)*	*0.76 (Fig. S64)*
7.LS_ PDOS(β)	*S46*	*-2.1*	*21.76*	*21.57*	*21.48*	*21.42*	*21.41*	*21.19*	*21.19*	*0.98 (Fig. S53)*	*0.89 (Fig. S65)*
8.HS_TDOS	*7*	*-0.5*	*11.27*	*10.73*	*10.52*	*10.44*	*10.63*	*10.65*	*10.15*	*0.75 (Fig. S54)*	*0.52 (Fig. S66)*
9.HS_ TDOS	*7*	*-0.7*	*14.89*	*14.14*	*13.91*	*13.85*	*13.82*	*13.68*	*13.18*	*0.93 (Fig. S55)*	*0.73 (Fig. S67)*
10.HS_ TDOS	*7*	*-1.9*	*54.78*	*54.66*	*54.63*	*54.58*	*54.45*	*54.45*	*54.21*	*0.86 (Fig. S56)*	*0.87 (Fig. S68)*
11.HS_ PDOS(α)	*S46*	*-0.7*	*8.05*	*7.67*	*7.49*	*7.431*	*7.26*	*7.26*	*6.94*	*0.94 (Fig. S57)*	*0.84 (Fig. S69)*
12.HS_ PDOS(α)	*S46*	*-2.0*	*29.17*	*29.10*	*29.07*	*29.04*	*28.97*	*28.97*	*28.56*	*0.64 (Fig. S58)*	*0.68 (Fig. S70)*

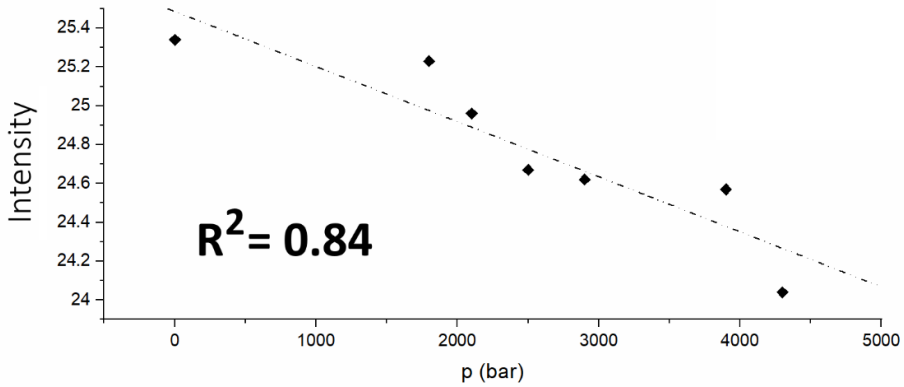

Figure S47. *Reported Intensity of the band of* ***1****$_{cry,LS}$ at -1.9 eV (1.LS_TDOS, Table S11) vs the pressure increase. Trend line reports the [I vs. p] correlation factor (R^2 = 0.84).*

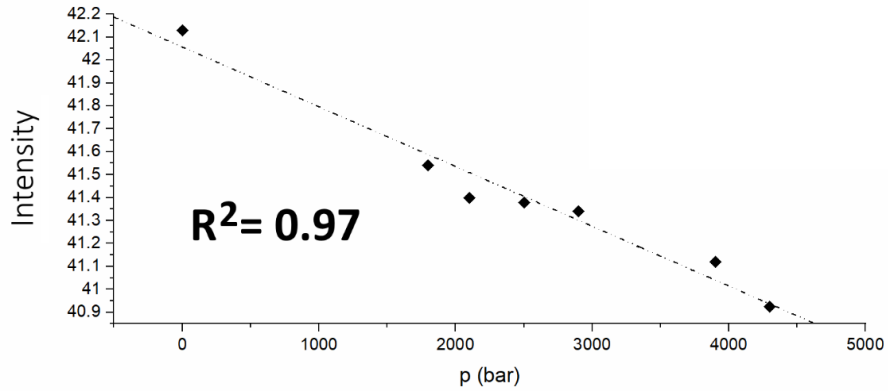

Figure S48. *Reported Intensity of the band of* ***1****$_{cry,LS}$ at -2.6 eV (2.LS_TDOS, Table S11) vs the pressure increase. Trend line reports the [I vs. p] correlation factor (R^2 = 0.97).*

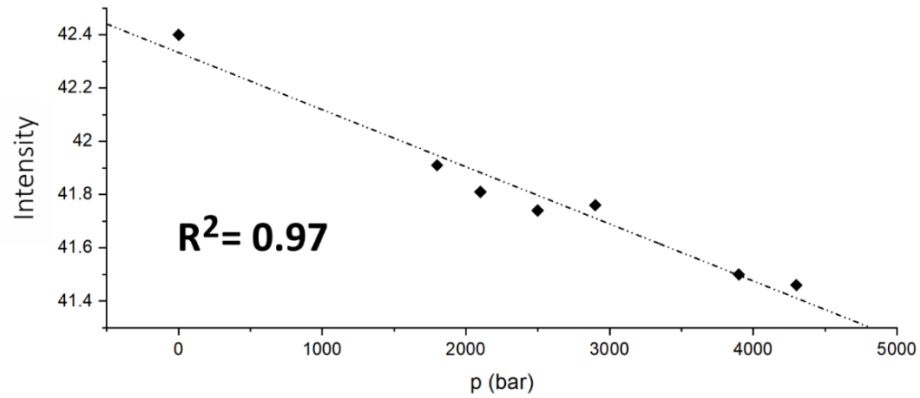

Figure S49. *Reported Intensity of the band of* ***1****$_{cry,LS}$ at -3.1 eV (3.LS_TDOS, Table S11) vs the pressure increase. Trend line reports the [I vs. p] correlation factor (R^2 = 0.97).*

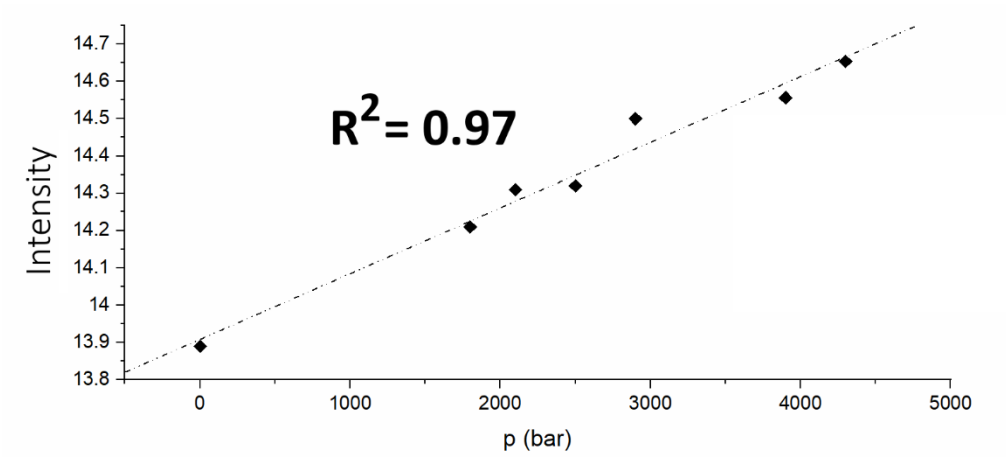

Figure S50. *Reported Intensity of the band of* ***1****$_{cry,LS}$ at -2.1 eV (4.LS_PDOS(α), Table S11) vs the pressure increase. Trend line reports the [I vs. p] correlation factor (R^2 = 0.97).*

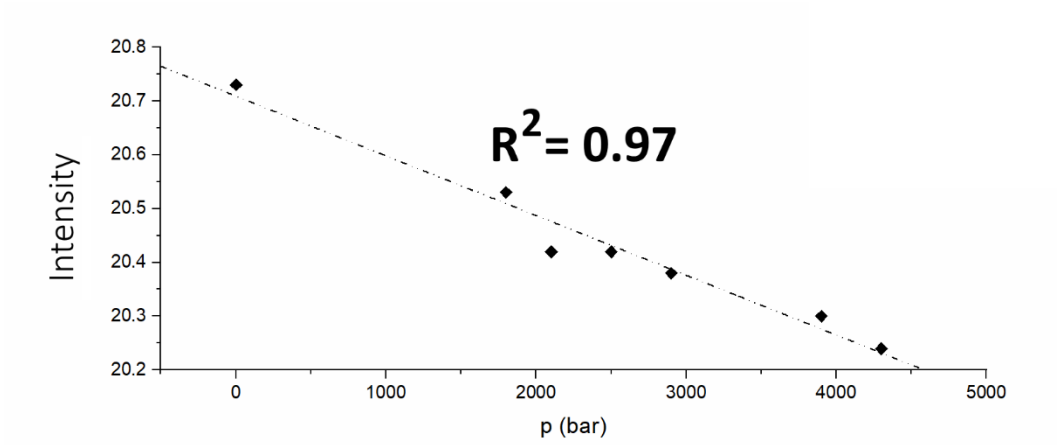

Figure S51. *Reported Intensity of the band of* ***1****$_{cry,LS}$ at -2.6 eV (5.LS_PDOS(α), Table S11) vs the pressure increase. Trend line reports the [I vs. p] correlation factor (R^2 = 0.97).*

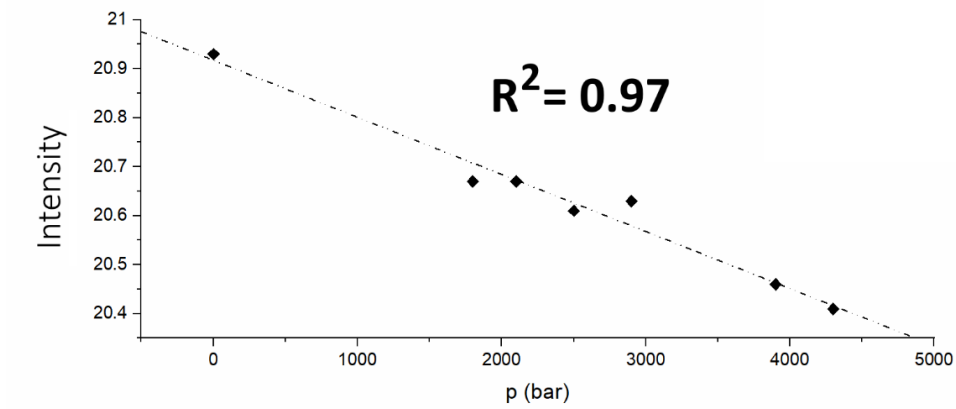

Figure S52. *Reported Intensity of the band of* ***1****$_{cry,LS}$ at -3.2 eV (6.LS_PDOS(α), Table S11) vs the pressure increase. Trend line reports the [I vs. p] correlation factor (R^2 = 0.97).*

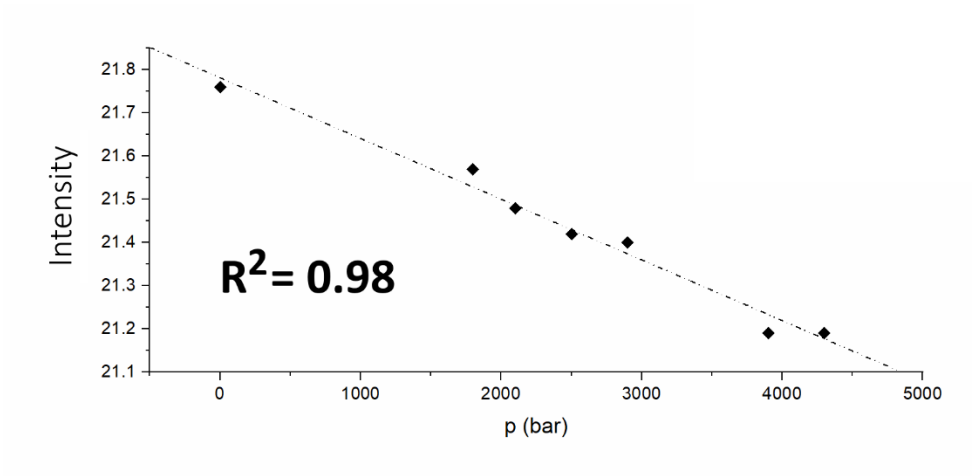

Figure S53. *Reported Intensity of the band of* ***1****$_{cry,LS}$ at -2.1 eV (7.LS_PDOS(β), Table S11) vs the pressure increase. Trend line reports the [I vs. p] correlation factor (R^2 = 0.98).*

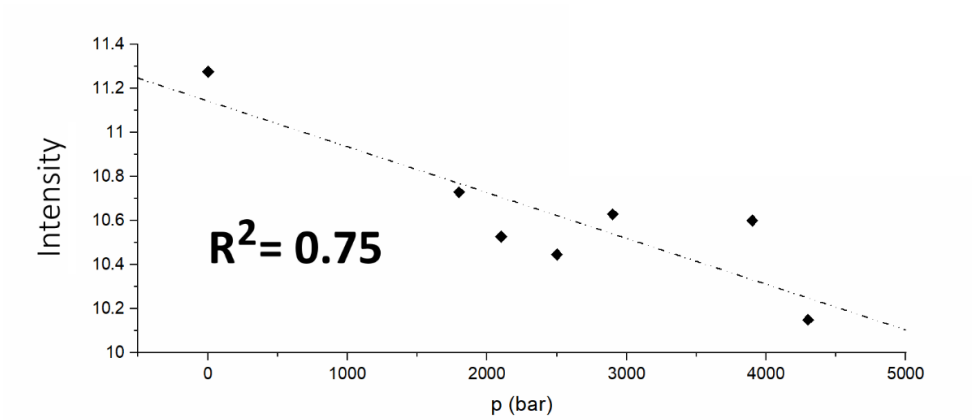

Figure S54. *Reported Intensity of the band of* ***1****$_{cry,HS}$ at -0.5 eV (8.HS_TDOS, Table S11) vs the pressure increase. Trend line reports the [I vs. p] correlation factor (R^2 = 0.75).*

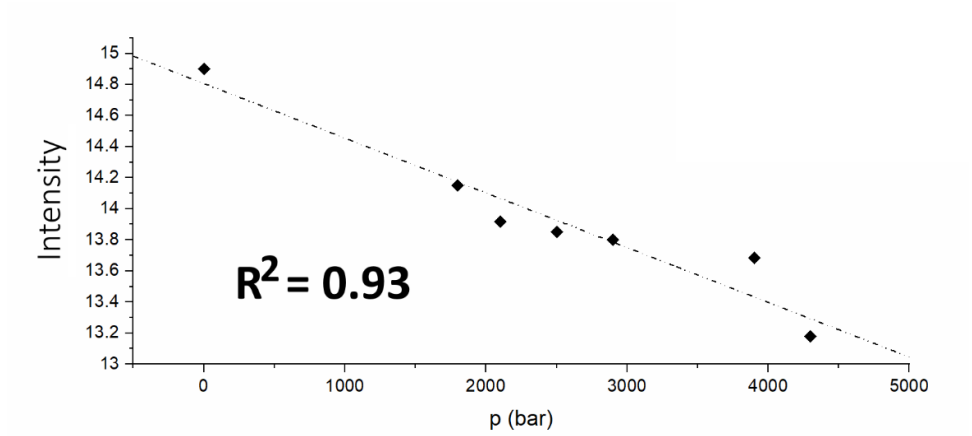

Figure S55. *Reported Intensity of the band of* ***1****$_{cry,HS}$ at -0.7 eV (9.HS_TDOS, Table S11) vs the pressure increase. Trend line reports the [I vs. p] correlation factor (R^2 = 0.93).*

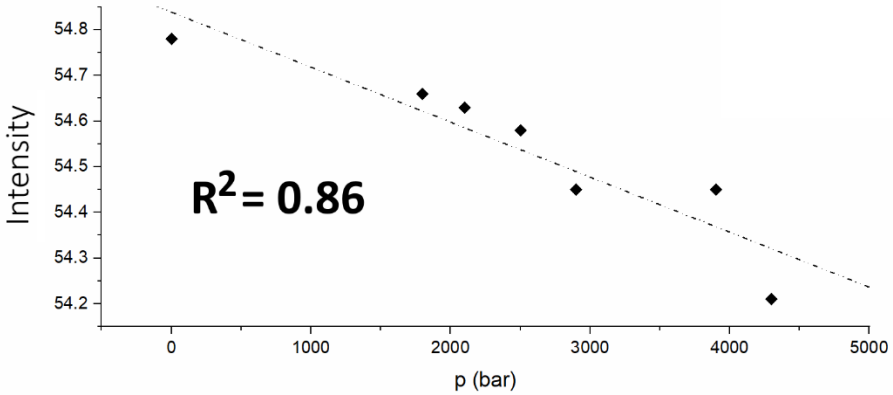

Figure S56. *Reported Intensity of the band of* ***1****$_{cry,HS}$ at -1.9 eV (10.HS_TDOS, Table S11) vs the pressure increase. Trend line reports the [I vs. p] correlation factor (R^2 = 0.86).*

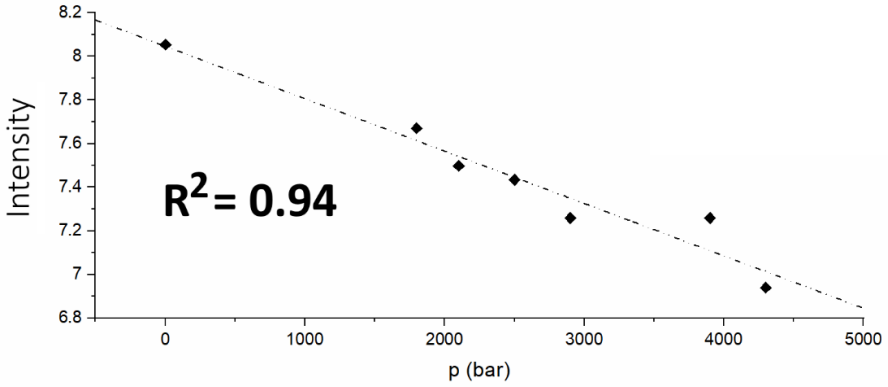

Figure S57. *Reported Intensity of the band of* ***1****$_{cry,HS}$ at -0.7 eV (11.HS_PDOS(α), Table S11) vs the pressure increase. Trend line reports the [I vs. p] correlation factor (R^2 = 0.94).*

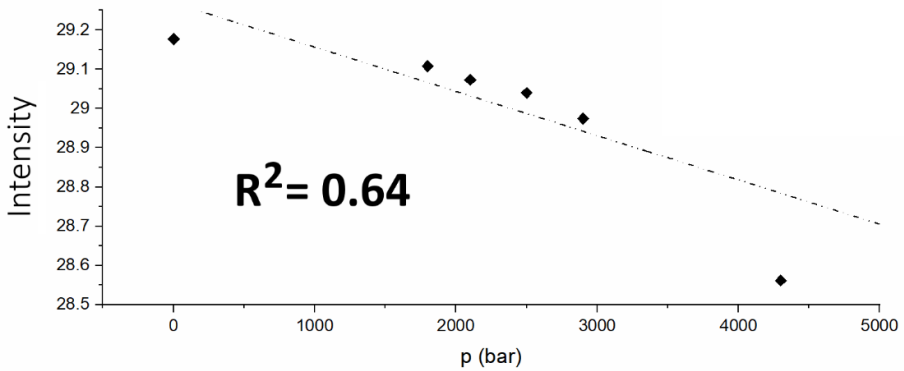

Figure S58. *Reported Intensity of the band of* ***1****$_{cry,HS}$ at -2.0 eV (12.HS_PDOS(α), Table S11) vs the pressure increase. Trend line reports the [I vs. p] correlation factor (R^2 = 0.64).*

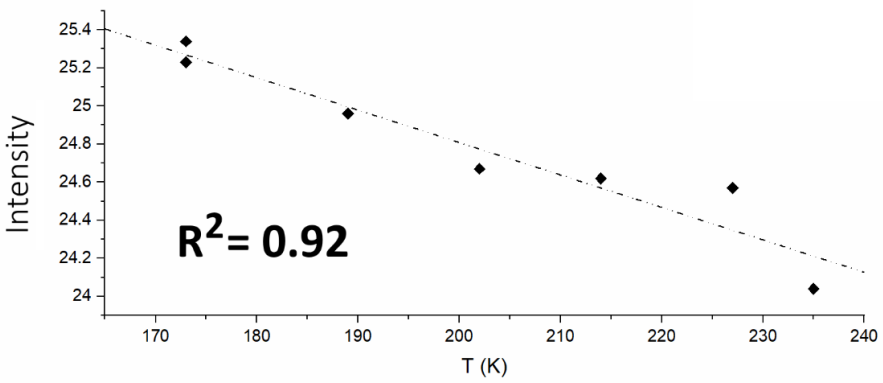

Figure S59. *Reported Intensity of the band of* ***1****$_{cry,LS}$ at -1.9 eV (1.LS_TDOS, Table S11) vs the measured $T_{1/2}$. Trend line reports the [I vs. $T_{1/2}$] correlation factor (R^2 = 0.92).*

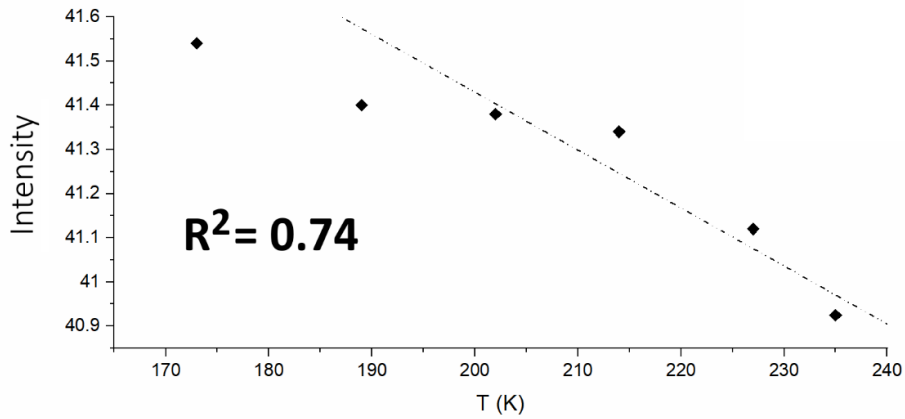

Figure S60. *Reported Intensity of the band of* ***1****$_{cry,LS}$ at -2.6 eV (2.LS_TDOS, Table S11) vs the measured $T_{1/2}$. Trend line reports the [I vs. $T_{1/2}$] correlation factor (R^2 = 0.74).*

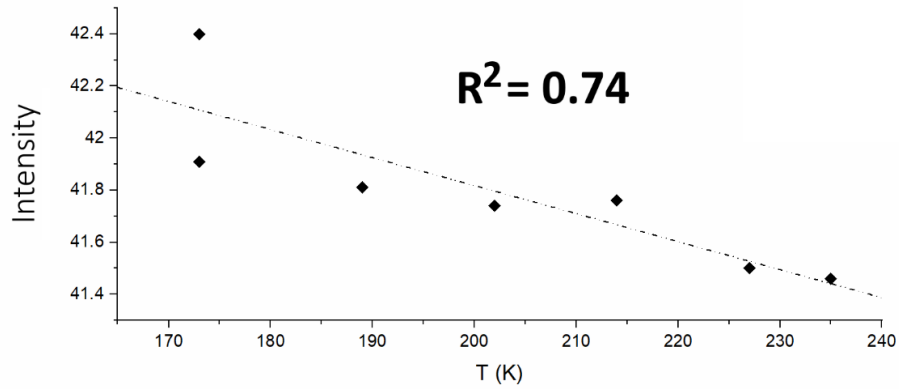

Figure S61. *Reported Intensity of the band of* ***1****$_{cry,LS}$ at -3.1 eV (3.LS_TDOS, Table S11) vs the measured $T_{1/2}$. Trend line reports the [I vs. $T_{1/2}$] correlation factor (R^2 = 0.74).*

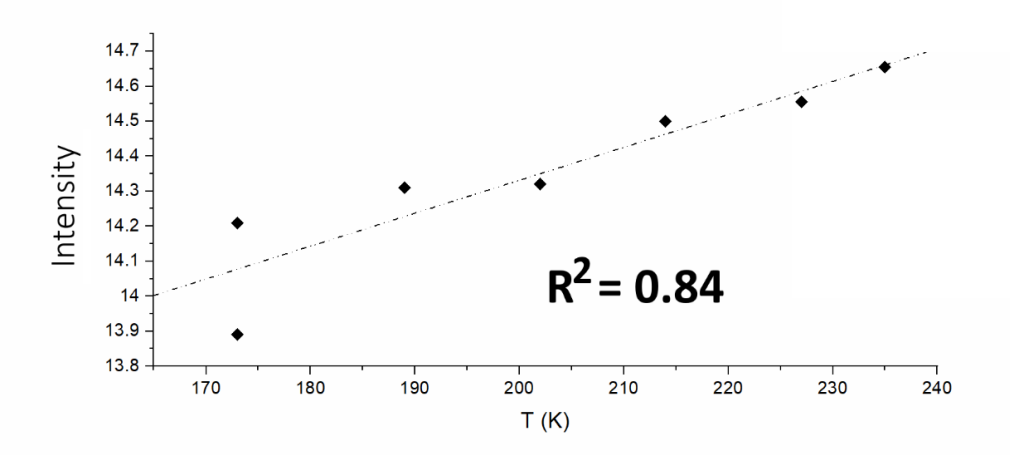

Figure S62. *Reported Intensity of the band of* ***1****$_{cry,LS}$ at -2.1 eV (4.LS_PDOS(α), Table S11) vs the measured $T_{1/2}$. Trend line reports the [I vs. $T_{1/2}$] correlation factor (R^2 = 0.84)*

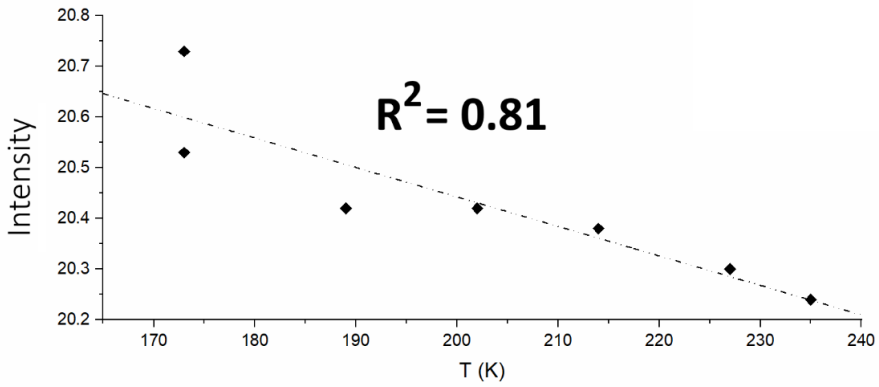

Figure S63. *Reported Intensity of the band of* ***1****$_{cry,LS}$ at -2.6 eV (5.LS_PDOS(α), Table S11) vs the measured $T_{1/2}$. Trend line reports the [I vs. $T_{1/2}$] correlation factor (R^2 = 0.81).*

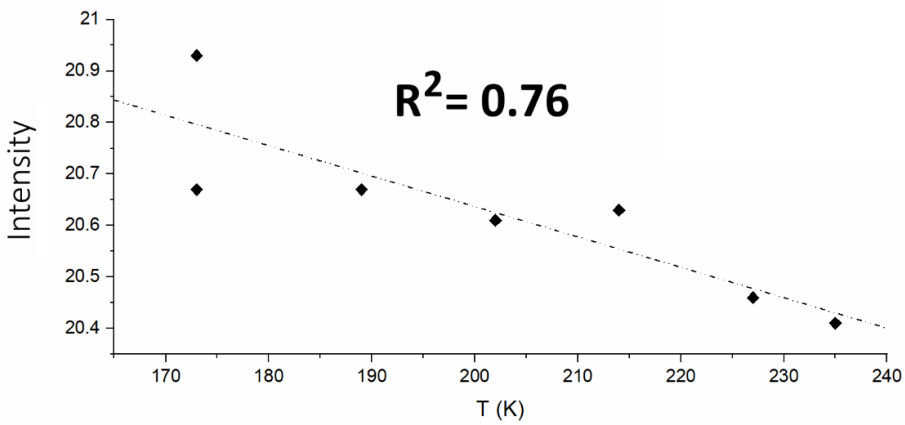

Figure S64. *Reported Intensity of the band of* ***1****$_{cry,LS}$ at -3.2 eV (6.LS_PDOS(α), Table S11) vs the measured $T_{1/2}$. Trend line reports the [I vs. $T_{1/2}$] correlation factor (R^2 = 0.76).*

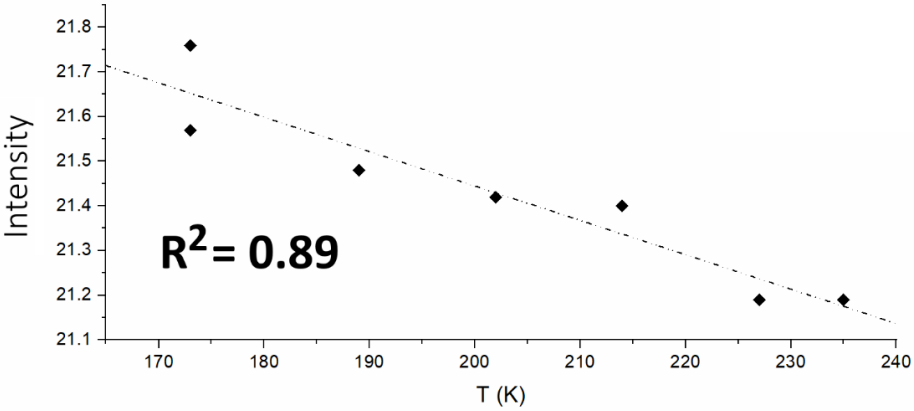

Figure S65. *Reported Intensity of the band of* ***1****$_{cry,LS}$ at -2.1 eV (7.LS_PDOS(β), Table S11) vs the measured $T_{1/2}$. Trend line reports the [I vs. $T_{1/2}$] correlation factor (R^2 = 0.89).*

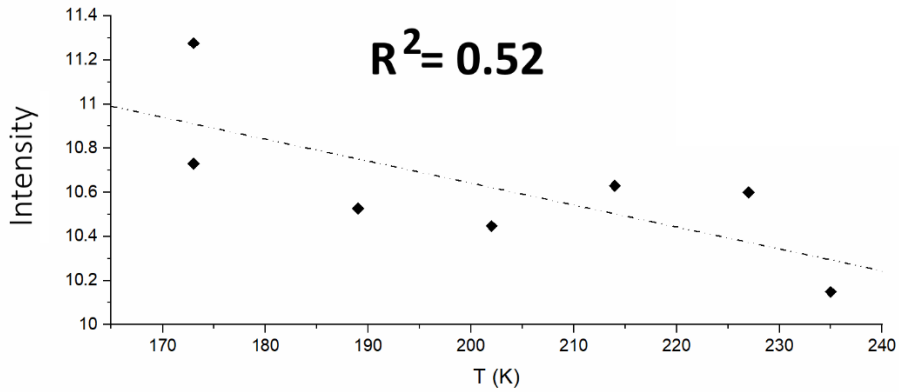

Figure S66. *Reported Intensity of the band of* ***1****$_{cry,HS}$ at -0.5 eV (8.HS_TDOS, Table S11) vs the measured $T_{1/2}$. Trend line reports the [I vs. $T_{1/2}$] correlation factor (R^2 = 0.52).*

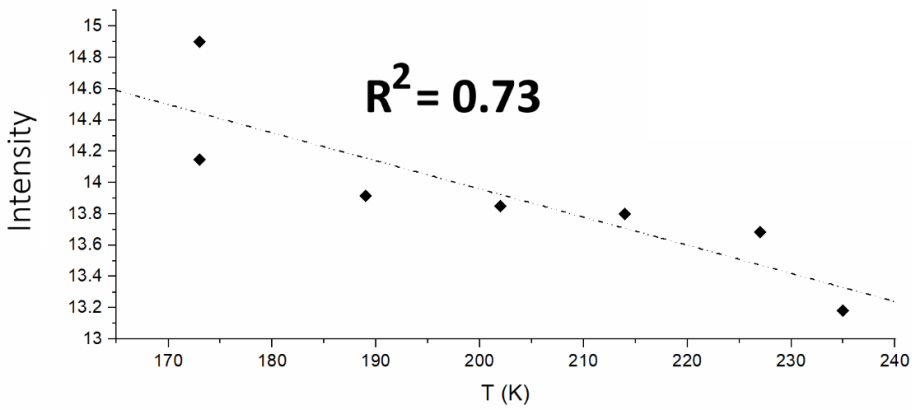

Figure S67. *Reported Intensity of the band of* ***1****$_{cry,HS}$ at -0.7 eV (9.HS_TDOS, Table S11) vs the measured $T_{1/2}$. Trend line reports the [I vs. $T_{1/2}$] correlation factor (R^2 = 0.73).*

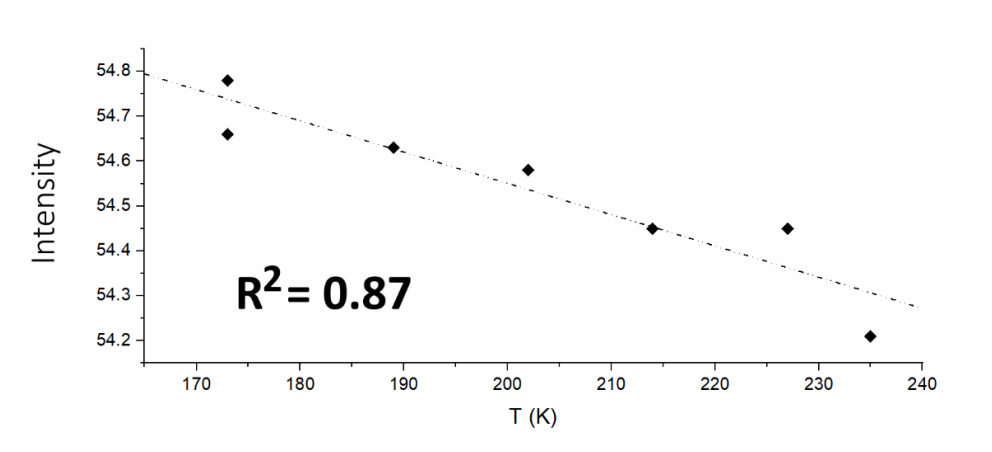

Figure S68. *Reported Intensity of the band of* ***1****$_{cry,HS}$ at -1.9 eV (10.HS_TDOS, Table S11) vs the measured* $T_{1/2}$*. Trend line reports the [I vs.* $T_{1/2}$*] correlation factor (*R^2 *= 0.87).*

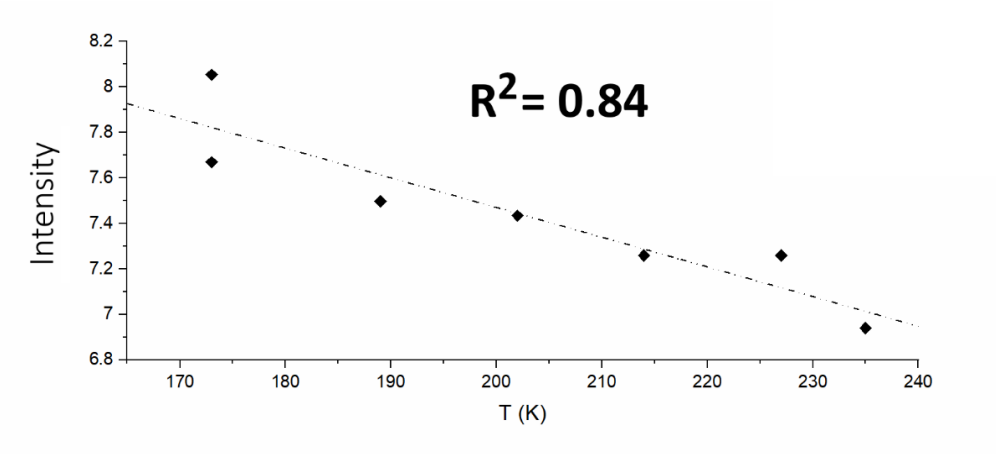

Figure S69. *Reported Intensity of the band of* ***1****$_{cry,HS}$ at -0.7 eV (11.HS_PDOS(α), Table S11) vs the measured* $T_{1/2}$*. Trend line reports the [I vs.* $T_{1/2}$*] correlation factor (*R^2 *= 0.84).*

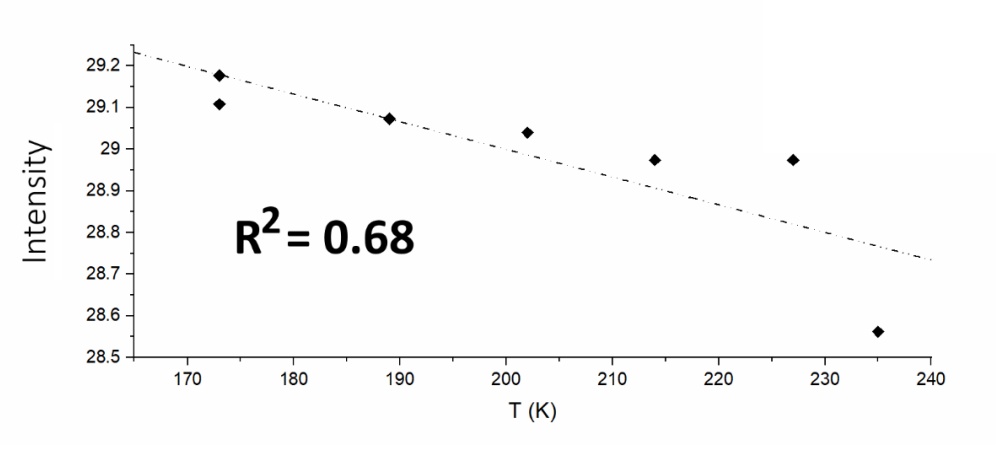

Figure S70. *Reported Intensity of the band of* ***1****$_{cry,HS}$ at -2.0 eV (12.HS_PDOS(α), Table S11) vs the measured* $T_{1/2}$*. Trend line reports the [I vs.* $T_{1/2}$*] correlation factor (*R^2 *= 0.68).*

3.1. LDOS: Cobalt Atoms

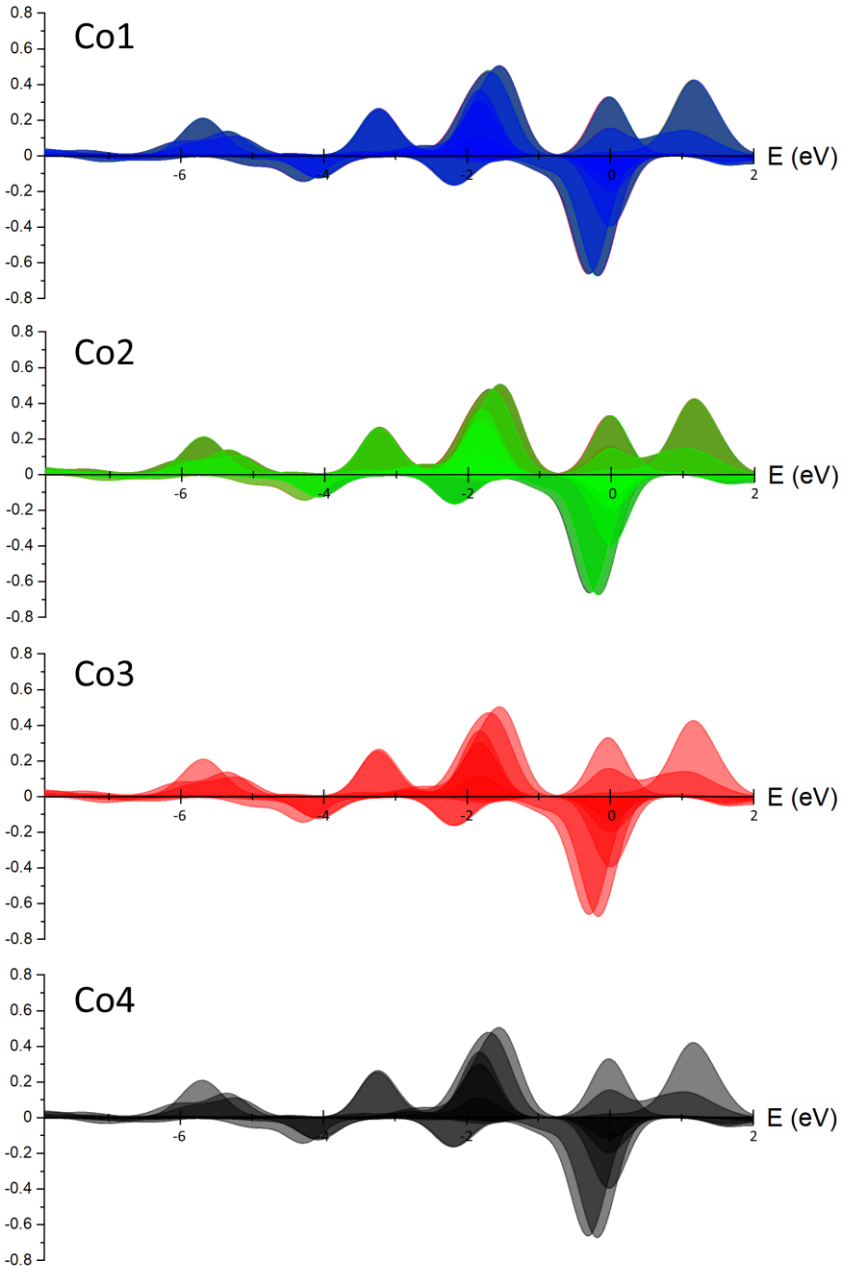

Figure S71. *Reported LDOS of the four Co^{II} ions for* ***$1_{cry,LS}$*** *at the pressure of 1 bar in the energy range between -8 eV and +2 eV. For each spin state are reported α- (+y axis) and β-orbitals (-y axis). Colour code: first Co^{II} (blue), second Co^{II} ion (green), third Co^{II} (red), fourth Co^{II} (black).*

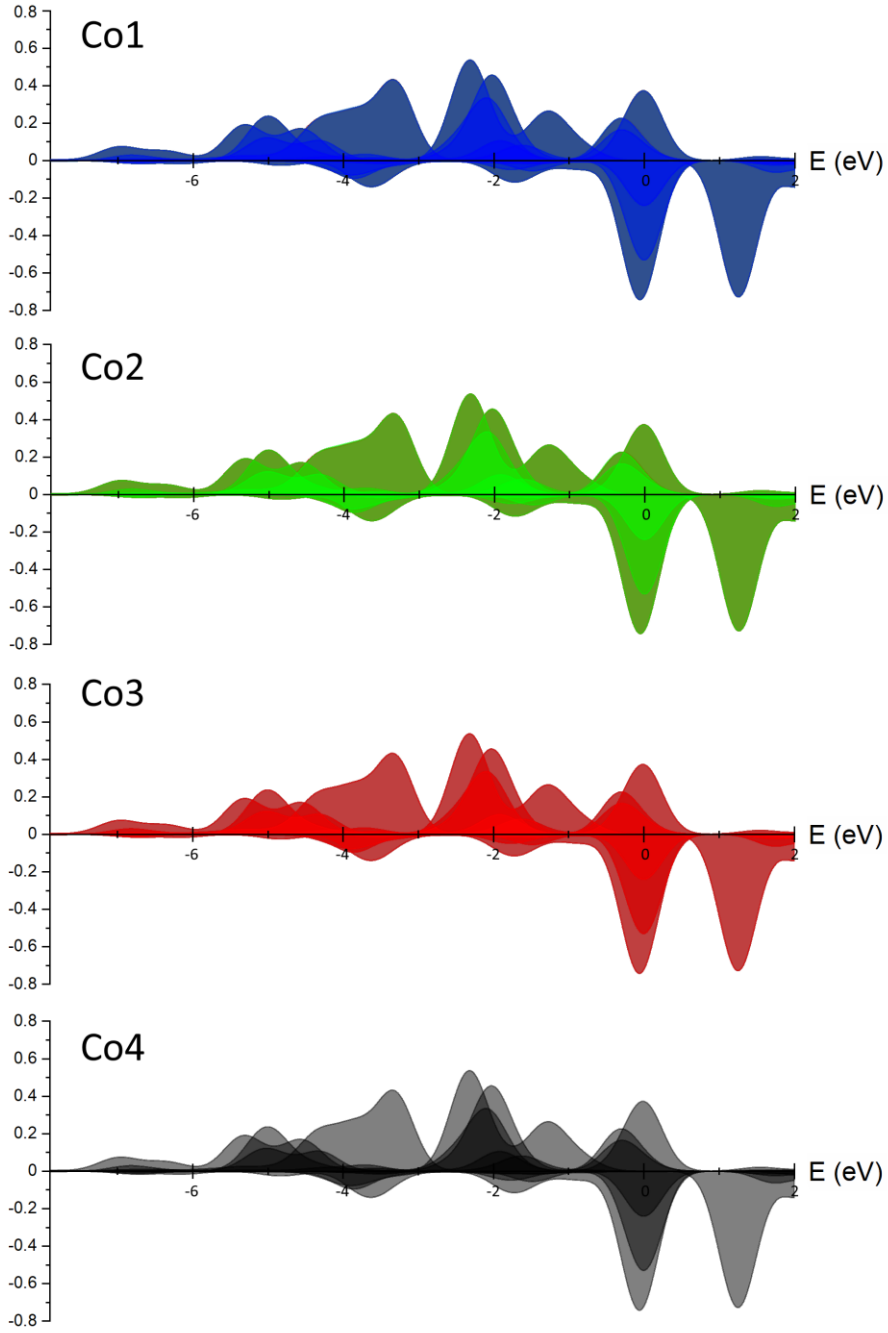

Figure S72. *Reported LDOS of the four Co^{II} ions for* ***1$_{cry,HS}$*** *at the pressure of 1 bar in the energy range between -8 eV and +2 eV. For each spin state are reported α- (+y axis) and β-orbitals (-y axis). Colour code: first Co^{II} (blue), second Co^{II} ion (green), third Co^{II} (red), fourth Co^{II} (black).*

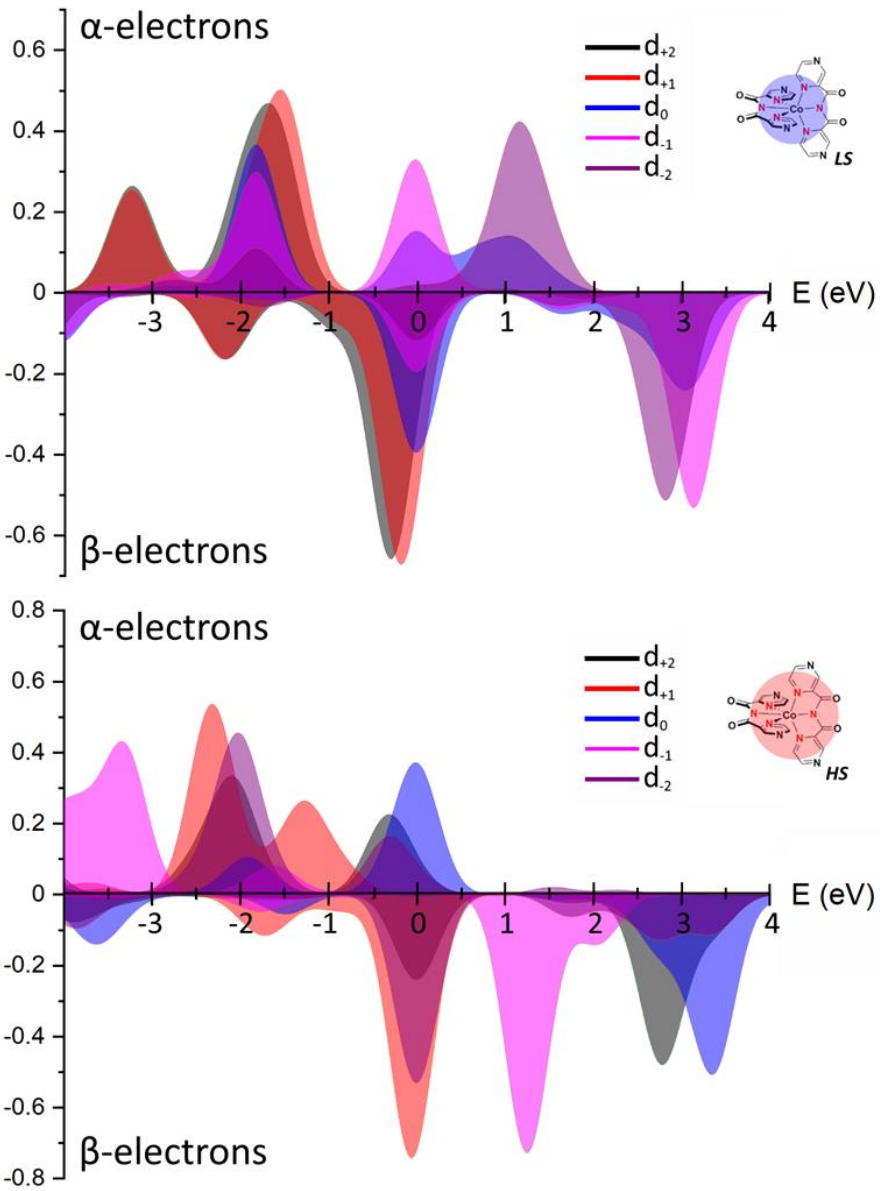

Figure S73. *Calculated energy of the five d-orbitals represented by complex functions (m_l = -2, -1, 0, +1, +2) for* ***1****$_{cry,LS}$ (top) and to* ***1****$_{cry,HS}$ (bottom) in the energy range between -4 eV and +4 eV. For each spin state the α- (+y axis) and β-orbitals (-y axis) are reported. Colour code: d_{+2} (black), d_{+1} (red), d_0 (blue), d_{-1} (magenta), d_{-2} (purple).*

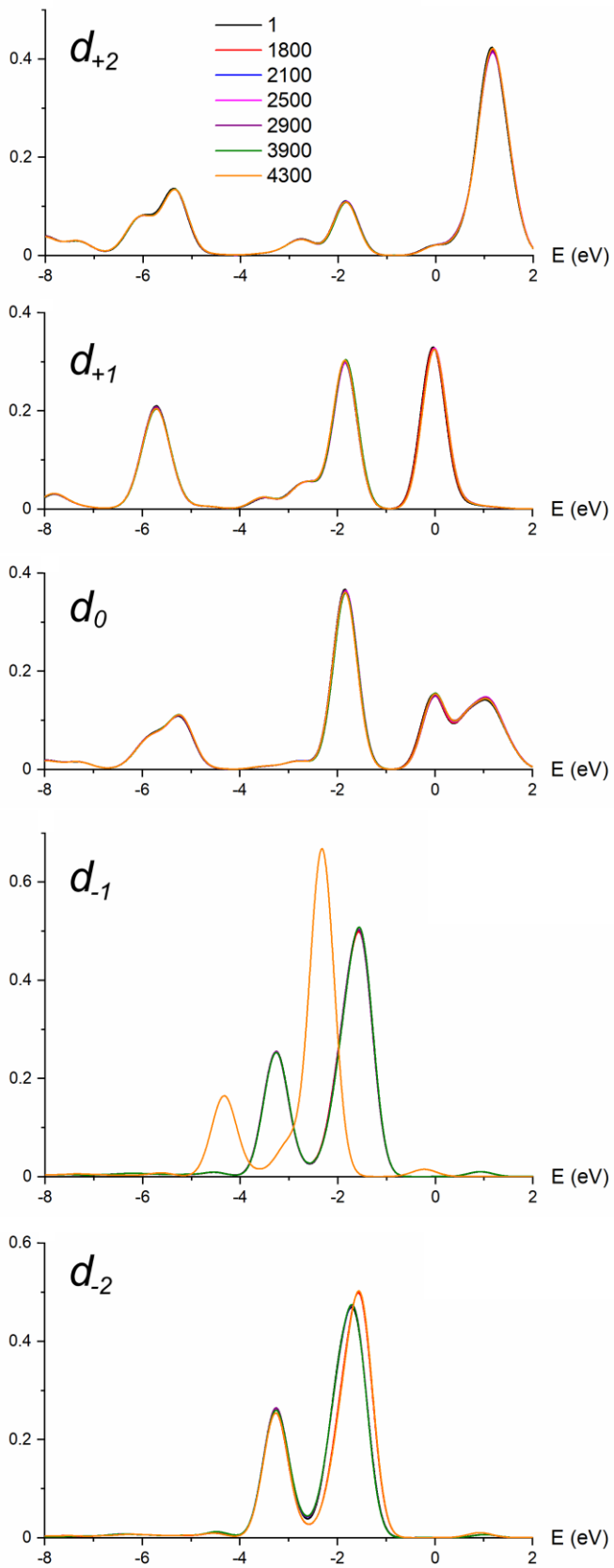

Figure S74. *Reported LDOS of the alfa d-orbitals of the Co^{II} ions of* ***1****$_{cry,LS}$ at the seven studied different pressures (p = 1, 1800, 2100, 2500, 2900, 3900, 4300 bar).*

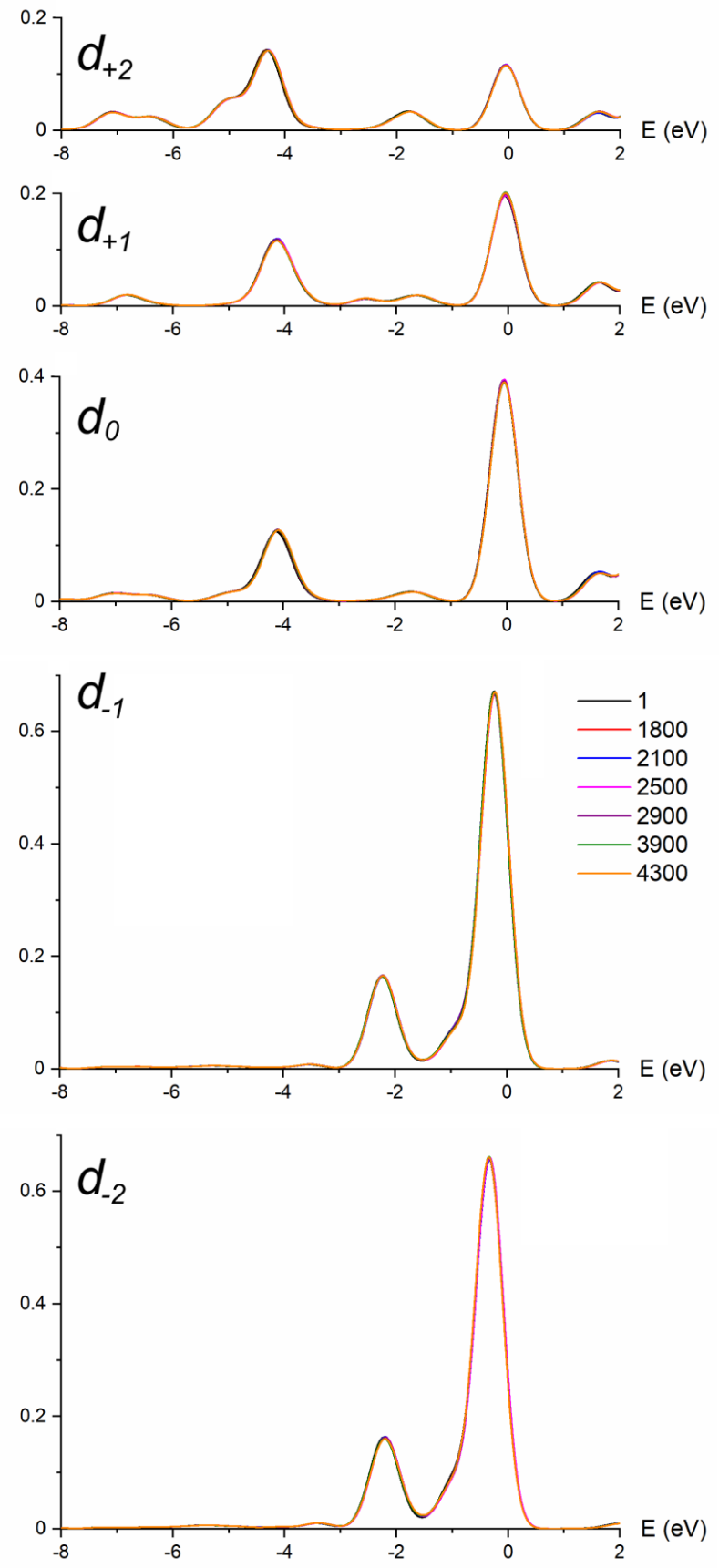

Figure S75. *Reported LDOS of the beta d-orbitals of the Co^{II} ions of* ***1$_{cry,LS}$*** *at the seven studied different pressures (p = 1, 1800, 2100, 2500, 2900, 3900, 4300 bar).*

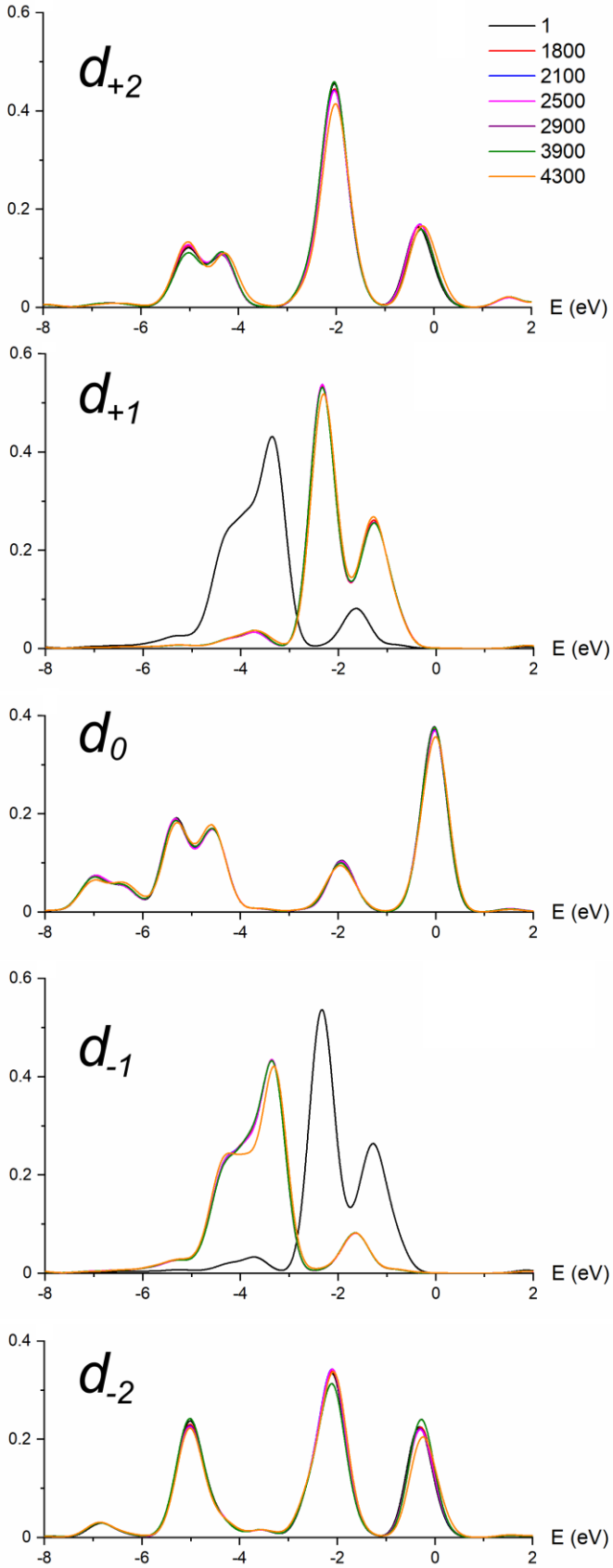

Figure S76. *Reported LDOS of the alfa d-orbitals of the Co^{II} ions of* ***1$_{cry,HS}$*** *at the seven studied different pressures (p = 1, 1800, 2100, 2500, 2900, 3900, 4300 bar).*

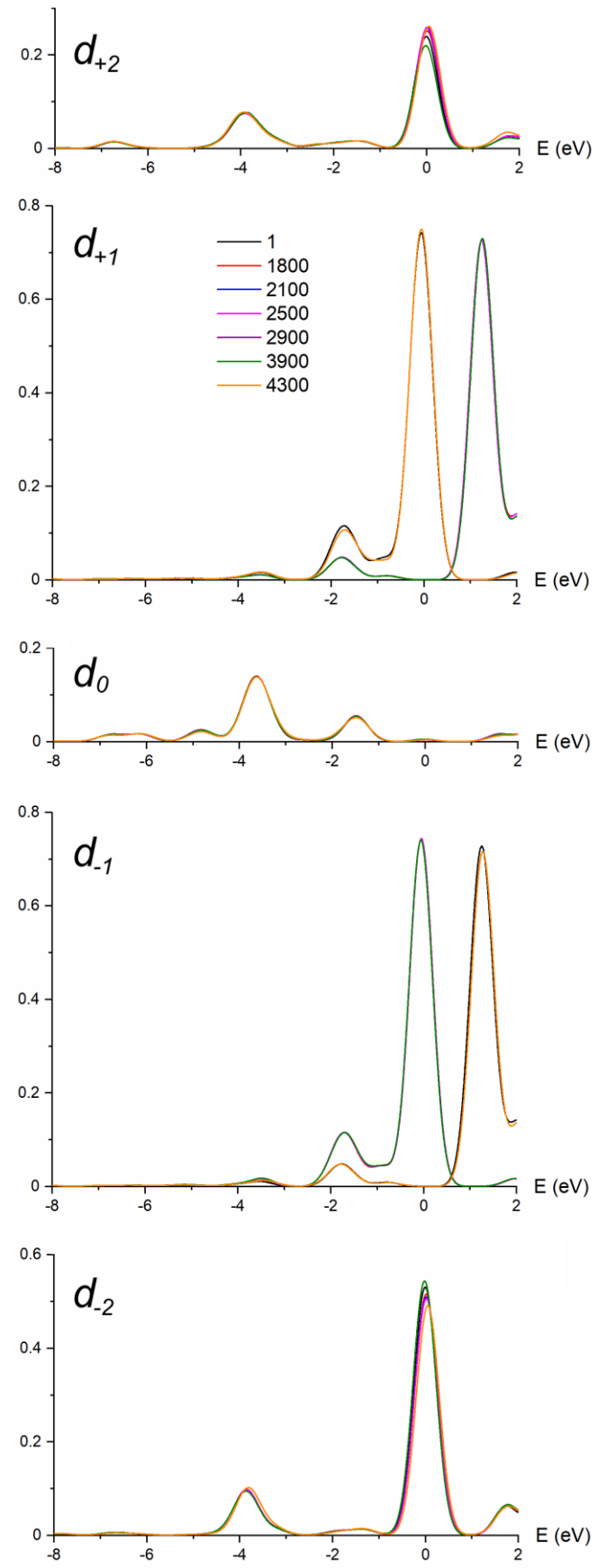

Figure S77. *Reported LDOS of the beta d-orbitals of the* Co^{II} *ions of* $\mathbf{1}_{cry,HS}$ *at the seven studied different pressures (p = 1, 1800, 2100, 2500, 2900, 3900, 4300 bar).*

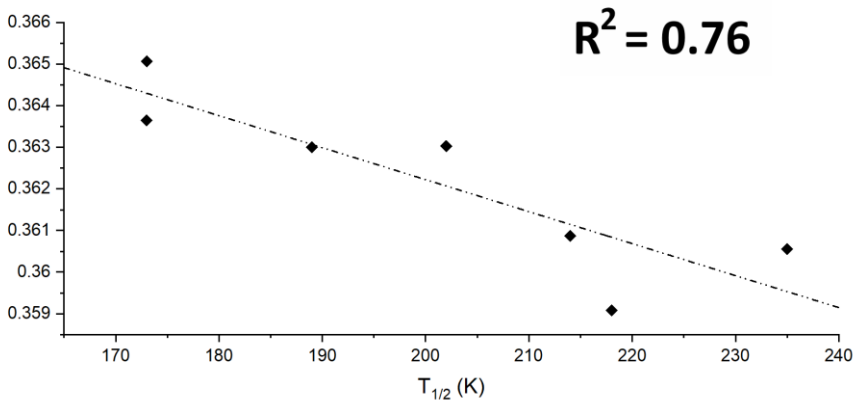

Figure S78. *Reported Intensity of the band of* ***1****$_{cry,LS}$ at -1.85 eV of Co(d$_0$) atomic orbitals vs the measured $T_{1/2}$. Trend line reports the [I vs. $T_{1/2}$] correlation factor (R^2 = 0.76).*

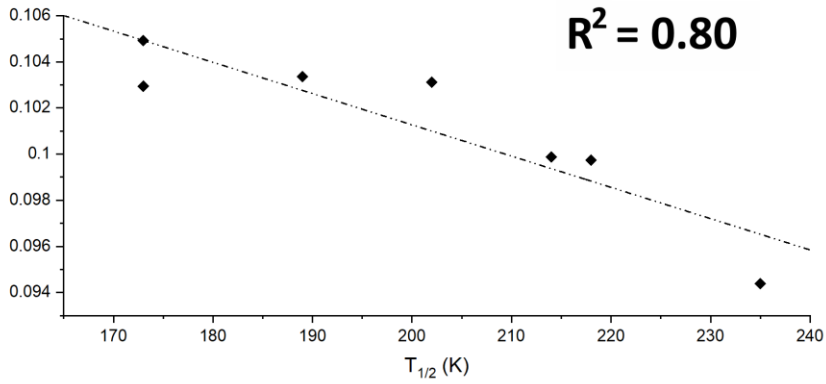

Figure S79. *Reported Intensity of the band of* ***1****$_{cry,HS}$ at -1.93 eV of Co(d$_0$) atomic orbitals vs the measured $T_{1/2}$. Trend line reports the [I vs. $T_{1/2}$] correlation factor (R^2 = 0.80).*

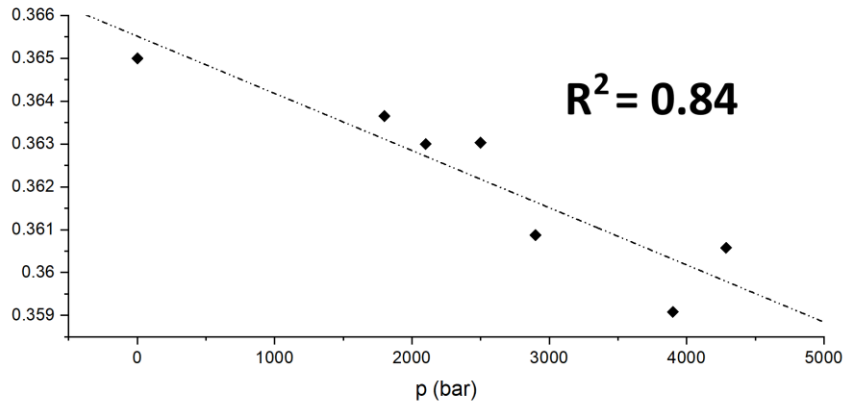

Figure S80. *Reported Intensity of the band of* ***1****$_{cry,LS}$ at -1.85 eV of Co(d$_0$) atomic orbitals vs the experimental pressures where the SCO phenomenon was monitored. Trend line reports the [I vs. p] correlation factor (R^2 = 0.84).*

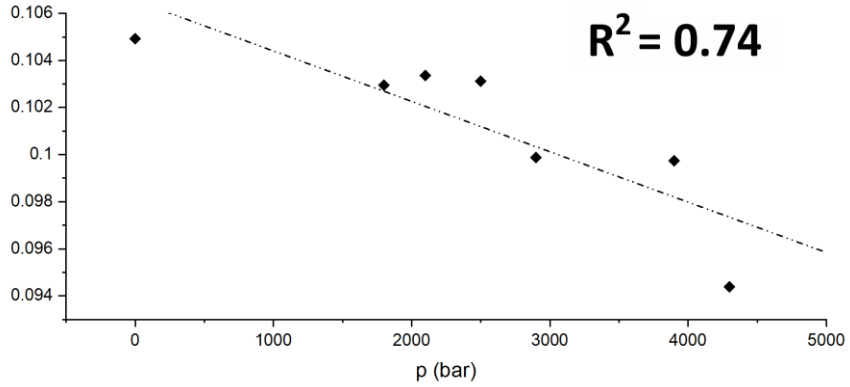

Figure S81. *Reported Intensity of the band of* ***1****$_{cry,HS}$ at -1.93 eV of Co(d$_0$) atomic orbitals vs the experimental pressures where the SCO phenomenon was monitored. Trend line reports the [I vs. p] correlation factor (R^2 = 0.74).*

3.2. LDOS: Nitrogen Atoms

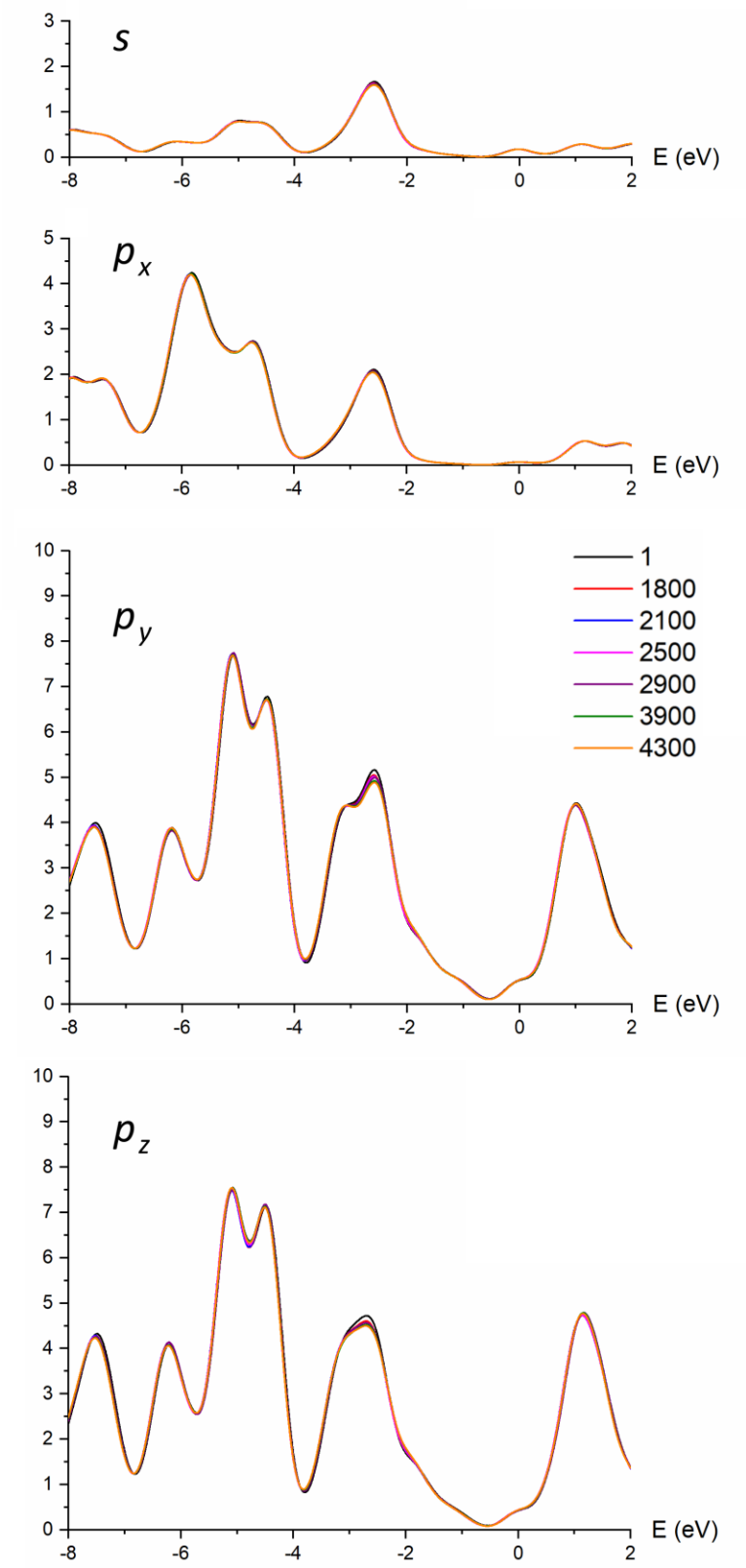

Figure S82. *Reported LDOS of the orbitals of the N atoms of* ***1****$_{cry,LS}$ at the seven studied different pressures (p = 1, 1800, 2100, 2500, 2900, 3900, 4300 bar).*

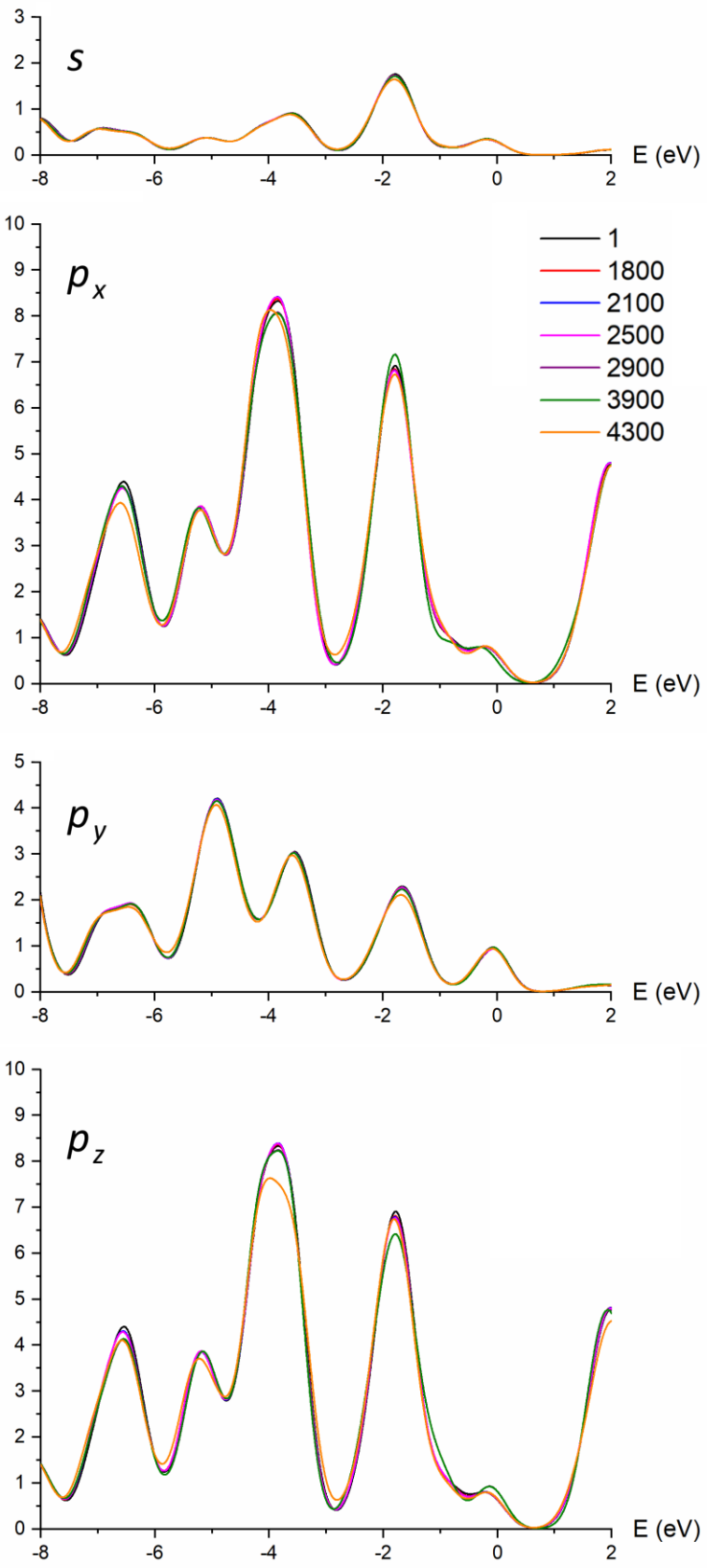

Figure S83. *Reported LDOS of the orbitals of the N atoms of* ***1****$_{cry,HS}$ at the seven studied different pressures (p = 1, 1800, 2100, 2500, 2900, 3900, 4300 bar).*

3.3. LDOS: Carbon Atoms

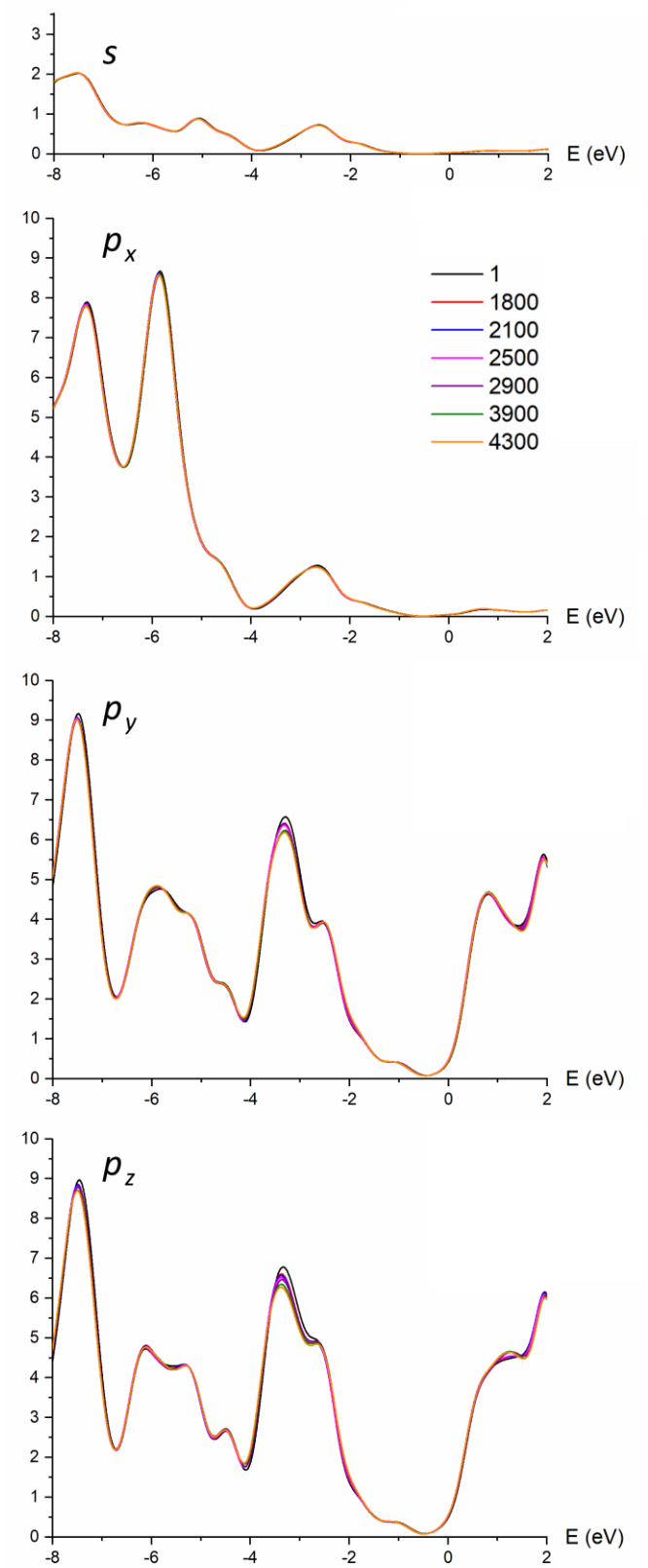

Figure S84. *Reported LDOS of the orbitals of the C atoms of* ***1****$_{cry,LS}$ at the seven studied different pressures (p = 1, 1800, 2100, 2500, 2900, 3900, 4300 bar).*

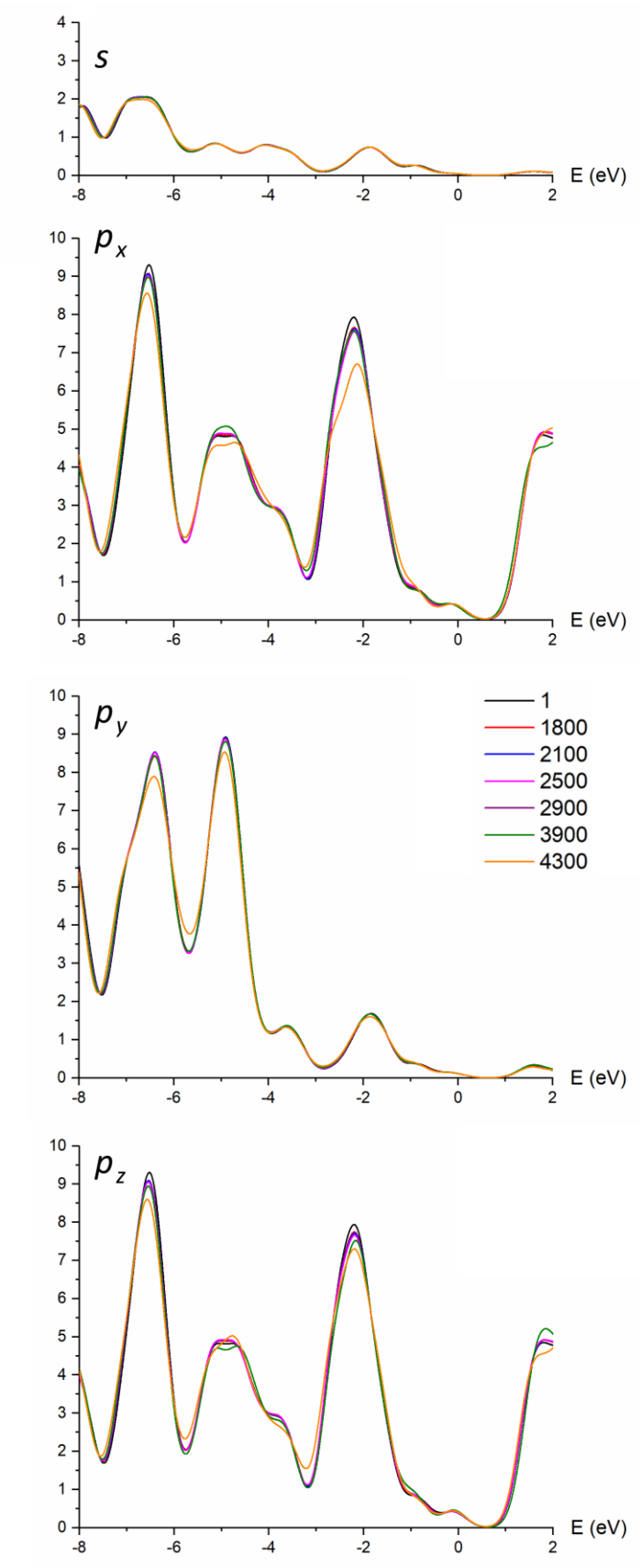

Figure S85. *Reported LDOS of the orbitals of the C atoms of* ***1****$_{cry,HS}$ at the seven studied different pressures (p = 1, 1800, 2100, 2500, 2900, 3900, 4300 bar).*

3.2. Molecular Orbitals of [Co(dpzca)$_2$]

Table S12. *Reported metal-centred MOs contributing to the main peak at 1.9eV in* ***1$_{cry,LS}$*** and ***1$_{cry,HS}$*** *TDOS (Figure 7). Last three columns on the right reports the correlation factor of the MOs energies against all seven employed different pressures; six different pressures (excluding results for p = 3900 bar); and the seven different measured $T_{1/2}$.*

p / bar		***1***	***1800***	***2100***	***2500***	***2900***	***3900***	***4300***	***R^2 (p) (all pressures)***	***R^2 (p) (p = 3900 bar excluded)***	***R^2 ($T_{1/2}$)***
$T_{1/2}$(exp.) / K		***173***	***173***	***189***	***202***	***214***	***227***	***235***			
1$_{cry,LS}$	277β	-2.08711	-1.9946	-1.98643	-1.97011	-1.94562	-1.91296	-1.90208	0.99 (Fig. S88)	0.99 (Fig. S88)	0.79 (Fig. S106)
	278β	-2.09528	-2.02181	-2.01364	-2.00004	-1.95378	-1.92929	-1.9184	0.98 (Fig. S89)	0.97 (Fig. S89)	0.85 (Fig. S107)
	279β	-2.09528	-2.02997	-2.01909	-2.0082	-1.95922	-1.94017	-1.92929	0.97 (Fig. S90)	0.96 (Fig. S90)	0.86 (Fig. S108)
	280β	-2.10072	-2.03813	-2.02725	-2.01909	-1.98915	-1.94017	-1.92929	0.98 (Fig. S91)	0.98 (Fig. S91)	0.85 (Fig. S109)
1$_{cry,HS}$	270α	-2.65311	-2.57964	-2.56604	-2.54971	-2.49801	-2.49529	-2.33746	0.82 (Fig. S92)	0.89 (Fig. S92)	0.84 (Fig. S110)
	271α	-2.64767	-2.5742	-2.56059	-2.54699	-2.49256	-2.48984	-2.31569	0.79 (Fig. S93)	0.88 (Fig. S93)	0.83 (Fig. S111)
	272α	-2.64495	-2.5742	-2.55787	-2.54154	-2.46807	-2.46535	-2.31569	0.84 (Fig. S94)	0.89 (Fig. S94)	0.88 (Fig. S112)
	273α	-2.6259	-2.54699	-2.53066	-2.54154	-2.46807	-2.46535	-2.25038	0.73 (Fig. S95)	0.83 (Fig. S95)	0.77 (Fig. S113)
	274α	-2.61502	-2.54154	-2.52522	-2.51161	-2.45991	-2.45719	-2.23678	0.74 (Fig. S96)	0.84 (Fig. S96)	0.79 (Fig. S114)
	275α	-2.61502	-2.53882	-2.52522	-2.50889	-2.45447	-2.45175	-2.22861	0.74 (Fig. S97)	0.84 (Fig. S97)	0.79 (Fig. S115)
	276α	-2.61229	-2.53882	-2.5225	-2.50889	-2.42726	-2.42454	-2.22861	0.79 (Fig. S98)	0.85 (Fig. S98)	0.85 (Fig. S116)
	273β	-2.24222	-2.16603	-2.1497	-2.13337	-2.098	-2.09256	-1.89391	0.75 (Fig. S99)	0.86 (Fig. S99)	0.79 (Fig. S117)
	274β	-2.2395	-2.16331	-2.14698	-2.13337	-2.08439	-2.07895	-1.88847	0.78 (Fig. S100)	0.87 (Fig. S100)	0.81 (Fig. S118)
	275β	-2.23406	-2.16059	-2.14426	-2.12793	-2.08167	-2.07895	-1.86942	0.75 (Fig. S101)	0.85 (Fig. S101)	0.80 (Fig. S119)
	276β	-2.21773	-2.14426	-2.12521	-2.1116	-2.08167	-2.07895	-1.8667	0.72 (Fig. S102)	0.85 (Fig. S102)	0.76 (Fig. S120)
	277β	-2.098	-2.01636	-1.99732	-1.98643	-1.92385	-1.92112	-1.73337	0.80 (Fig. S103)	0.88 (Fig. S103)	0.83 (Fig. S121)
	279β	-2.08167	-2.00004	-1.98371	-1.96738	-1.91296	-1.90752	-1.72248	0.80 (Fig. S104)	0.88 (Fig. S104)	0.83 (Fig. S122)
	280β	-2.07895	-1.99732	-1.98099	-1.96738	-1.91024	-1.9048	-1.70615	0.78 (Fig. S105)	0.87 (Fig. S105)	0.82 (Fig. S123)

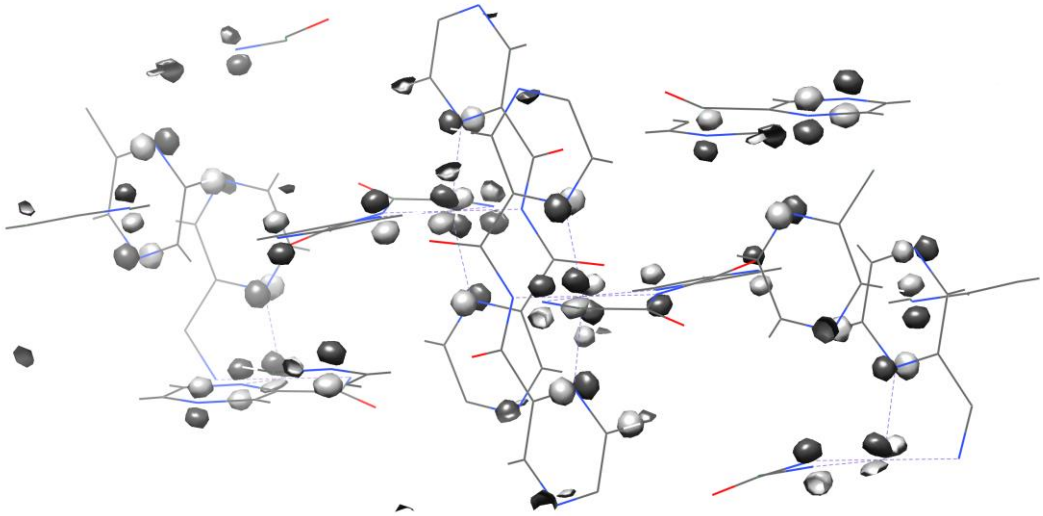

Figure S86. *Plotted MOs 277α (t_{2g} shaped) for* ***1****$_{cry,HS}$ calculated at the pressure of 1bar (ρ cutoff = 0.04).*

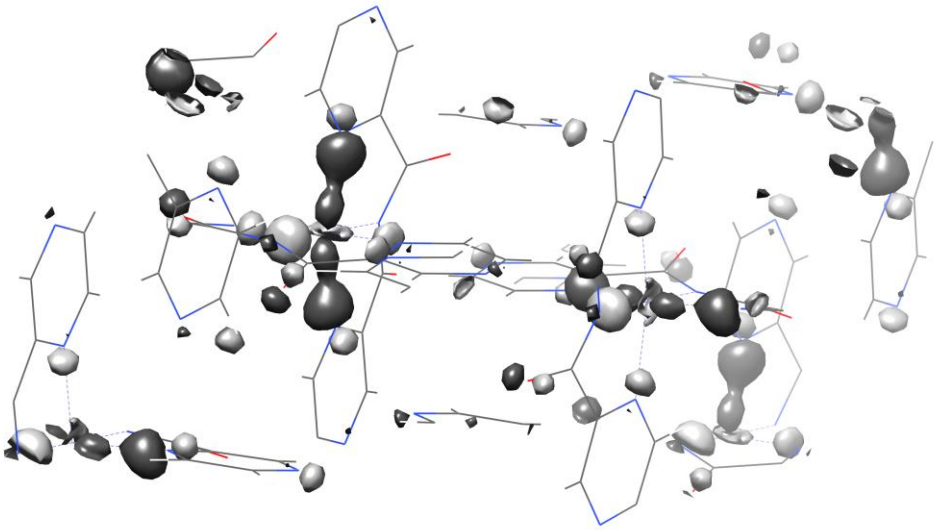

Figure S87. *Plotted MOs 277β (e_g shaped) for* ***1****$_{cry,HS}$ calculated at the pressure of 1bar (ρ cutoff = 0.04).*

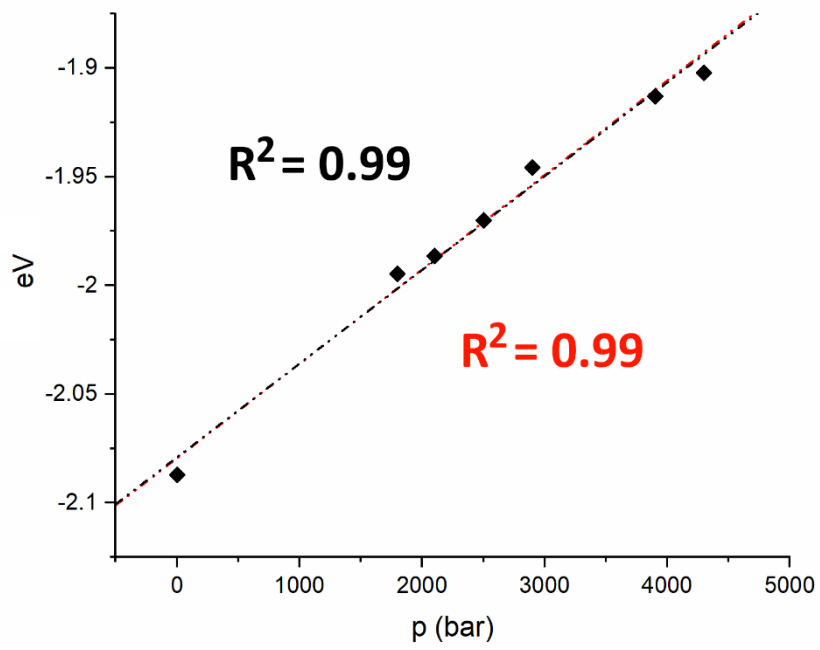

Figure S88. *Reported trend for the variation of MO-277β in* ***1****$_{cry,LS}$ at seven different pressures (R^2 = 0.99) and six different pressures (except p = 3900 bar, R^2 = 0.99).*

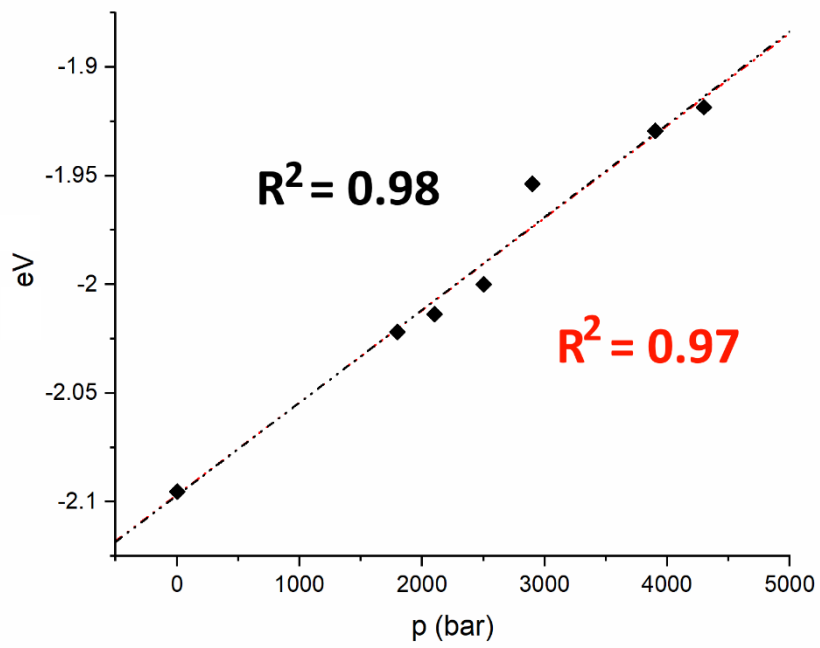

Figure S89. *Reported trend for the variation of MO-278β in* ***1****$_{cry,LS}$ at seven different pressures (R^2 = 0.98) and six different pressures (except p = 3900 bar, R^2 = 0.97).*

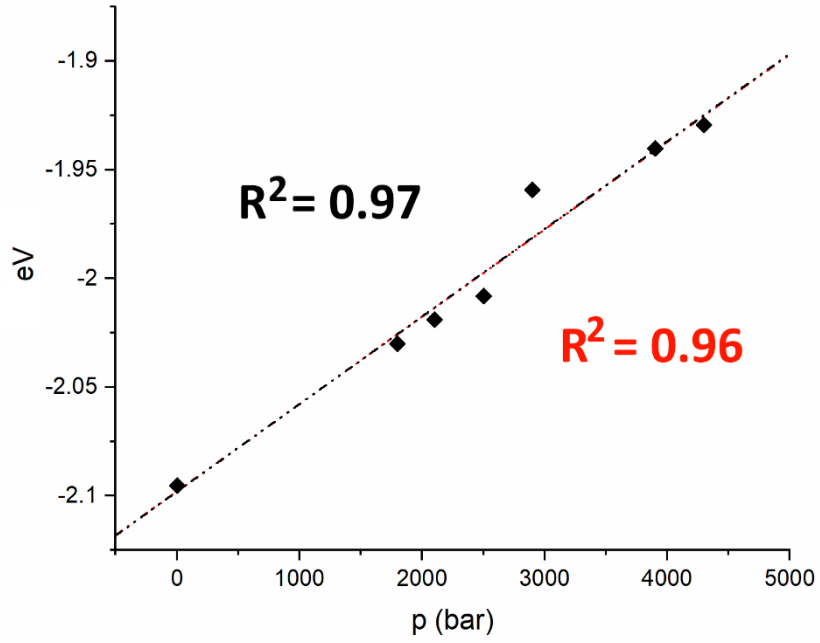

Figure S90. *Reported trend for the variation of MO-279β in* ***1****$_{cry,LS}$ at seven different pressures (R^2 = 0.97) and six different pressures (except p = 3900 bar, R^2 = 0.96).*

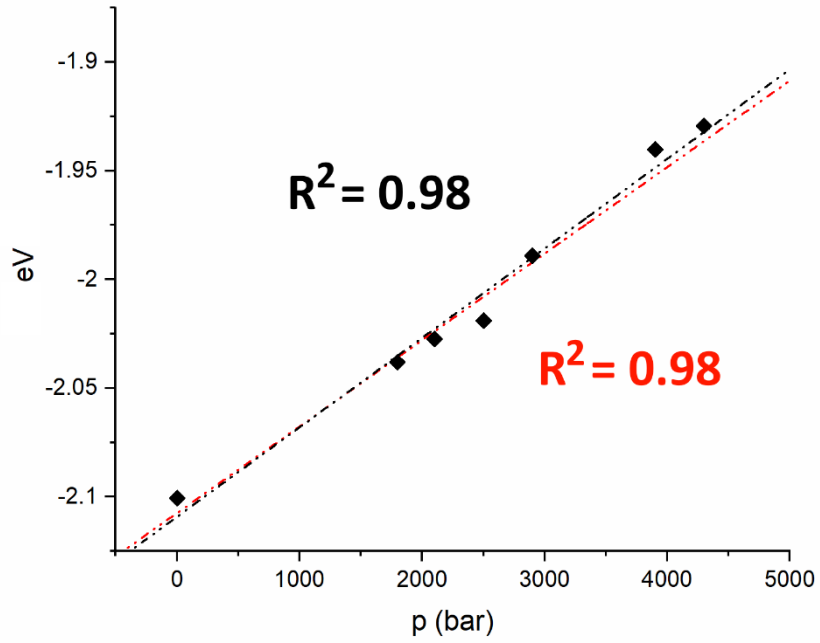

Figure S91. *Reported trend for the variation of MO-280β in* ***1****$_{cry,LS}$ at seven different pressures (R^2 = 0.98) and six different pressures (except p = 3900 bar, R^2 = 0.98).*

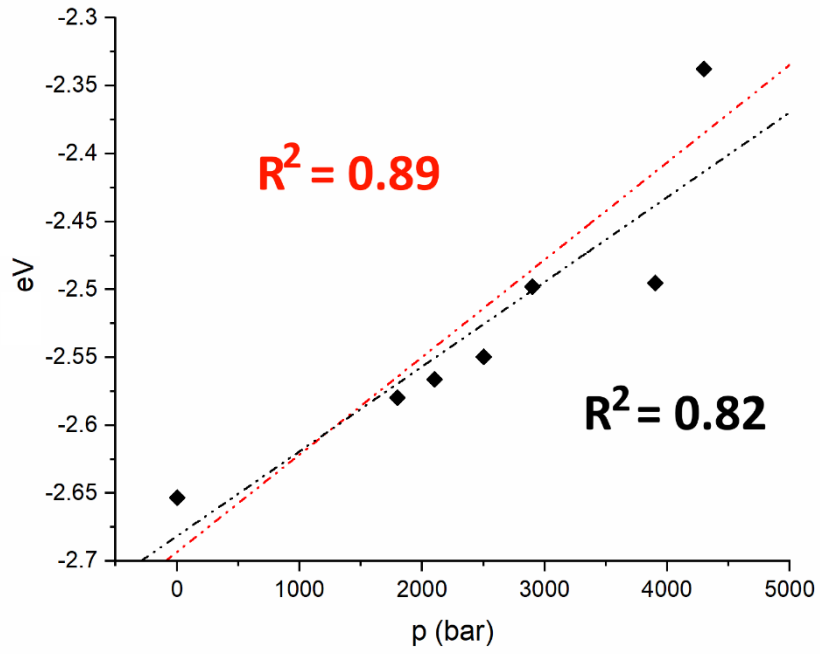

Figure S92. *Reported trend for the variation of MO-270α in* ***1****$_{cry,HS}$ at seven different pressures (R^2 = 0.82) and six different pressures (except p = 3900 bar, R^2 = 0.89).*

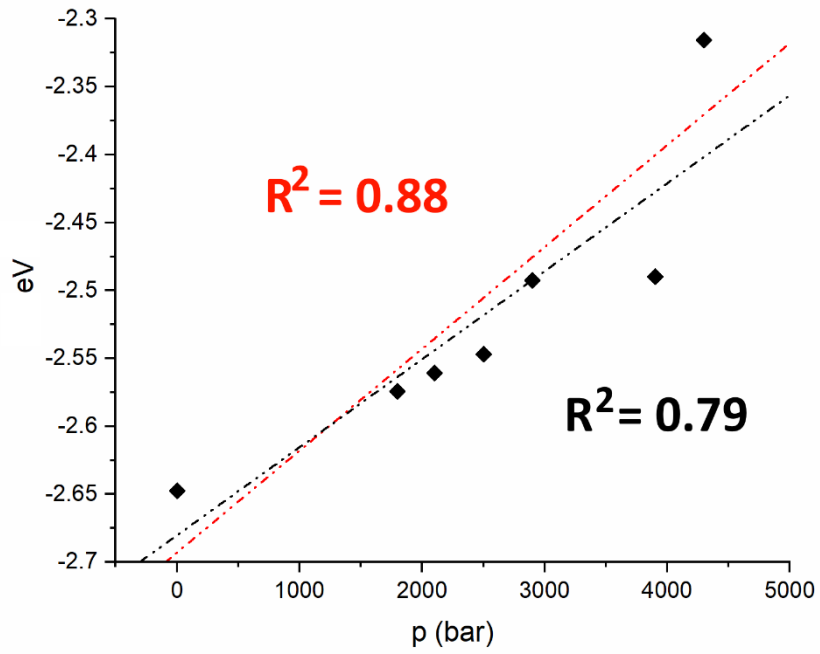

Figure S93. *Reported trend for the variation of MO-271α in* ***1****$_{cry,HS}$ at seven different pressures (R^2 = 0.79) and six different pressures (except p = 3900 bar, R^2 = 0.88).*

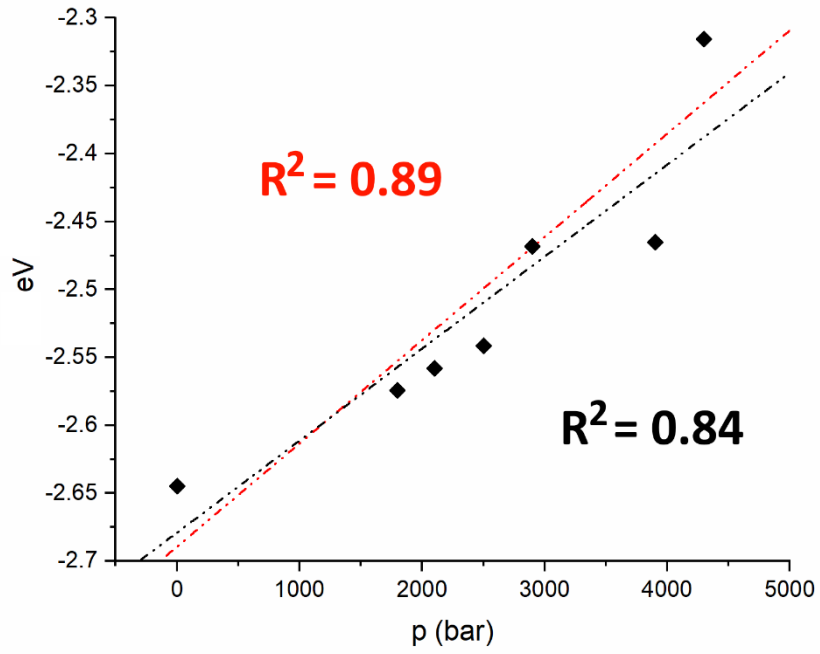

Figure S94. *Reported trend for the variation of MO-272α in* $\mathbf{1}_{cry,HS}$ *at seven different pressures* (R^2 = 0.84) *and six different pressures (except p = 3900 bar,* R^2 = 0.89).

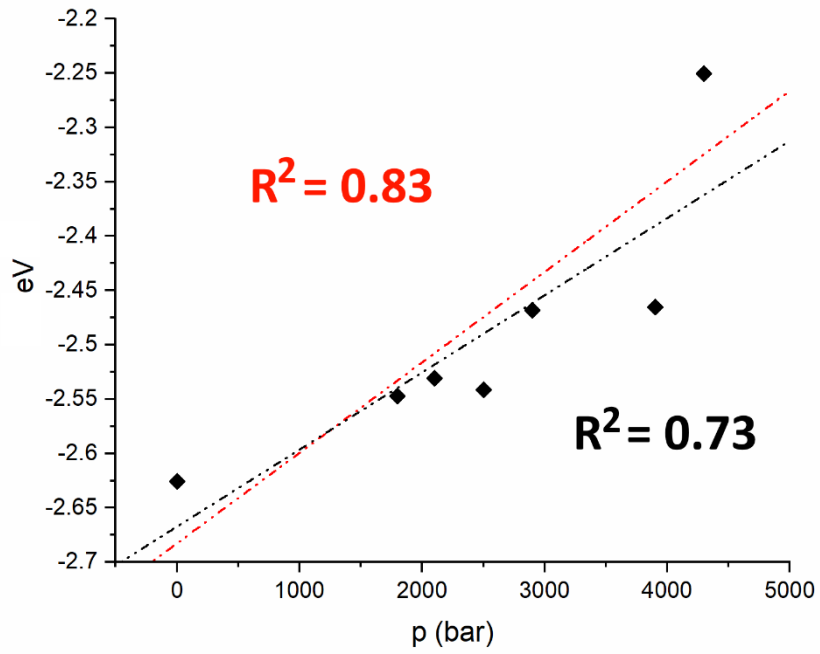

Figure S95. *Reported trend for the variation of MO-273α in* $\mathbf{1}_{cry,HS}$ *at seven different pressures* (R^2 = 0.73) *and six different pressures (except p = 3900 bar,* R^2 = 0.83).

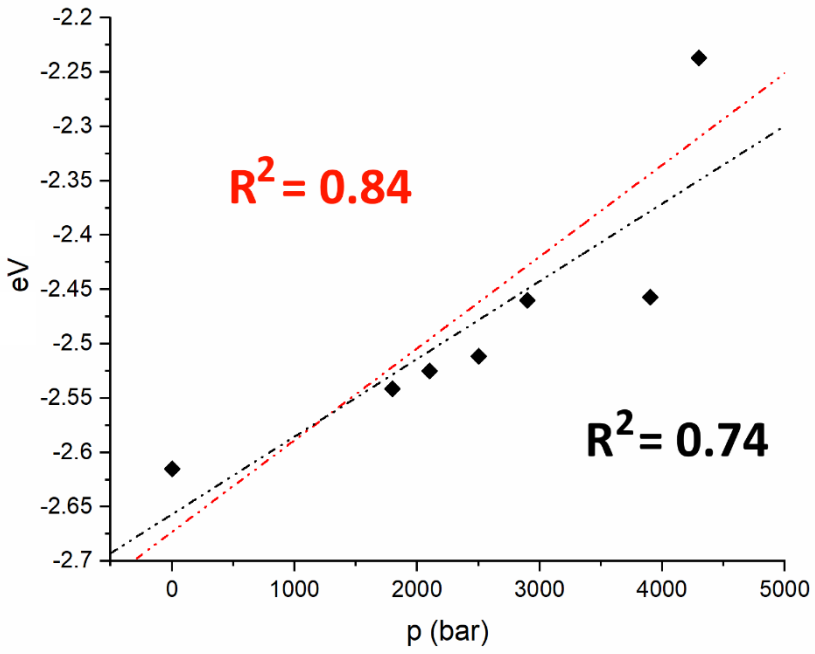

Figure S96. *Reported trend for the variation of MO-274α in* $\mathbf{1}_{cry,HS}$ *at seven different pressures* (R^2 = 0.74) *and six different pressures (except p = 3900 bar,* R^2 = 0.84).

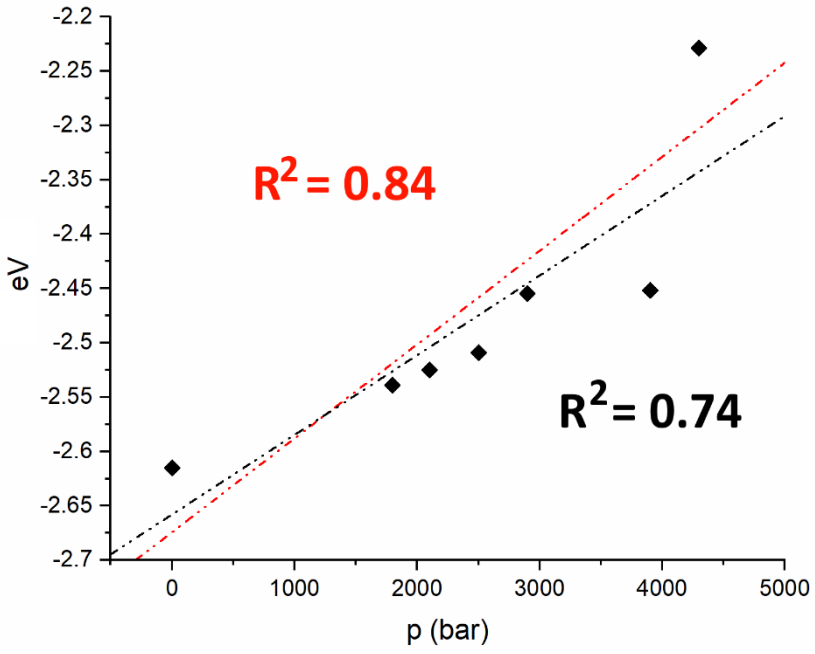

Figure S97. *Reported trend for the variation of MO-275α in* $\mathbf{1}_{cry,HS}$ *at seven different pressures* (R^2 = 0.74) *and six different pressures (except p = 3900 bar,* R^2 = 0.84).

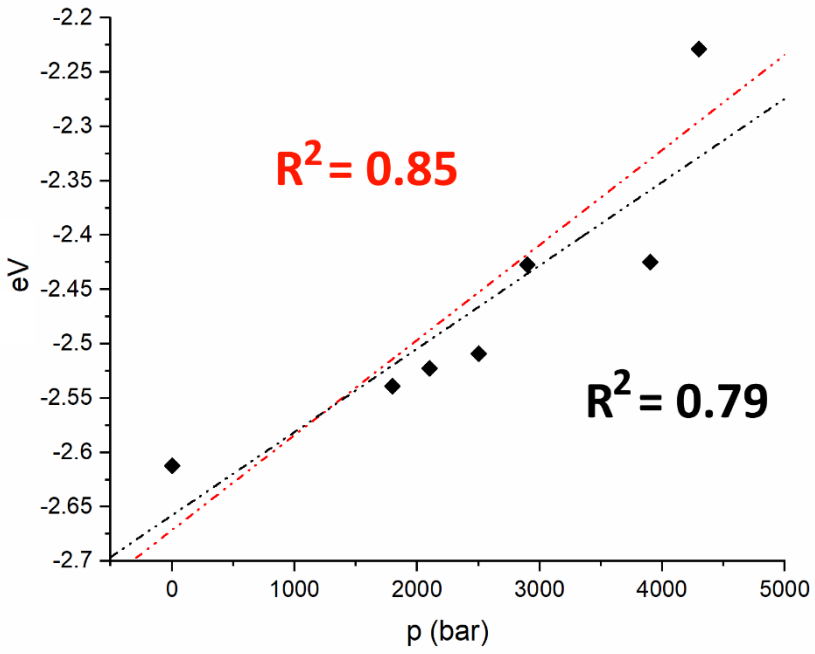

Figure S98. *Reported trend for the variation of MO-276α in* $\mathbf{1}_{cry,HS}$ *at seven different pressures* (R^2 = 0.79) *and six different pressures (except p = 3900 bar,* R^2 = 0.85).

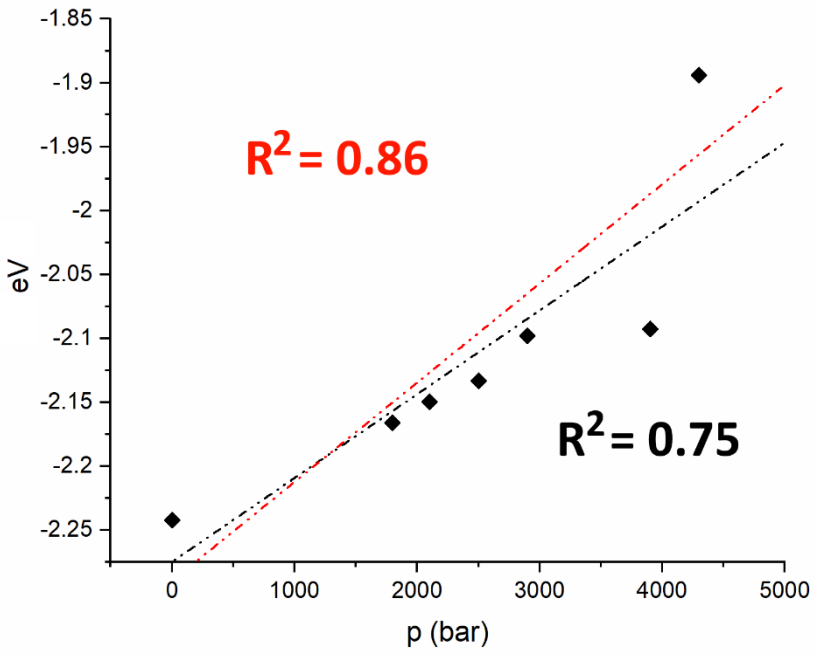

Figure S99. *Reported trend for the variation of MO-273β in* $\mathbf{1}_{cry,HS}$ *at seven different pressures* (R^2 = 0.75) *and six different pressures (except p = 3900 bar,* R^2 = 0.86).

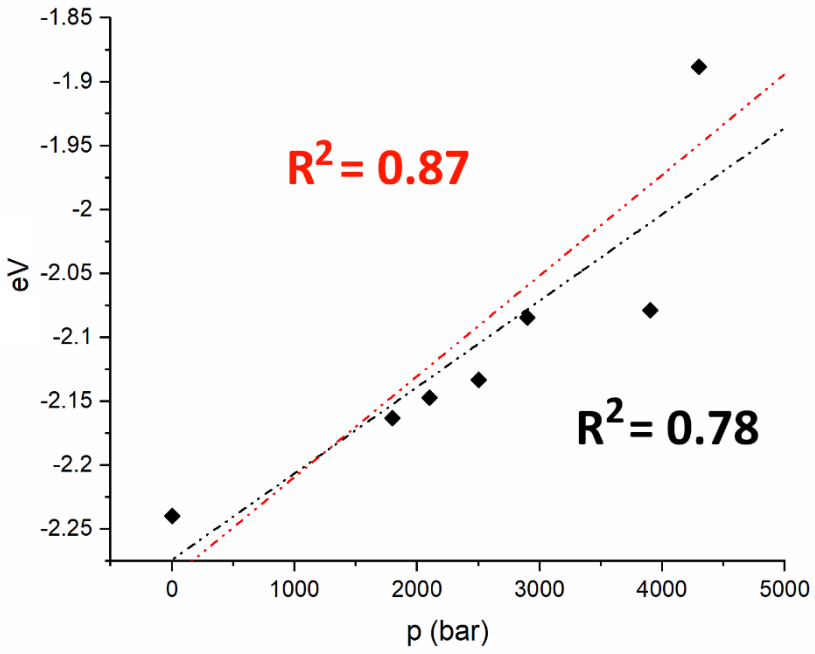

Figure S100. *Reported trend for the variation of MO-274β in* $\mathbf{1}_{cry,HS}$ *at seven different pressures* (R^2 = 0.78) *and six different pressures (except p = 3900 bar,* R^2 = 0.87).

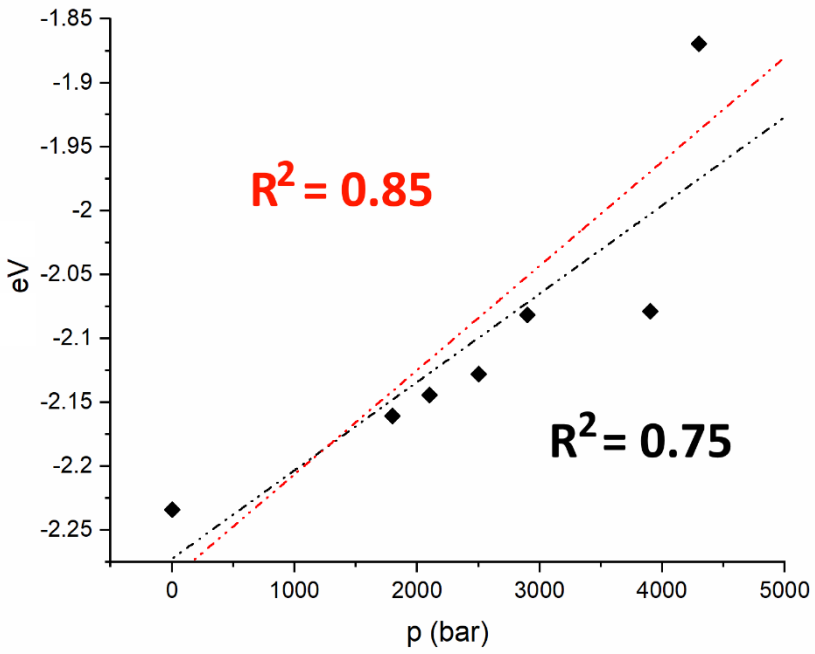

Figure S101. *Reported trend for the variation of MO-275β in* $\mathbf{1}_{cry,HS}$ *at seven different pressures* (R^2 = 0.75) *and six different pressures (except p = 3900 bar,* R^2 = 0.85).

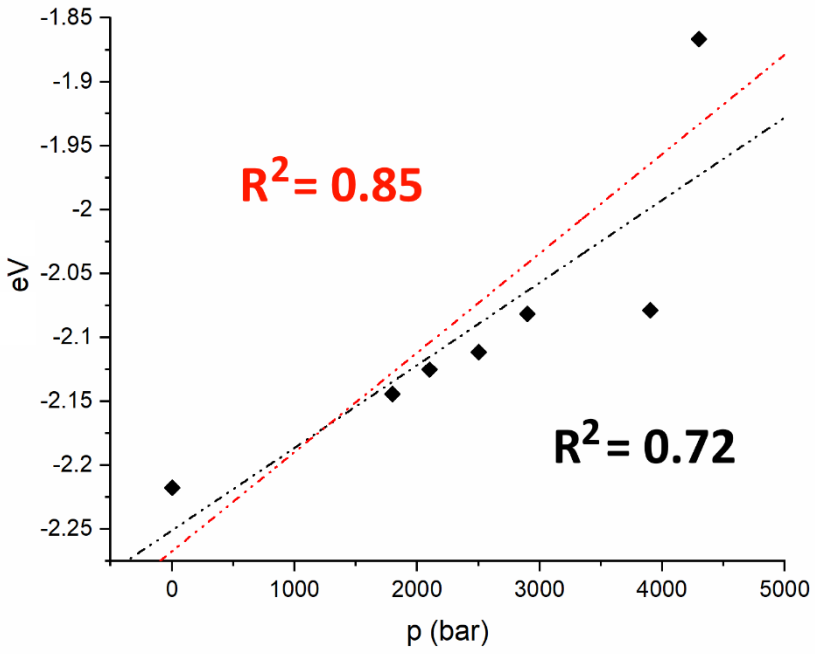

Figure S102. *Reported trend for the variation of MO-276β in* $\mathbf{1}_{cry,HS}$ *at seven different pressures* (R^2 = 0.72) *and six different pressures (except p = 3900 bar,* R^2 = 0.85).

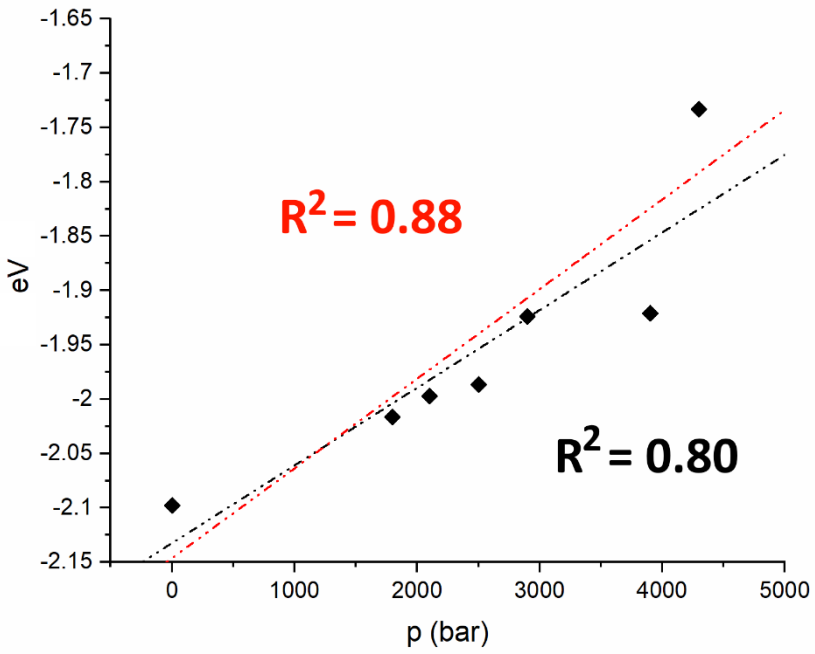

Figure S103. *Reported trend for the variation of MO-277β in* $\mathbf{1}_{cry,HS}$ *at seven different pressures* (R^2 = 0.80) *and six different pressures (except p = 3900 bar,* R^2 = 0.88).

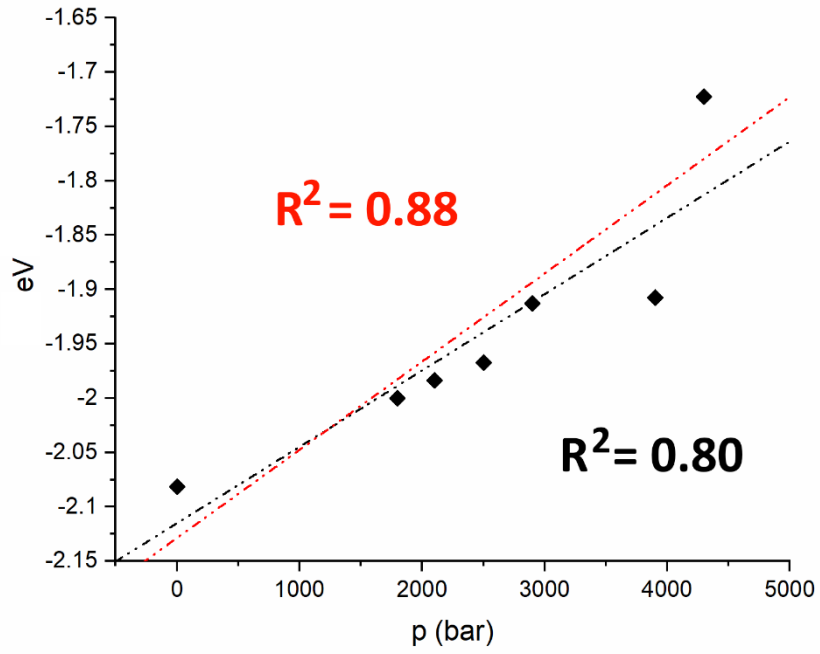

Figure S104. *Reported trend for the variation of MO-279β in* $\mathbf{1}_{cry,HS}$ *at seven different pressures* (R^2 = 0.80) *and six different pressures (except p = 3900 bar,* R^2 = 0.88).

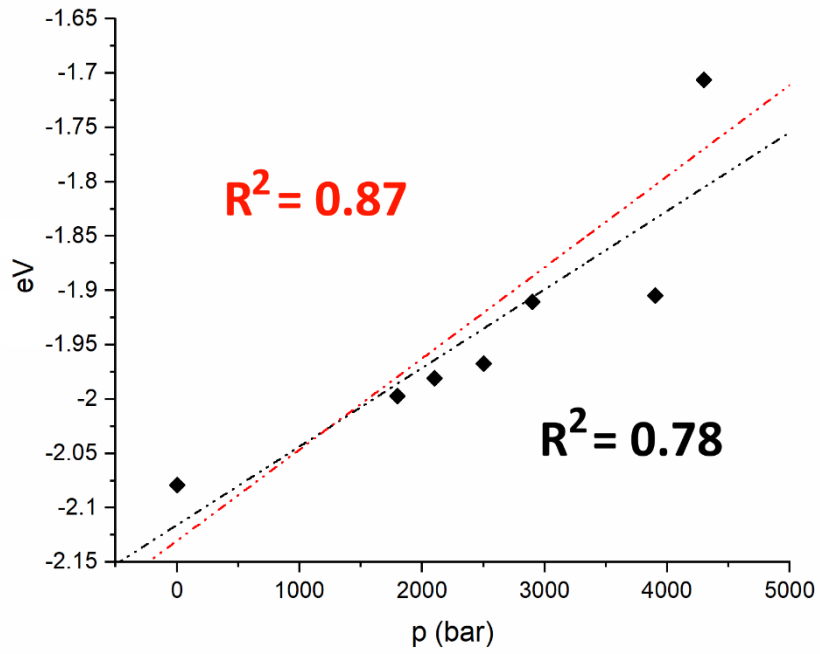

Figure S105. *Reported trend for the variation of MO-280β in* $\mathbf{1}_{cry,HS}$ *at seven different pressures* (R^2 = 0.78) *and six different pressures (except p = 3900 bar,* R^2 = 0.87).

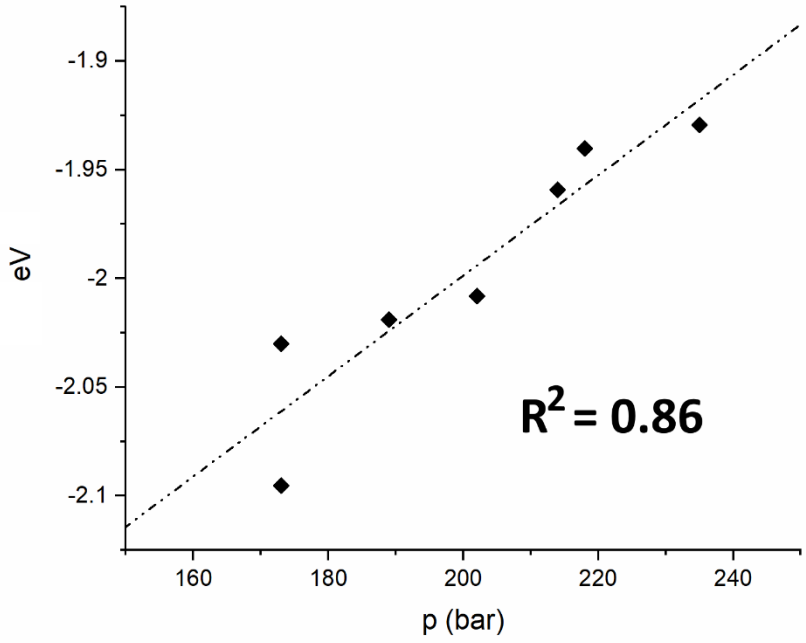

Figure S106. *Reported trend for the variation of MO-279β in* ***1****$_{cry,LS}$ versus the measured* $T_{1/2}$ *at seven different pressures* (R^2 *= 0.86).*

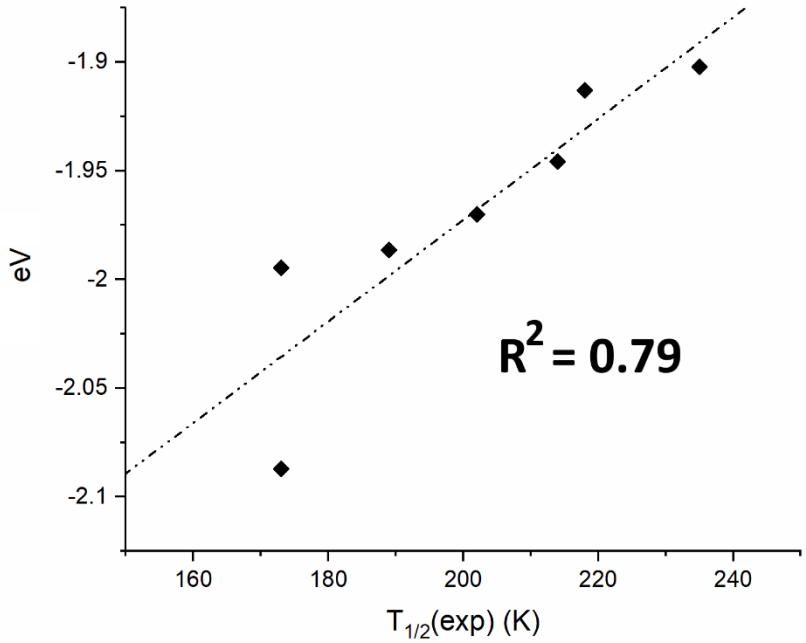

Figure S107. *Reported trend for the variation of MO-277β in* ***1****$_{cry,LS}$ versus the measured* $T_{1/2}$ *at seven different pressures* (R^2 *= 0.79).*

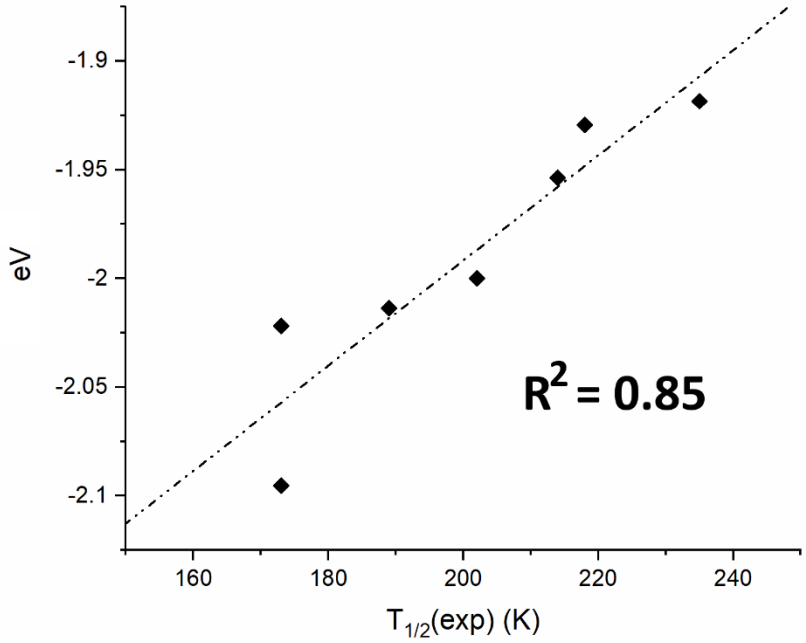

Figure S108. *Reported trend for the variation of MO-278β in* ***1****$_{cry,LS}$ versus the measured* $T_{1/2}$ *at seven different pressures* (R^2 *= 0.85).*

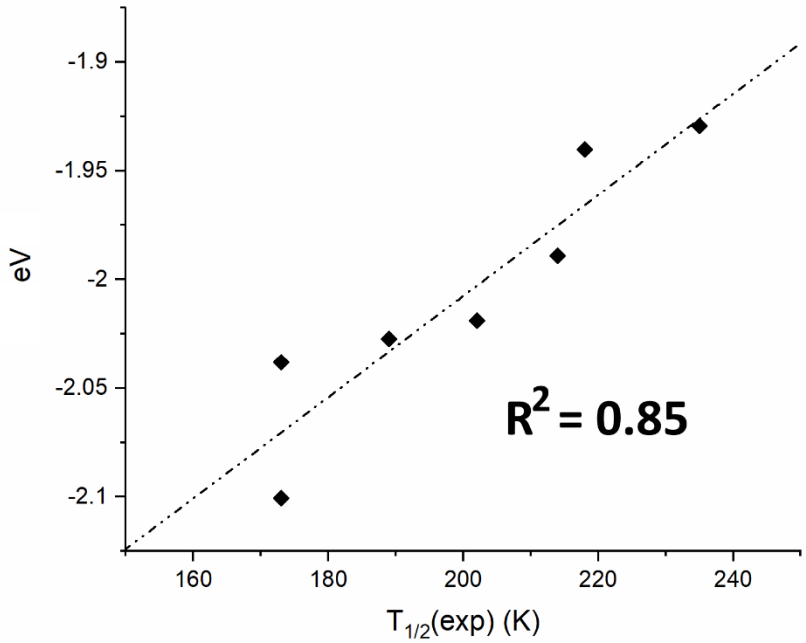

Figure S109. *Reported trend for the variation of MO-280β in* ***1****$_{cry,LS}$ versus the measured* $T_{1/2}$ *at seven different pressures* (R^2 *= 0.85).*

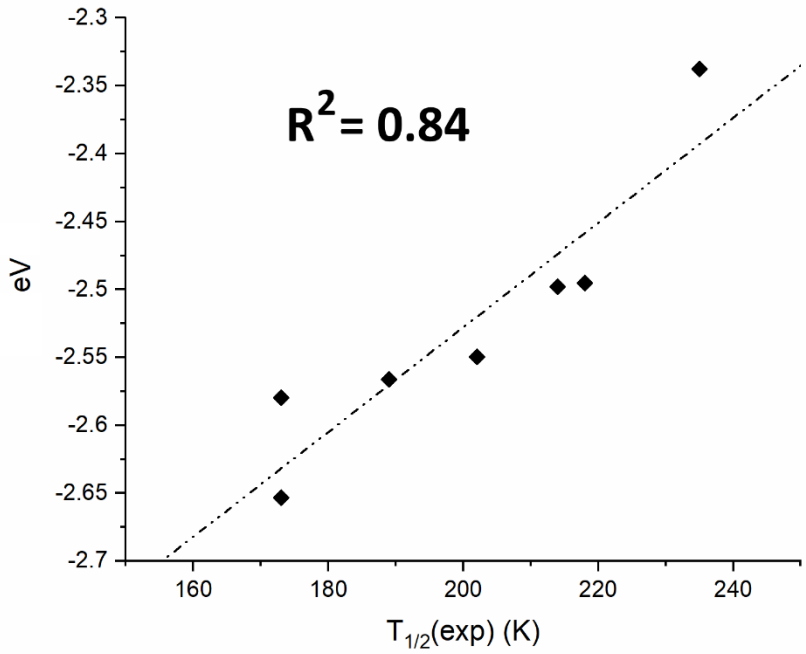

Figure S110. *Reported trend for the variation of MO-270α in* $\mathbf{1}_{cry,HS}$ *versus the measured* $T_{1/2}$ *at seven different pressures* (R^2 = 0.84).

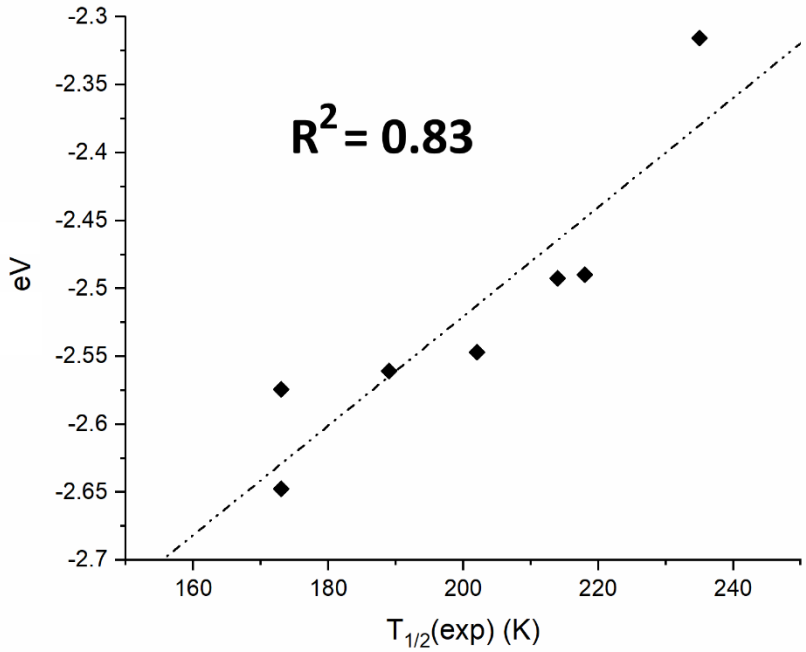

Figure S111. *Reported trend for the variation of MO-271α in* $\mathbf{1}_{cry,HS}$ *versus the measured* $T_{1/2}$ *at seven different pressures* (R^2 = 0.83).

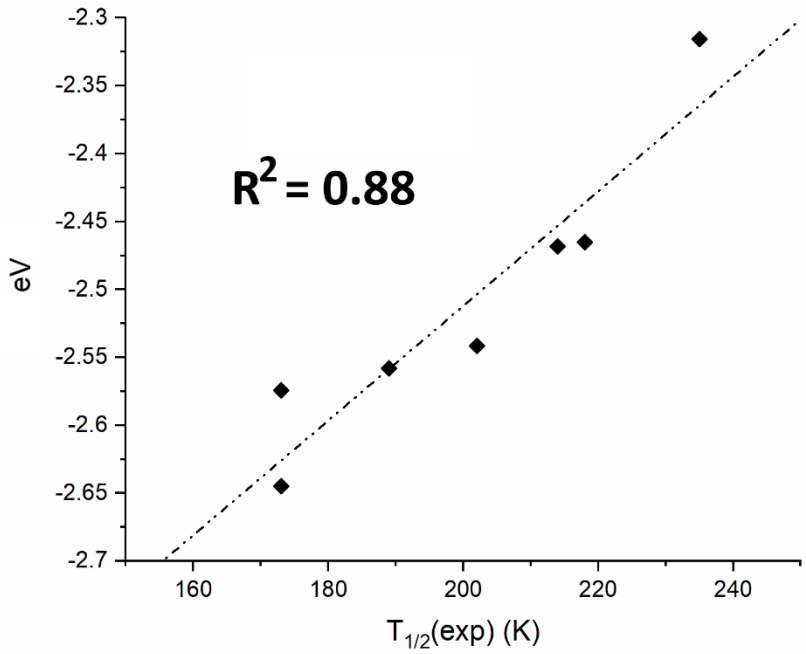

Figure S112. *Reported trend for the variation of MO-272α in* $\mathbf{1}_{cry,HS}$ *versus the measured* $T_{1/2}$ *at seven different pressures* (R^2 = 0.88).

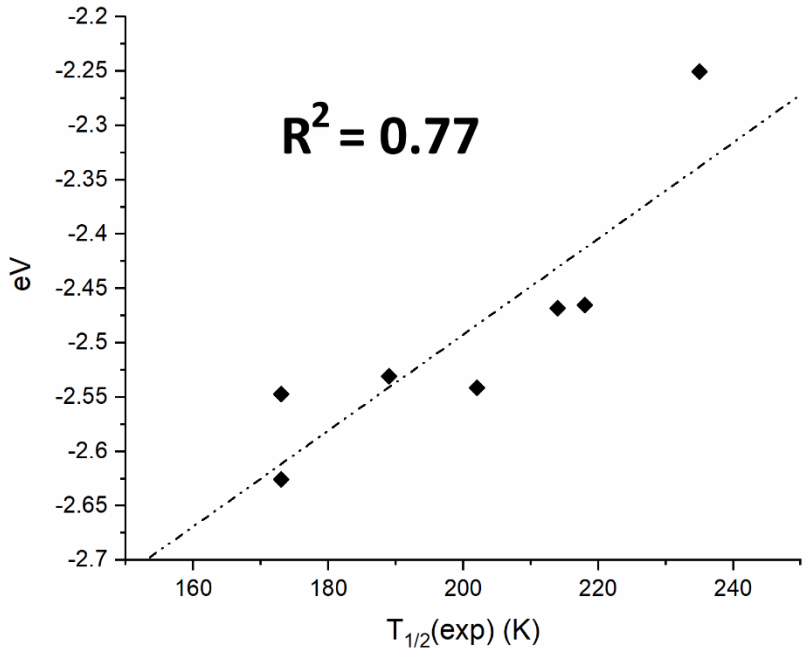

Figure S113. *Reported trend for the variation of MO-273α in* $\mathbf{1}_{cry,HS}$ *versus the measured* $T_{1/2}$ *at seven different pressures* (R^2 = 0.77).

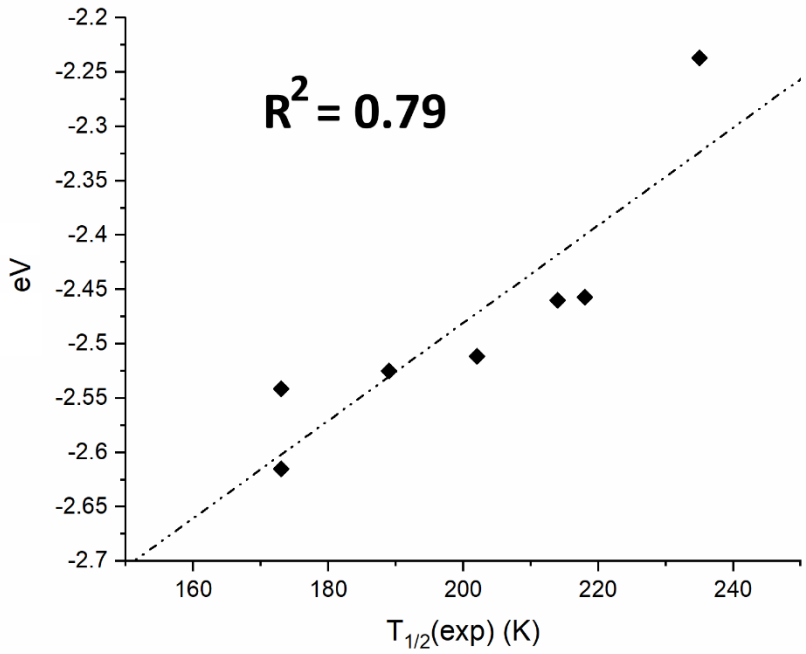

Figure S114. *Reported trend for the variation of MO-274α in* $\mathbf{1}_{cry,HS}$ *versus the measured* $T_{1/2}$ *at seven different pressures* (R^2 *= 0.79).*

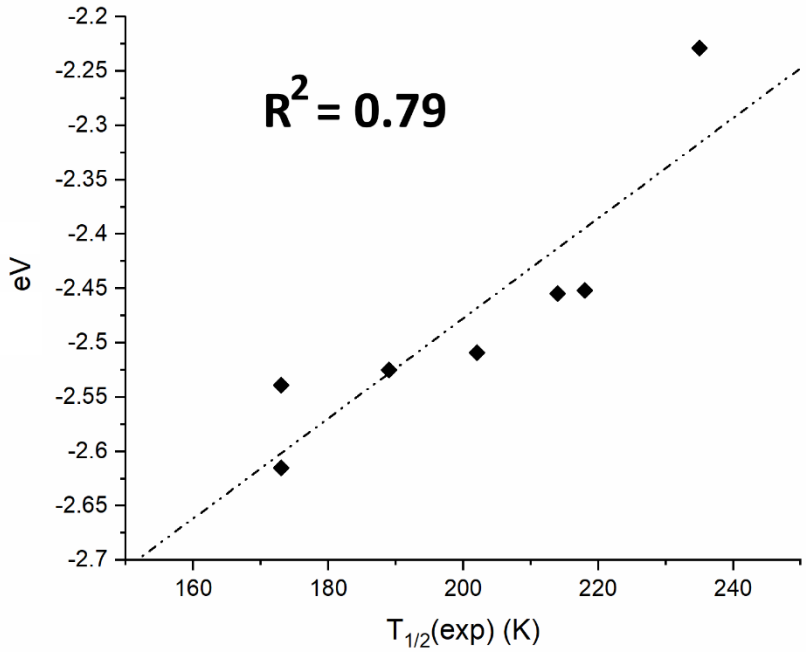

Figure S115. *Reported trend for the variation of MO-275α in* $\mathbf{1}_{cry,HS}$ *versus the measured* $T_{1/2}$ *at seven different pressures* (R^2 *= 0.79).*

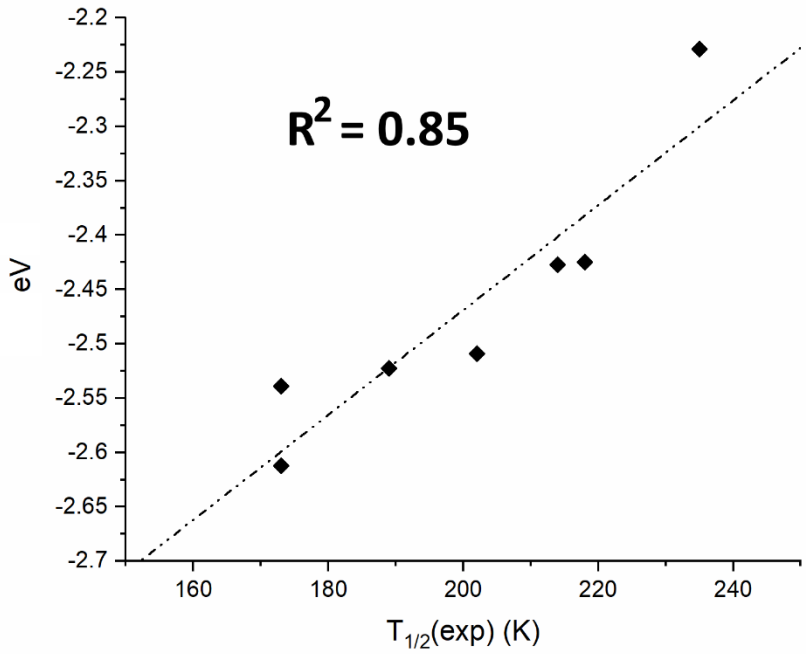

Figure S116. *Reported trend for the variation of MO-276α in* $\mathbf{1}_{cry,HS}$ *versus the measured* $T_{1/2}$ *at seven different pressures* (R^2 *= 0.85).*

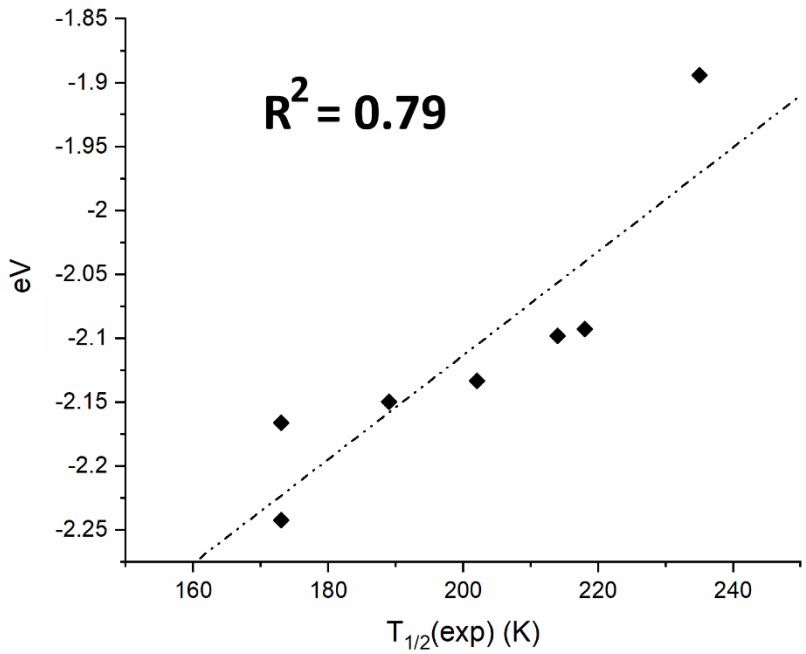

Figure S117. *Reported trend for the variation of MO-273β in* $\mathbf{1}_{cry,HS}$ *versus the measured* $T_{1/2}$ *at seven different pressures* (R^2 *= 0.79).*

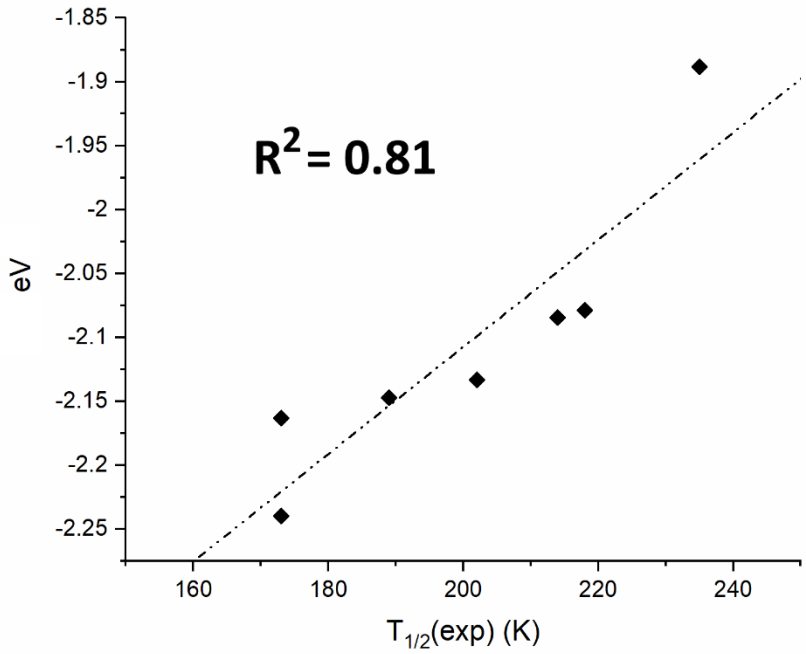

Figure S118. *Reported trend for the variation of MO-274β in* $\mathbf{1}_{cry,HS}$ *versus the measured* $T_{1/2}$ *at seven different pressures* (R^2 *= 0.81).*

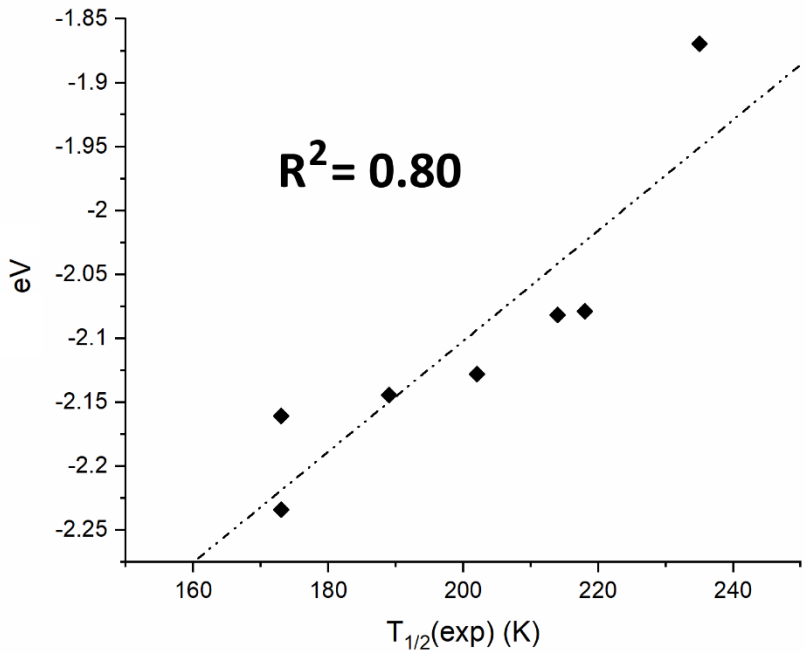

Figure S119. *Reported trend for the variation of MO-275β in* $\mathbf{1}_{cry,HS}$ *versus the measured* $T_{1/2}$ *at seven different pressures* (R^2 *= 0.80).*

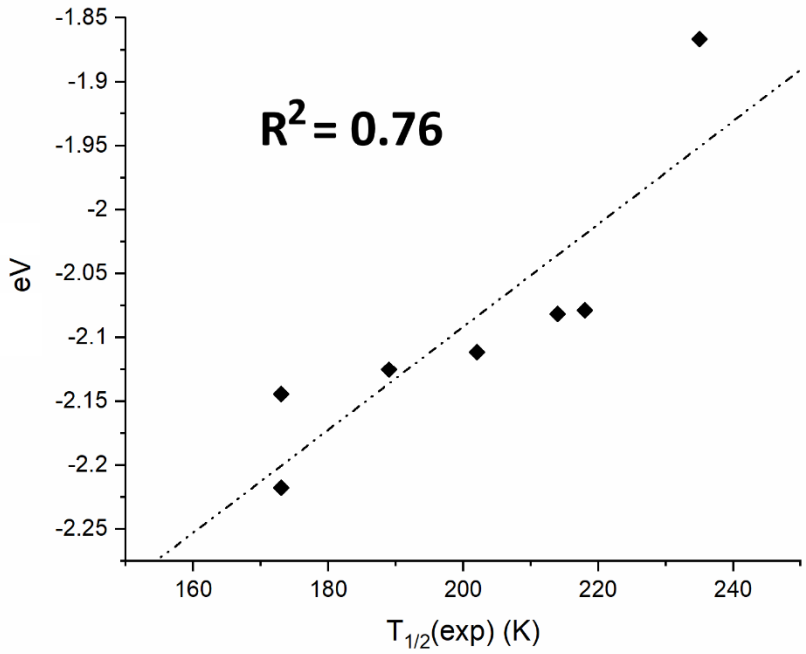

Figure S120. *Reported trend for the variation of MO-276β in* ***1****$_{cry,HS}$ versus the measured* $T_{1/2}$ *at seven different pressures* (R^2 *= 0.76).*

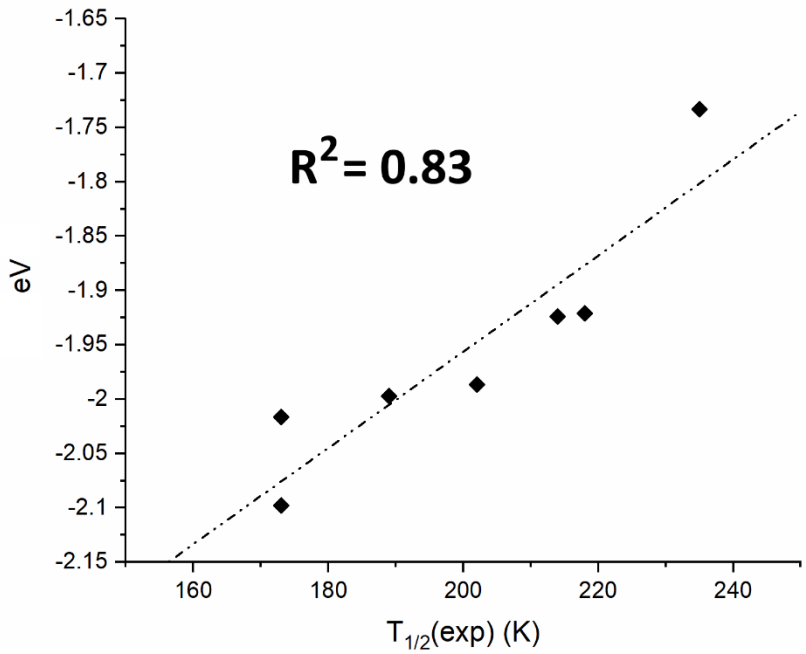

Figure S121. *Reported trend for the variation of MO-277β in* ***1****$_{cry,HS}$ versus the measured* $T_{1/2}$ *at seven different pressures* (R^2 *= 0.83).*

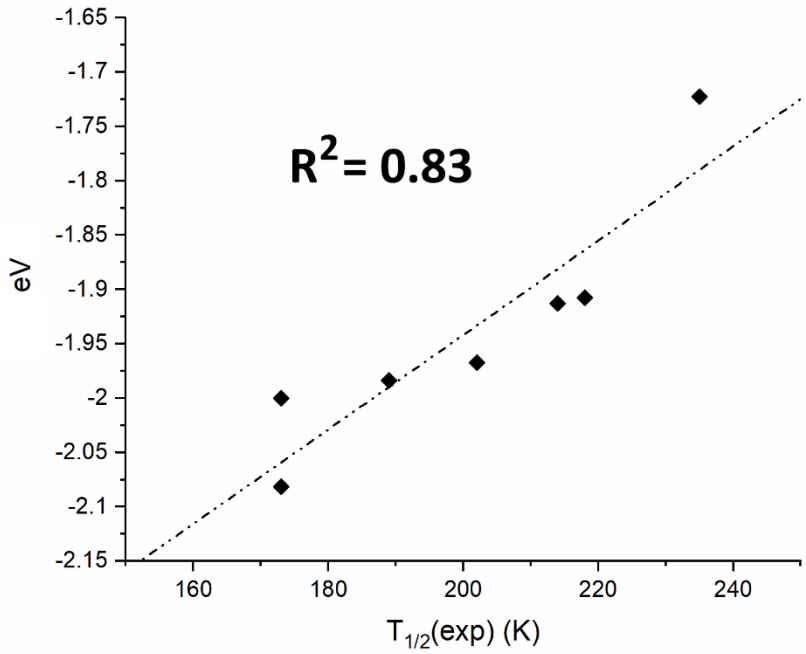

Figure S122. *Reported trend for the variation of MO-279β in* ***1****$_{cry,HS}$ versus the measured* $T_{1/2}$ *at seven different pressures* (R^2 *= 0.83).*

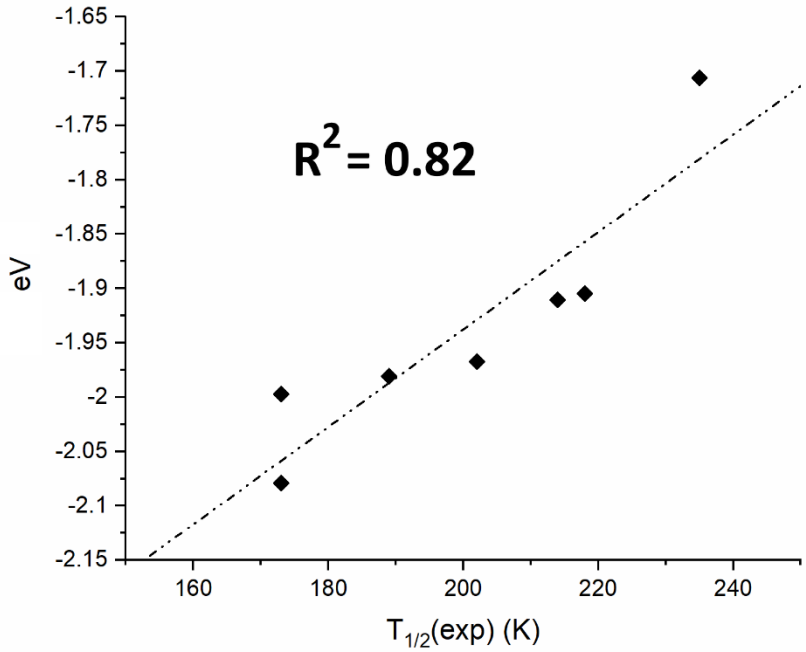

Figure S123. *Reported trend for the variation of MO-280β in* ***1****$_{cry,HS}$ versus the measured* $T_{1/2}$ *at seven different pressures* (R^2 *= 0.82).*

Table S13. *Calculated values of the frontier MOs (HOMO/LUMO) and the HOMO-LUMO gap (Δ(MOs) for* ***1****$_{cry,LS}$* and ***1****$_{cry,HS}$. Last two columns on the right reports the correlation factor for each of the three studied terms (HOMO, LUMO, HOMO-LUMO gap) for* ***1****$_{cry,LS}$* and ***1****$_{cry,HS}$ against the seven pressures employed for this study and the relative experimental $T_{1/2}$ measured at that pressure conditions.*

p / bar		***1***	***1800***	***2100***	***2500***	***2900***	***3900***	***4300***	***R^2 (p)***	***R^2 ($T_{1/2}$(exp))***
$T_{1/2}$(exp.) / K		***173***	***173***	***189***	***202***	***214***	***227***	***235***		
1*$_{cry,LS}$*	***HOMO***	2.884681	2.971757	2.985363	2.999241	3.009037	3.056112	3.073147	0.99 (Fig. S124)	0.81 (Fig. S127)
	LUMO	3.330947	3.39816	3.409044	3.419929	3.446868	3.483059	3.495332	0.99 (Fig. S125)	0.87 (Fig. S128)
	Δ(MOs)	0.446267	0.426403	0.423681	0.420688	0.437831	0.426947	0.422185	0.40 (Fig. S126)	0.14 (Fig. S129)
1*$_{cry,HS}$*	***HOMO***	1.683025	1.768741	1.783435	1.800578	1.845477	1.850919	2.057617	0.78 (Fig. S124)	0.74 (Fig. S127)
	LUMO	2.861823	2.932028	2.94645	2.960872	3.028629	3.032438	3.210836	0.80 (Fig. S125)	0.79 (Fig. S128)
	Δ(MOs)	1.178798	1.163287	1.163015	1.160566	1.183152	1.181519	1.153219	0.05 (Fig. S126)	0.01 (Fig. S129)

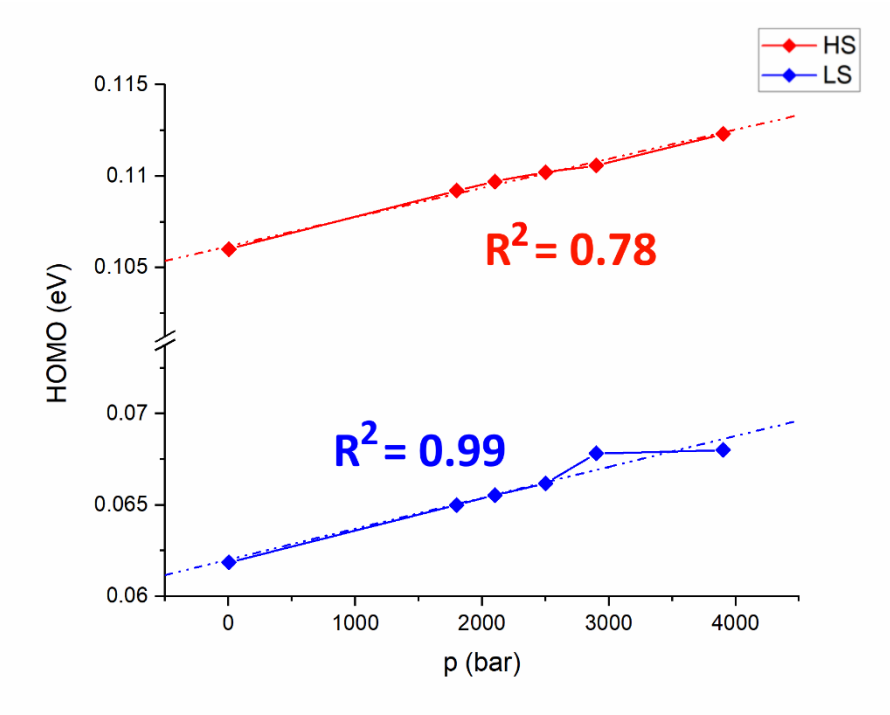

Figure S124. *Reported trend for the variation of the HOMO energy levels at the pressure increase for* ***1****$_{cry,HS}$ (R^2 = 0.78) and* ***1****$_{cry,LS}$ (R^2 = 0.99).*

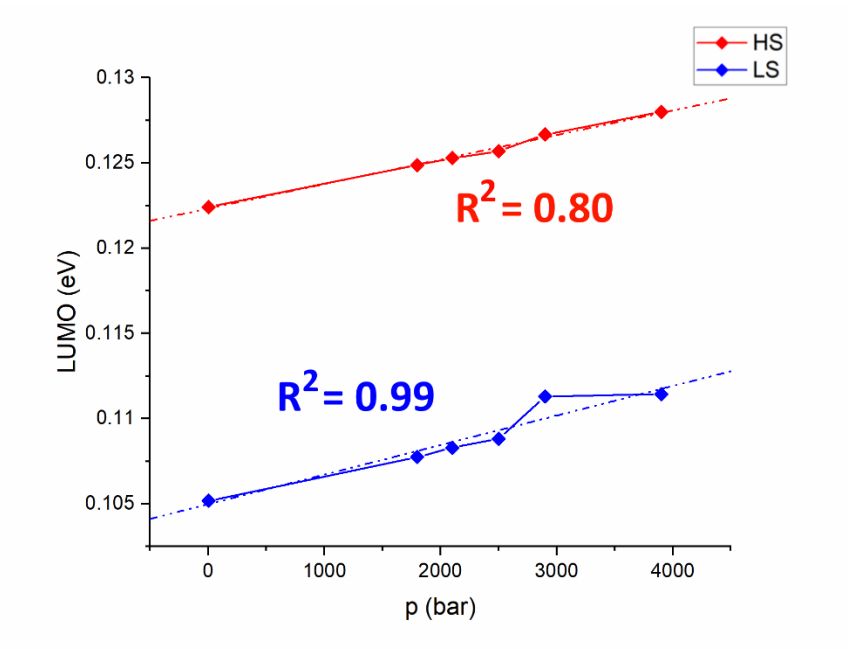

Figure S125. *Reported trend for the variation of the HOMO energy levels at the pressure increase for* ***1****$_{cry,HS}$ (R^2 = 0.80 and* ***1****$_{cry,LS}$ (R^2 = 0.99).*

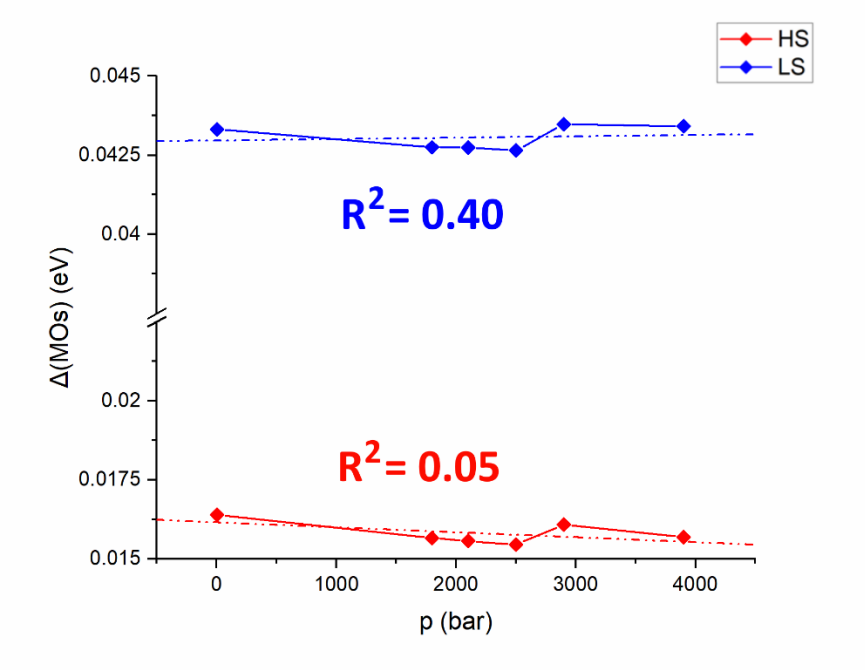

Figure S126. *Reported trend for the variation of the HOMO-LUMO gap (ΔMOs) at the pressure increase for* ***1****$_{cry,HS}$ (R^2 = 0.40) and* ***1****$_{cry,LS}$ (R^2 = 0.05).*

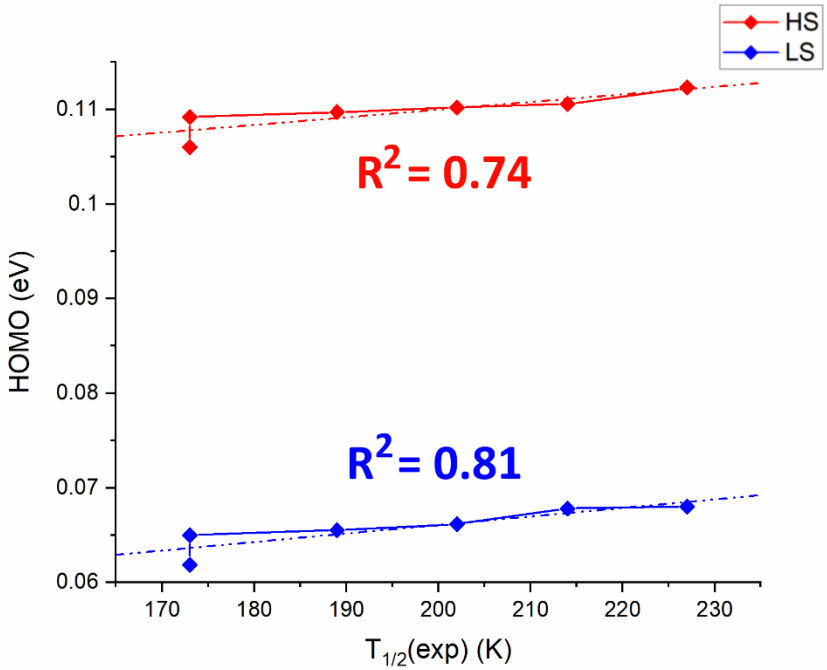

Figure S127. *Reported trend for the variation of the HOMO energy levels of* ***1****$_{cry,HS}$ (R^2 = 0.74) and* ***1****$_{cry,LS}$ (R^2 = 0.81) at the measured $T_{1/2}$ at the pressure increase.*

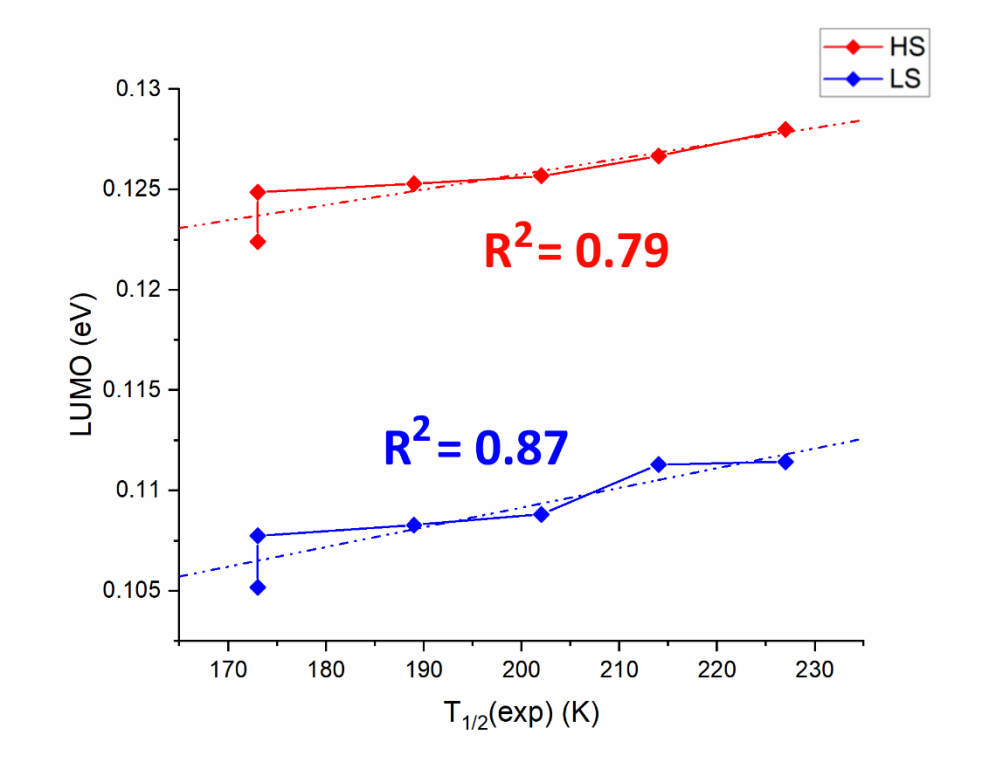

Figure S128. *Reported trend for the variation of the LUMO energy levels of* ***1****cry,HS* *(R^2 = 0.79) and* ***1****cry,LS* *(R^2 = 0.87) at the measured* $T_{1/2}$ *at the pressure increase.*

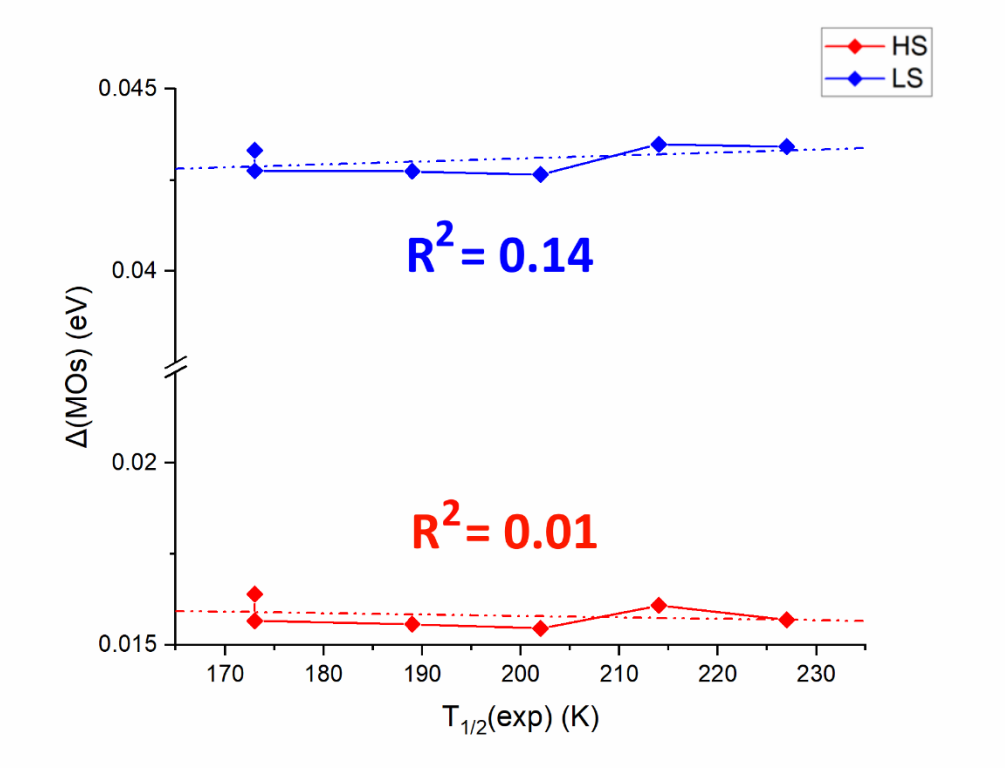

Figure S129. *Reported trend for the variation of the HOMO-LUMO gap (ΔMOs) of* ***1****cry,HS* *(R^2 = 0.14) and* ***1****cry,LS* *(R^2 = 0.01) at the measured* $T_{1/2}$ *at the pressure increase.*

4. Additional Data for *Gradual SCO* Modelling

4.1. CP2K 6.1 Calculated IR Spectra

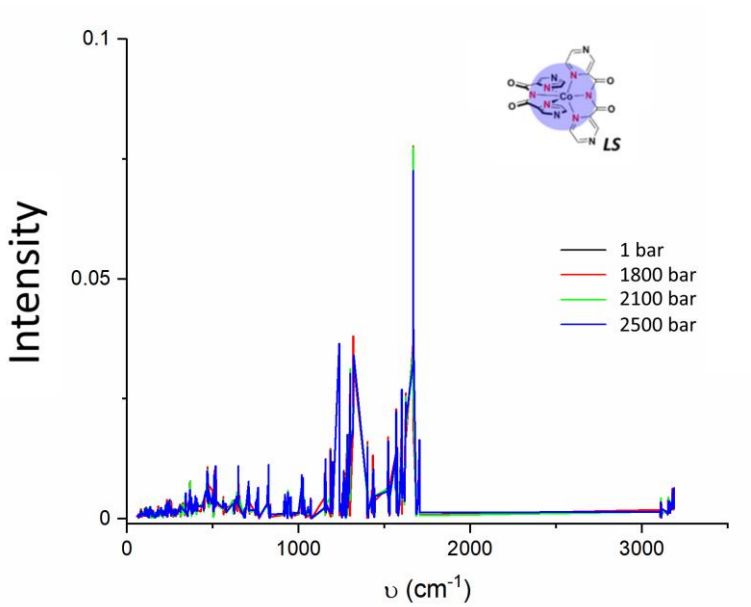

Figure S130. *Reported IR spectra calculated with CP2K6.1 code for crystalline* ***1****$_{cry,LS}$ at the four different pressures (p = 1, 1800, 2100, 2500 bar) where the SCO transition was modelled properly.*

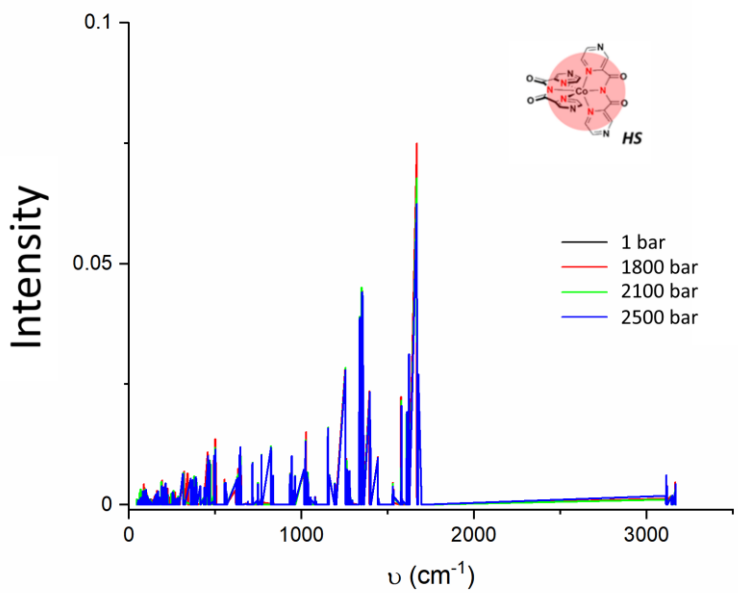

Figure S131. *Reported IR spectra calculated with CP2K6.1 code for crystalline* ***1****$_{cry,HS}$ at three different pressures (p = 1, 1800, 2100, 2500 bar) where the SCO transition was modelled properly.*

4.2. IR/Raman Spectra ORCA4.1 code

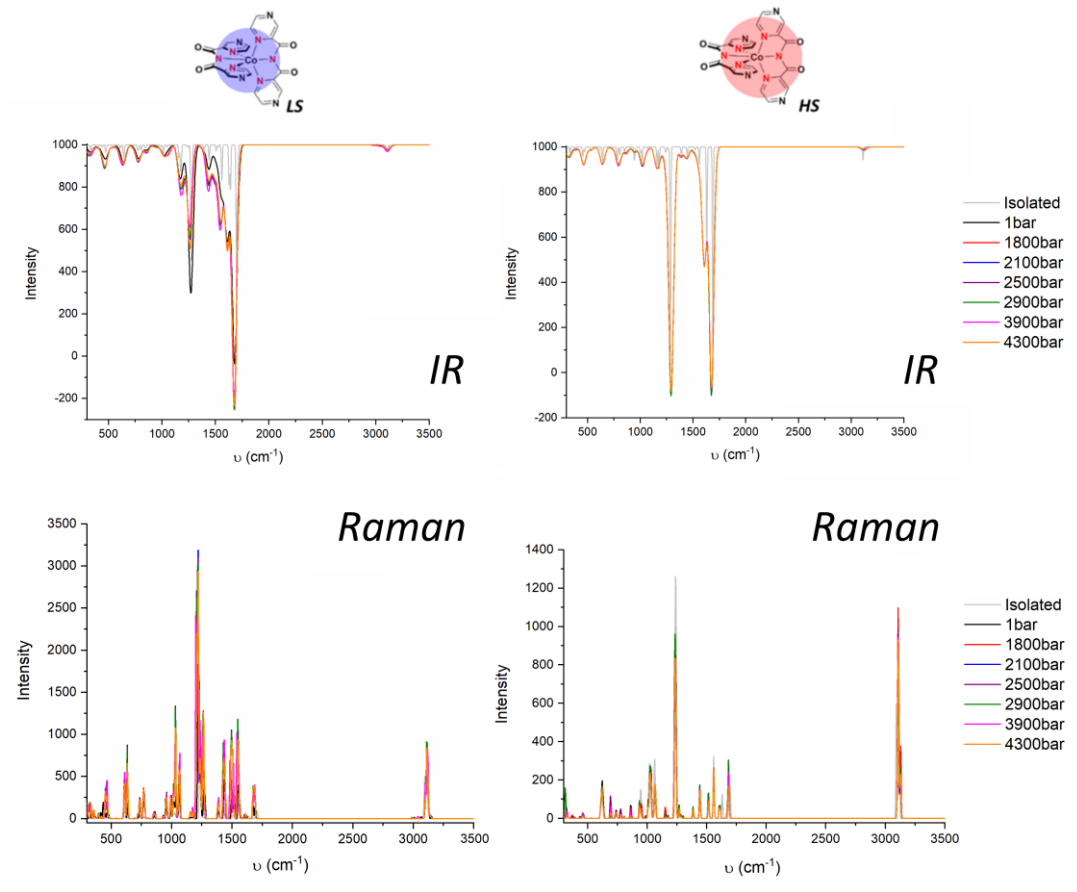

Figure S132. *Calculated IR and Raman spectra for* ***1****$_{cf,LS}$ (left) and* ***1****$_{cf,HS}$ (right) obtained by extrapolation from the crystalline cell and re-optimised using ORCA4.1 code using RI-PBE-def2-TZVPP level of theory (w = 10).*

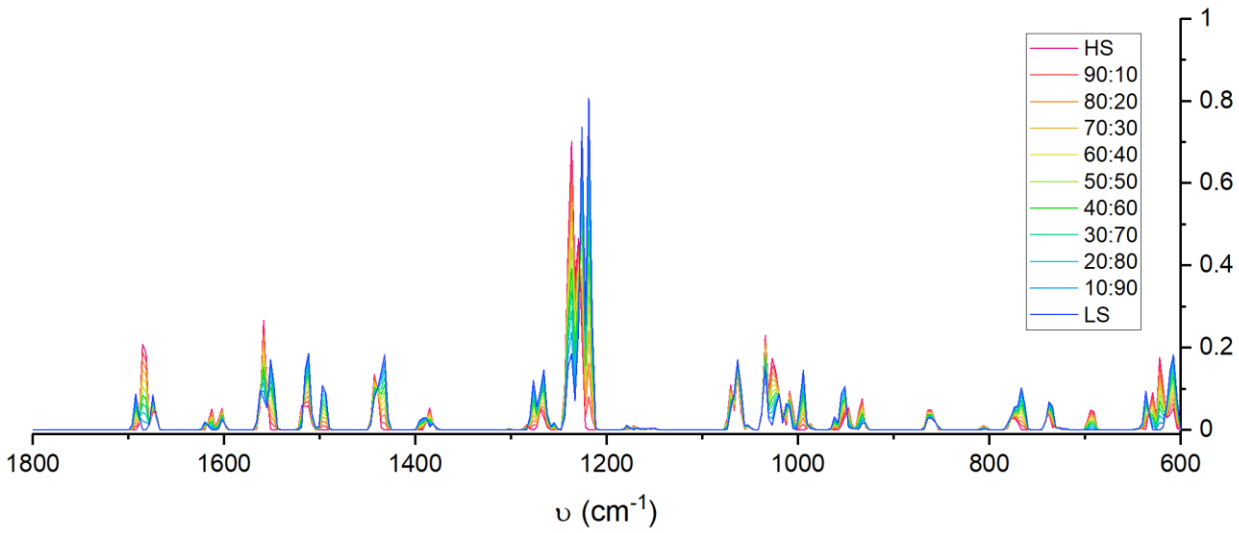

Figure S133. *Variation of the calculated Raman Spectrum of* ***1****$_{cf}$ at p = 1 bar, from* ***1****$_{cf,LS}$ and* ***1****$_{cf,HS}$. Spectra were obtained using ORCA4.1 code: RI-PBE-def2-TZVPP level of theory (w = 5).*

4.3. Thermodynamic Terms

Table S14. *Summary table of the thermodynamic contribution (H_{el}) for* ***1$_{cry,HS}$*** and ***1$_{cry,LS}$*** *at different pressure (from 1 bar to 2900 bar). Results are reported in eV.*

	H_{el} (eV)		
p / bar	***HS***	***LS***	**Δ**
1	-46632.1965	-46632.5185	0.3220
1800	-46632.1911	-46632.5068	0.3157
2100	-46632.1854	-46632.5027	0.3173
2500	-46632.1801	-46632.4962	0.3161
2900	-46631.4015	-46632.4855	1.0840
3900	-46631.3854	-46632.4632	1.0780
4300	-46630.8149	-46632.4516	1.6363

Table S15. *Summary table of the thermodynamic contribution (S_{el}) for* ***1$_{cry,HS}$*** and ***1$_{cry,LS}$*** *at different pressure (from 1 bar to 2900 bar). Results are reported in eV.*

	S_{el} (eV)		
p / bar	***HS***	***LS***	**Δ**
1	0.000214	0.000134	0.00080
1800	0.000214	0.000134	0.00080
2100	0.000214	0.000134	0.00080
2500	0.000214	0.000134	0.00080
2900	0.000214	0.000134	0.00080
3900	0.000214	0.000134	0.00080

Table S16. *Summary table of the thermodynamic contribution (H_{vib}) for* ***1***$_{cry,LS}$ *at different pressure (from 1 bar to 2900 bar). Results are reported in eV.*

p / bar	**1**	**1800**	**2100**	**2500**	**2900**	**3900**
T / K			***H_{vib} (LS) / eV***			
25	34.205	34.213	34.213	34.220	34.224	33.951
50	34.243	34.250	34.250	34.258	34.263	34.005
75	34.337	34.344	34.344	34.351	34.357	34.117
100	34.486	34.492	34.492	34.498	34.504	34.281
125	34.683	34.688	34.689	34.695	34.701	34.492
150	34.924	34.930	34.931	34.936	34.941	34.746
155	34.977	34.983	34.984	34.989	34.995	34.801
160	35.032	35.038	35.039	35.044	35.050	34.859
165	35.089	35.095	35.096	35.100	35.106	34.917
170	35.147	35.153	35.154	35.159	35.164	34.978
175	35.207	35.213	35.214	35.219	35.224	35.040
180	35.269	35.274	35.275	35.280	35.286	35.103
185	35.332	35.338	35.339	35.343	35.349	35.168
190	35.396	35.402	35.403	35.408	35.413	35.235
195	35.463	35.469	35.470	35.474	35.479	35.303
200	35.530	35.536	35.537	35.542	35.547	35.372
225	35.893	35.899	35.900	35.904	35.909	35.744
250	36.293	36.300	36.301	36.305	36.310	36.152
275	36.732	36.739	36.740	36.744	36.748	36.598
300	37.207	37.214	37.215	37.219	37.223	37.079
325	37.717	37.725	37.726	37.729	37.734	37.596
350	38.262	38.269	38.271	38.274	38.278	38.147
375	38.840	38.847	38.848	38.852	38.856	38.729
400	39.448	39.456	39.457	39.461	39.465	39.343

Table S17. *Summary table of the thermodynamic contribution (H_{vib}) for* ***1***$_{cry,HS}$ *at different pressure (from 1 bar to 2900 bar). Results are reported in eV.*

p / bar	**1**	**1800**	**2100**	**2500**	**2900**	**3900**
T / K			***H_{vib} (HS) / eV***			
25	34.046	34.059	34.068	34.064	34.124	34.218
50	34.098	34.112	34.119	34.116	34.174	34.258
75	34.215	34.227	34.232	34.230	34.284	34.356
100	34.385	34.397	34.401	34.399	34.448	34.510
125	34.602	34.613	34.616	34.615	34.660	34.713
150	34.861	34.871	34.874	34.873	34.915	34.960
155	34.918	34.927	34.930	34.930	34.970	35.015
160	34.976	34.985	34.988	34.988	35.028	35.071
165	35.036	35.045	35.048	35.047	35.087	35.129
170	35.097	35.106	35.109	35.108	35.147	35.188
175	35.159	35.168	35.171	35.171	35.209	35.249
180	35.223	35.232	35.235	35.235	35.272	35.311
185	35.289	35.298	35.301	35.300	35.337	35.375
190	35.356	35.365	35.368	35.367	35.404	35.441
195	35.425	35.433	35.436	35.436	35.472	35.508
200	35.495	35.503	35.506	35.506	35.542	35.576
225	35.868	35.876	35.879	35.879	35.912	35.942
250	36.277	36.285	36.288	36.288	36.319	36.346
275	36.722	36.730	36.733	36.733	36.762	36.787
300	37.203	37.211	37.214	37.214	37.241	37.264
325	37.718	37.726	37.729	37.730	37.755	37.775
350	38.267	38.275	38.278	38.278	38.303	38.321
375	38.848	38.856	38.858	38.859	38.882	38.899
400	39.459	39.467	39.470	39.470	39.493	39.508

Table S18. *Summary table of the thermodynamic contribution (S_{vib}) for* ***1***$_{cry,LS}$ *at different pressure (from 1 bar to 2900 bar). Results are reported in eV.*

p / bar	**1**	**1800**	**2100**	**2500**	**2900**	**3900**
T / K			***S_{vib} (LS) / eV***			
25	0.000	0.000	0.000	0.000	0.000	0.000
50	0.001	0.001	0.001	0.001	0.001	0.002
75	0.003	0.003	0.003	0.003	0.003	0.004
100	0.004	0.004	0.004	0.004	0.004	0.005
125	0.006	0.006	0.006	0.006	0.006	0.007
150	0.008	0.008	0.008	0.008	0.008	0.009
155	0.008	0.008	0.008	0.008	0.008	0.010
160	0.009	0.008	0.008	0.009	0.009	0.010
165	0.009	0.009	0.009	0.009	0.009	0.010
170	0.009	0.009	0.009	0.009	0.009	0.011
175	0.010	0.010	0.010	0.010	0.010	0.011
180	0.010	0.010	0.010	0.010	0.010	0.011
185	0.010	0.010	0.010	0.010	0.010	0.012
190	0.011	0.011	0.011	0.011	0.011	0.012
195	0.011	0.011	0.011	0.011	0.011	0.012
200	0.011	0.011	0.011	0.011	0.011	0.013
225	0.013	0.013	0.013	0.013	0.013	0.014
250	0.015	0.015	0.015	0.015	0.015	0.016
275	0.016	0.016	0.016	0.016	0.016	0.018
300	0.018	0.018	0.018	0.018	0.018	0.020
325	0.020	0.020	0.020	0.020	0.020	0.021
350	0.021	0.021	0.021	0.021	0.021	0.023
375	0.023	0.023	0.023	0.023	0.023	0.024
400	0.024	0.024	0.024	0.024	0.024	0.026

Table S19. *Summary table of the thermodynamic contribution (S_{vib}) for* ***1***$_{cry,HS}$ *at different pressure (from 1 bar to 2900 bar). Results are reported in eV.*

p / bar	**1**	**1800**	**2100**	**2500**	**2900**	**3900**
T / K			***S_{vib} (HS) / eV***			
25	0.000	0.000	0.000	0.000	0.000	0.000
50	0.002	0.002	0.002	0.002	0.002	0.001
75	0.003	0.004	0.003	0.003	0.003	0.003
100	0.005	0.005	0.005	0.005	0.005	0.005
125	0.007	0.007	0.007	0.007	0.007	0.006
150	0.009	0.009	0.009	0.009	0.009	0.008
155	0.010	0.010	0.009	0.010	0.009	0.008
160	0.010	0.010	0.010	0.010	0.010	0.009
165	0.010	0.010	0.010	0.010	0.010	0.009
170	0.011	0.011	0.011	0.011	0.010	0.010
175	0.011	0.011	0.011	0.011	0.011	0.010
180	0.011	0.011	0.011	0.011	0.011	0.010
185	0.012	0.012	0.012	0.012	0.011	0.011
190	0.012	0.012	0.012	0.012	0.012	0.011
195	0.013	0.013	0.012	0.012	0.012	0.011
200	0.013	0.013	0.013	0.013	0.013	0.012
225	0.015	0.015	0.014	0.015	0.014	0.013
250	0.016	0.016	0.016	0.016	0.016	0.015
275	0.018	0.018	0.018	0.018	0.018	0.017
300	0.020	0.020	0.020	0.020	0.019	0.018
325	0.021	0.021	0.021	0.021	0.021	0.020
350	0.023	0.023	0.023	0.023	0.023	0.022
375	0.025	0.025	0.024	0.025	0.024	0.023
400	0.026	0.026	0.026	0.026	0.026	0.025

References

1. Hutter, J.; Iannuzzi, M.; Schiffmann, F.; VandeVondele, J., CP2K: atomistic simulations of condensed matter systems. *Wiley Interdiscip. Rev. Comput. Mol. Sci.* **2014,** *4* (1), 15-25.
2. Krack, M., Pseudopotentials for H to Kr optimized for gradient-corrected exchange-correlation functionals. *Theor. Chem. Acc.* **2005,** *114* (1-3), 145-152.
3. Hartwigsen, C.; Gœdecker, S.; Hutter, J., Relativistic separable dual-space Gaussian pseudopotentials from H to Rn. *Phys. Rev. B* **1998,** *58* (7), 3641.
4. Goedecker, S.; Teter, M.; Hutter, J., Separable dual-space Gaussian pseudopotentials. *Phys. Rev. B* **1996,** *54* (3), 1703-1710.
5. Caldeweyher, E.; Bannwarth, C.; Grimme, S., Extension of the D3 dispersion coefficient model. *J. Chem. Phys.* **2017,** *147* (3), 034112.
6. Dudarev, S. L.; Botton, G. A.; Savrasov, S. Y.; Humphreys, C. J.; Sutton, A. P., Electron-energy-loss spectra and the structural stability of nickel oxide: An LSDA+U study. *Phys. Rev. B* **1998,** *57* (3), 1505-1509.
7. Aryasetiawan, F.; Karlsson, K.; Jepsen, O.; Schönberger, U., Calculations of Hubbard U from first-principles. *Phys. Rev. B* **2006,** *74* (12), 125106.
8. Miller, R. G.; Narayanaswamy, S.; Clark, S. M.; Jameson, G. B.; Tallon, J. L.; Brooker, S., Pressure induced separation of phase-transition-triggered-abrupt vs gradual components of spin crossover. *Dalton Trans.* **2015,** *44*, 20843-20849 and front cover.
9. Perdew, J. P.; Ruzsinszky, A.; Csonka, G. I.; Vydrov, O. A.; Scuseria, G. E.; Constantin, L. A.; Zhou, X.; Burke, K., Restoring the density-gradient expansion for exchange in solids and surfaces. *Phys. Rev. Lett.* **2008,** *100* (13), 136406.
10. Vydrov, O. A.; Van Voorhis, T., Nonlocal van der Waals density functional: The simpler the better. *J. Chem. Phys.* **2010,** *133* (24), 244103.
11. Sabatini, R.; Gorni, T.; de Gironcoli, S., Nonlocal van der Waals density functional made simple and efficient. *Phys. Rev. B* **2013,** *87* (4), 041108.
12. Neese, F., Software update: the ORCA program system, version 4.0. *WIREs Comput. Mol. Sci.* **2018,** *8* (1), e1327.
13. Perdew, J. P.; Yue, W., Accurate and simple density functional for the electronic exchange energy: Generalized gradient approximation. *Phys. Rev. B* **1986,** *33* (12), 8800-8802.
14. Weigend, F.; Ahlrichs, R., Balanced basis sets of split valence, triple zeta valence and quadruple zeta valence quality for H to Rn: Design and assessment of accuracy. *Phys. Chem. Chem. Phys.* **2005,** *7* (18), 3297-3305.
15. Weigend, F., Accurate Coulomb-fitting basis sets for H to Rn. *Phys. Chem. Chem. Phys.* **2006,** *8* (9), 1057-1065.
16. Neese, F., *Wiley Interdiscip. Rev. Comput. Mol. Sci.* **2012,** *2*, 73.
17. Buron-Le Cointe, M.; Hébert, J.; Baldé, C.; Moisan, N.; Toupet, L.; Guionneau, P.; Létard, J. F.; Freysz, E.; Cailleau, H.; Collet, E., Intermolecular Control of Thermoswitching and Photoswitching Phenomena in Two Spin-Crossover Polymorphs. *Phys. Rev. B: Condens. Matter Mater. Phys.* **2012,** *85*, 064114.

18. Lufaso, M. W.; Woodward, P. M., Jahn–Teller distortions, cation ordering and octahedral tilting in perovskites. *Acta Crystallogr. B Struct. Sci. Cryst.* **2004,** *60* (1), 10-20.
19. McCusker, J. K.; Rheingold, A. L.; Hendrickson, D. N., Variable-Temperature Studies of Laser-Initiated $^5T_2$ - $^1A_1$ Intersystem Crossing in Spin-Crossover Complexes: Empirical Correlations between Activation Parameters and Ligand Structure in a Series of Poly pyridyl Ferrous Complexes. *Inorg. Chem.* **1996,** *35*, 2100-2112.
20. Marchivie, M.; Guionneau, P.; Létard, J. F.; Chasseau, D., Photo-Induced Spin-Transition: the Role of the Iron(II) Environment Distortion. *Acta Crystallogr., Sect. B: Struct. Sci.* **2005,** *61*, 25.
21. Kuehne, I. A.; Barker, A.; Zhang, F.; Stamenov, P.; O'Doherty, O.; Müller-Bunz, H.; Stein, M.; Rodriguez, B. J.; MORGAN, G. G., Modulation of Jahn-Teller Distortion and Electromechanical Response in a Mn 3+ Spin Crossover Complex. *J. Phys. Condens. Matter* **2020,** *32* (40), 404002.
22. Ketkaew, R.; Tantirungrotechai, Y.; Harding, P.; Chastanet, G.; Guionneau, P.; Marchivie, M.; Harding, D. J., OctaDist: A tool for calculating distortion parameters in spin crossover and coordination complexes. *Dalton Trans.* **2021,** *50*, 1086-1096.
23. Humphrey, W.; Dalke, A.; Schulten, K., VMD: visual molecular dynamics. *J. Mol. Graph.* **1996,** *14* (1), 33-38.